Application of the Adjoint Modal Formalism for the Design of Nanooptical Structures

Dissertation
zur Erlangung des akademischen Grades
doctor rerum naturalium (Dr. rer. nat.)

vorgelegt dem Rat der Physikalisch-Astronomischen Fakultät
der Friedrich-Schiller-Universität zu Jena

von Diplom-Physiker Thomas Kaiser
geboren am 13.09.1983 **in** Rodewisch

1. Gutachter: Prof. Dr. Thomas Pertsch, Friedrich-Schiller-Universität Jena, Germany
2. Gutachter: Prof. Dr. N. Asger Mortensen, Syddansk Universitet Odense, Denmark
3. Gutachter: Prof. Dr. Stefan Linden, Universität Bonn, Germany

Tag der Disputation: 19. April 2018

Zusammenfassung

Die vorliegende Arbeit behandelt die Analyse und das Design funktionaler nanooptischer Strukturen mit Hilfe modaler Methoden. Diese basieren auf dem Reziprozitätstheorem der Elektrodynamik und erlauben es, den machtvollen mathematischen Apparat der Funktionalanalysis und Operatorenalgebra analog zur Quantenmechanik zu benutzen. In seiner klassischen Formulierung gilt diese modale Behandlung allerdings ausschließlich für hermitesche Operatoren, d.h. verlustfreie Systeme.

In der Nanooptik, speziell im Gebiet der Plasmonik, spielt des Verhalten von Metallen bei optischen Frequenzen eine tragende Rolle. Diese zeichnen sich durch hohe dissipative Verluste aus, die im Rahmen der verlustfreien modalen Theorie nicht mehr störungstheoretisch behandelt werden können.

Beim Vorliegen einer nicht-hermiteschen Eigenwertgleichung für das elektromagnetische Feld muss ein Übergang zum *adjungierten* modalen Formalismus vollzogen werden. Während die gewonnenen Ausdrücke ihre intuitive physikalische Interpretation im Zusammenhang mit Energie und Energieflussdichte verlieren, können die wesentlichsten mathematischen Eigenschaften erhalten werden. Diese sind die Orthogonalität der Eigenfunktionen, welche in eine Biorthogonalität bzgl. eines adjungierten Moden*paares* übergeht, sowie die Vollständigkeit des aus ihnen aufgespannten Vektorraumes, welche die Entwicklung von Lösungen der Helmholtzgleichung in Eigenfunktionen überhaupt erst ermöglicht. Die adjungierten Moden stehen hierbei physikalisch im Zusammenhang mit den rückwärts propagierenden Moden eines optischen Systems.

Nach der einführenden Darstellung des mathematischen Formalismus wird dieser in der vorliegenden Arbeit auf das Problem einer Verallgemeinerung des Impedanzbegriffes für die Nanooptik angewandt. Ziel ist es, einen Ausdruck zu finden, der eine Berechnung von komplexen, zusammengesetzten Systemen in Analogie zur Elektrotechnik ermöglicht. Ausgangspunkt ist die Inversion der formalen analytischen Lösung für die modalen Reflexionskoeffizienten an der Ebene zwischen zwei verschiedenen, beliebigen optischen Systemen. Es wird gezeigt, dass eine skalare Behandlung ausschließlich möglich ist für den Fall, dass die physikalische Interaktion über jeweils *ein* dominant interagierendes adjungiertes Modenpaar in beiden Systemen geschieht. Dies ist die *Fundamental Mode Approximation* (FMA), deren Gültigkeit von zentraler Bedeutung ist für die Beschreibbarkeit photonischer Strukturen analog zu homogenen Materialien durch sog. effektive Parameter.

Unter dieser Voraussetzung wird ein verallgemeinerter Ausdruck für das Impedanzverhältnis zweier photonischer Strukturen hergeleitet und es wird gezeigt, unter welchen Voraussetzungen sich die Beiträge der unterschiedlichen Eigenmoden so trennen lassen, dass sich für beide Strukturen ein Absolutwert für die Impedanz angeben lässt. Im Fall ei-

nes Surface Plasmon Polariton (SPP) wird die Rechnung explizit analytisch durchgeführt und ein Ausdruck für die Impedanz eines SPPs gewonnen, der in völliger Analogie zur Verwendung des Begriffes in der Elektrotechnik steht. Zur Verdeutlichung dieser Analogie wird gezeigt, dass die in der Elektrotechnik gebräuchlichen Ausdrücke für Impedanzen verschiedener Strukturen wie Mikrowellen-Wellenleitern als Spezialfall perfekter Leiter in dem hier dargelegten Formalismus enthalten sind. Die gewonnen Ergebnisse werden weiterhin anhand der Beispiele eines BRAGG Reflektors für SPPs und der Kopplung in einen nanostrukturierten Wellenleiter illustriert.

Im Bereich der Nanoantennen wird das adjungierte Modenpaar durch ein- und auswärts propagierende Moden der lokalisierten Struktur gebildet. Der Resonanzmechanismus einer Antenne wird in der Arbeit so beeinflusst, dass die veränderte modale Kopplung an die Umgebung die Rückkopplung und damit die Antennenresonanz verstärkt. Konkret wird eine Gitterstruktur mit einem BRAGG Gitter zweiter Ordnung zu diesem Zweck eingesetzt. Die Realisierung erfolgt durch Hinzufügen einer Ringstruktur zu einer zentralen Nanodisk mittels fokussiertem Ionenstrahlschreiben. Die Eigenmoden sind durch Hankel SPPs gegeben. Die experimentelle Charakterisierung durch Scanning Near-Field Optical Microscopy (SNOM) und nichtlineare Photoemission Electron Microscopy (n-PEEM) bestätigt eine Erhöhung der zentralen Intensität um einen Faktor ≈ 5. Zur Interpretation der n-PEEM Bilder wird in der Arbeit ein Modell entwickelt, dass die Photoelektronenausbeute semiklassisch unter der Annahme einer Proportionalität zur Absorptionsrate für 3-Photonen-Absorption als zeitliches Integral der beitragenden Komponenten des elektrischen Feldes beschreibt. Eine sehr gute Übereinstimmung mit rigorosen Simulationsergebnissen und analytischen Überlegungen zu Hankel SPPs wird demonstriert.

Der letzte Teil der Arbeit behandelt die Hybridisierung eines adjungierten BLOCH Modenpaars mittels einer lokalisierten plasmonischen Partikelresonanz. Das konkret behandelte System untersucht dielektrische Schichtwellenleiter auf denen ein regelmäßiges Gitter aus plasmonischen Nanostrukturen aufgebracht ist. Zum Einsatz kommt die sog. Cut-Wire Pair Geometrie, die eine effektive magnetische Antwort des Systems bei optischen Frequenzen zu erzeugen vermag. Es wird demonstriert, dass eine Anregung der plasmonischen Strukturen durch die longitudinale Komponente des elektrischen Feldes der fundamentalen Wellenleitermode möglich ist. Die Dispersionskurve des hybridisierten Zustandes zeigt eine über die Gitterperiode und Partikelgröße spektral einstellbare Resonanz. Während diese bei dichten Gittern, d.h. kleiner Periode, die erwartbare Signatur der Lorentz-förmigen Resonanz des plasmonischen Partikels zeigt, verändert diese ihre Form je näher die plasmonische Resonanz der Bandkante kommt, wo eine Hybridisierung mit der adjungierten Rückwärtsmode einsetzt. Es treten einstellbare Wendepunkte, Punkte unendlicher Gruppengeschwindigkeit und Bereiche mit negativer Gruppengeschwindigkeit in der Dispersionskurve auf. Diese Ergebnisse müssen im Lichte der Literatur über die Gruppengeschwindigkeit in dissipativen Systemen gesehen werden, die in einer »adjungierten Feldgeschwindigkeit« ihre Verallgemeinerung auf den dissipativen Fall findet, wie bereits vor einigen Jahren gezeigt wurde. Neben der Möglichkeit des Einsatzes in der integriert optischen Sensorik stellt das hier untersuchte System daher eine einfach herzustellende Plattform für die Erforschung extremer Lichtzustände dar.

Contents

I. Introduction

Light has fascinated and stimulated the mind of the physicist ever since. Nothing else has so much influenced the advancement of our understanding about nature. It was the first phenomenon that was described in a quantized manner by PLANCK [1], led to a new understanding of space and time [2, 3], and thus witnessed the birth of the two most important theories in contemporary Theoretical Physics. The question whether light should be described by rays, waves or particles has been a longstanding issue.

A convincing solution was found when HERTZ proved that light is an electromagnetic *field* [4, 5] in the sense that MAXWELL had described [6]. This is still the state-of-the art when describing light: We either treat it as a classical field by MAXWELL's equations or as a quantized field. Within this thesis, we do the former.

The problem of describing light was now conceptually shifted to the realm of mathematical field theory. Its behavior is »encoded« and somehow hidden from the physicist in the *field equations* for which the mathematician develops strategies how to solve them. HELMHOLTZ and GREEN contributed significantly to the mathematical understanding and two principle methods evolved: The modal method which describes the problem in terms of the eigenfunctions of a field operator or the GREEN's function method which describes the response of the system to a point-like excitation in space or time (or both).

This thesis is entirely devoted to the first method and we want to develop a modally resolved picture of the scientific questions we encounter in this thesis. Modal methods largely rely on the findings in the mathematical field of functional analysis [7]. The properties of the modes depend entirely on the properties of the field operator. In our case, this will be the HELMHOLTZ operator introduced in Chapter II. In analogy to quantum mechanics one often calls any operator under consideration the »Hamiltonian« $\hat{H}$ of the system.

In quantum mechanics, the property of utmost importance is that $\hat{H}$ is self-adjoint, which is the case when it is real-valued. In optics, this is realized when the involved materials are lossless, *i. e.* no dissipation occurs. For decades, this requirement has not

been much of a problem for the fields in optics where modal methods are used extensively, namely resonator, fiber and waveguide optics, although authors like SIEGMAN argued already in the 1970s that a laser cavity as an open resonator is not free of dissipation and requires a generalization of the theoretical framework [8–10].

In the last decade, the research area of plasmonics and nanophotonics emerged. The driving force was the possibility to overcome ABBE's diffraction limit [11] and »squeeze more light into tinier space«. However, the designs largely depend on the use of noble metals at optical frequencies which suffer from high Ohmic losses. In this way, we have to deal with a non-selfadjoint operator and its eigenmodes. The question on the implications for quantum mechanics was treated since approximately the same time [12, 13]. Hence, we have to come to a modal understanding of dissipative systems.

The tremendous increase in available computational power during the last three decades has caused a paradigm shift in applied photonics. It is possible today to solve Maxwell's equations with ab-initio (also called rigorous) techniques even for very complicated 3D problems. But how can we bridge the gap between the fundamental theory and bare computational results? The chosen numerical method has to provide more than just the electromagnetic field solution and modal methods are very well suited for this purpose [14–18]. It is important that we can find model parameters which describe the systems we wish to treat in a simple way. One extends the applicability of a certain concept by generalizing the underlying quantities. This became known as the »effective parameter« approach, especially when dealing with man-made photonic crystals and metamaterials. These two concepts make use of sub-wavelength ingredients below the diffraction limit with the aim to manipulate the flow of light in ways which are not achievable by using just the homogeneous materials alone [19, 20]. If the effective parameter approach is successful, the structure can be treated as if it was a genuine homogeneous material. Among such parameters, the »refractive index« and the impedance gained the most importance.

Especially the impedance has a long history in electromagnetics. Since its introduction by HEAVISIDE [21] just about the same time HERTZ discovered the electromagnetic waves, the impedance gained the meaning of a »wave resistance« and represented the ratio of the electric to the magnetic field strength for a plane wave. However, SCHELKUNOFF pointed out already in the 1930's that the impedance must be seen as a property of the wave *in* the medium rather than the medium alone [22]. The quantity quickly became the most important one for the emerging field of electronics and allowed the construction of

complicated circuits by simple components such as coils, capacitors and resistances.

Optics did, however, not so strongly benefit from the impedance framework, since the ratio E/H is not spatially constant, *e. g.* in an optical waveguide. Proposals how to heuristically overcome this reached from taking just the ratio of the average field strengths, the average of the ratio of them or line integrals in analogy to an »optical voltage« and »optical current«, so that already in the 1960s a situation with mutually contradicting definitions existed [23].

Modern micro- and nanophotonics has brought up a multitude of structures for which the applicability of an impedance concept would be highly beneficial. The first research area in modern photonics where the question was treated again was the field of lossless photonic crystals. The same heuristic approaches were made and, not surprisingly, led to unsatisfactory results, which were highly geometry-dependent [24–26]. A promising approach was found in the so-called »BLOCH-impedance« – the ratio of the surface-averaged electric and magnetic field components – which was shown to be an analytical solution being compatible with MAXWELL's equations [27, 28]. The applicability of this quantity has a prerequisite, namely the »*Fundamental Mode Approximation*« (FMA), which was later on also applied to the delicate task of assigning effective parameters to metamaterials. It was shown that the validity of this approximation is a general requirement for describing a metamaterial by effective parameters *at all* [29–34]. We will come back to this point later in the thesis.

A violation of the FMA requires that the concept of a scalar impedance value must be abandoned. LAWRENCE and co-workers showed that, for frequencies above WOOD's anomaly [35], impedance matrices have to be introduced [36–38].

In plasmonics, with the vision of integrated circuits at optical speeds in mind, one tried to stretch the understanding of the radio wave frequency domain to optics. Especially ENGHETA, ALÙ and co-workers contributed substantial work to the field of »lumped circuit« elements for optics [39–42]. The similarity in the working principle of a plasmonic metal-insulator-metal waveguide[1] and a hollow-core waveguide in the RF regime, for instance, facilitated the use of traditional concepts for this kind of structure [43–45]. However, this requires that the quasi-static limit is reached and that heuristic analogies can be found for a specific structure. The impedance of a dipole emitter or nanoantenna in the dipole-limit was also alternatively defined by GREFFET and co-workers in conjunction with the quantum-optical GREEN tensor [46].

[1] This is a structure where sub-wavelength waveguiding occurs in a dielectric which is sandwiched between two noble metal layers.

Nanoantennas. Soon after the discovery of electromagnetic waves, the natural question was how to efficiently convert localized electromagnetic energy into propagating one and vice versa. The first wireless transmission experiments were carried out by MARCONI in the Swiss Alps in 1895. In his Nobel Prize speech of 1909 [47], MARCONI referred to the transducers he used as »antennas«.

It is interesting to note that the principal idea of using light scattering from very small particles as a nanoscale light source was developed quite fast. It was SYNGE who expressed this idea in a letter to EINSTEIN in 1928 [48]. However, it was viewed more as a problem of microscopy instead of an »electronics-for-light-problem«.

The following decades saw a tremendous development of antenna theory, technology and applications in the RF regime, with an ever increasing frequency of operation up to the lower GHz band used for modern wireless communication. These efforts were accompanied by another strong driving force of 20$^{\text{th}}$ century technology: miniaturization. With the invention of the transistor and breathtaking advancements in solid-state physics in the background, brilliant minds such as FEYNMAN started to realize that a manipulation of matter on the nano- or even atomic scale should in principle be possible. In his visionary talk »There's plenty of room at the bottom« [49], he correctly envisioned nanoscience as an entirely new field of physics, which would be not so much driven by new fundamental insights into nature, but by the tremendous possibilities for technological applications. The subsequent technological advances revolutionized the field of electronics in the last decades of the 20$^{\text{th}}$ century.

Building antennas for the optical frequency domain came in reach with the advancements of nanofabrication technology and promised to solve a conceptual problem that light emission has. Due to the diffraction limit, the free electromagnetic field cannot localize on length scales smaller than half of the wavelength. A quantum emitter like a radiating atom is, however, much smaller and there is a huge impedance mismatch which makes the process inefficient [50, 51]. The near-fields of nanooptical systems are needed to bridge that gap.

Since the 1980s, optical nanoparticles have been used as antennas, first in the field of Scanning Near-Field Optical Microscopy (SNOM) [52–64] and in the enhancement of light emission [65–73]. A scanning probe is used to sample the photonic near-field, which was at first also viewed as an antenna problem. Nonlinear spectroscopy, like Surface- or Tip Enhanced Raman Spectroscopy, benefit greatly from nanoantennas [74–84].

There are strong efforts in research to replace current electronic devices by photonic

ones. This »optical circuitry« has inspired nanoscale light generation, routing and emitting devices. Plasmonics could play a great role to reduce the size of the devices due to its ability to overcome the diffraction limit. Nanoantennas are the key ingredient to compensate the mismatch between free-space radiation and the nanoscale circuit [85–90]. Key features for interconnects such as tuning [91–95], electric detection [96, 97] or generation of surface plasmons [98–101] involved nanoantennas and displayed the enormous potential of this development.

The spectrally broad metallic nanoantenna resonance promises also a high temporal resolution [102]. Electromagnetic energy can thus be localized both in space and time on a very small scale, enabling »coherent control« over the fields [103]. The availability of reliable ultrafast laser sources together with the possibilities of nanoantennas have led to the demonstration of complete spatiotemporal control over the electromagnetic field [104–107].

It should be mentioned that other modern developments and keywords such as surface plasmon lasing (SPASER) [108–114] or the creation of artificial photonic sheets and materials (»metamaterials« and »metasurfaces«) have also been addressed in the context of optical nanoantennas [115–118] and exploit their properties. The lines are blurred between the research areas and one might quickly get the impression that in nanooptics »everything is an antenna«, which is neither fully true nor fully false. In this thesis, we have concentrated on works where the classical antenna functionality as a receiving or emitting transducer between the nanoscale and the far-field was in the focus.

The quantity of utmost importance for a nanoantenna is the »quality factor« Q, which is proportional to the ratio between the stored energy and radiated power at the resonance frequency [51, 119, 120]. It is the central goal for nanoantenna design, to increase this value.

A multitude of geometries had been suggested to build nanoantennas for the optical frequency range. The simplest is the monomer, which makes use of the localized resonance of a single particle. The theory of MIE, published as early as 1908, provided an analytical solution for the light scattering from a spherical nanoparticle [121]. It is possible to fabricate such particles chemically in solution, which increases their availability. Consequently, one of the first intensively investigated nanoantenna geometries were spheres or spheroid particles [66, 67, 122]. Another design are rod-type structures which function as an open cavity [123–131]. The recent years have also brought a different type of monomer nanoantenna, the all-dielectric one, which makes the first two MIE

resonances overlap spectrally in a high-index dielectric [118, 132–141]. Another interesting approach is the »traveling wave« antenna which is also of the all-dielectric type and exploits the leakage radiation of guided modes into their surrounding [142]

In analogy to the RF regime, also dimers were used as nanoantenna where the gap between two particles acts as a feed [143–145]. The two monomer plasmon modes interact strongly, which leads to the effect of hybridization [146]. The energy levels split into a lower-frequency »bonding« mode and a higher frequency »antibonding« one, a terminology which stems from the hybridization of atomic orbitals in molecular physics [147]. Due to their multipolar characteristics, they are referred to as »bright« and »dark« modes [148]. When spheres are used as constituents for the dimer, the current density in the metal can be reduced compared to other geometries [149]. This leads to lower Ohmic losses and a higher radiation efficiency of the antenna [150]. This design is found to be in remarkable similarity to the original experiments by HERTZ, but several orders of magnitudes higher in frequency. A similar consideration led to the »bow-tie« design, involving two facing triangles with edges as sharp as possible and a very small gap in between [151–154]. The sharp edge is enhancing the electric field and leads to a spectrally broadband operation. However, the achievable enhancement factors are usually limited by fabrication characteristics, so that bow-tie antennas may be outperformed by dipole-rod antennas in practice [51].

Apart from these relatively simple monomer or dimer geometries, there were efforts to increase the functionality by lending concepts from RF engineering, *e. g.* to introduce directionality (YAGI-UDA-antenna) [71, 72, 155–157] or polarization dependence [158, 159]. An interesting class of structures is created by exploiting BABINET's principle [160]. Instead of creating a certain structure from noble metal on a substrate, a hole with almost arbitrary shape is milled into a metal film. Such holes or hole-arrays were created with a multitude of shapes, from simple circular geometries [161, 162] over C-shaped designs [163] to bow-ties [164, 165]. They may also make use of the effect of extraordinary optical transmission (EOT), where a constructive interference of excited surface waves leads to an unexpected peak in device throughput [166].

Structure of this thesis

Within this thesis, we will entirely use the modal formalism to analyze and design functional nanophotonic structures. Chapter II lays the foundations for the mathematical fra-

mework in the form of the adjoint modal formalism, which is fully valid for dissipative systems. We will employ a description entirely based on a modal decomposition into adjoint modes and also introduce the numerical means used to calculate these modes.

In Chapter III, we apply the formalism to the question how a rigorous impedance definition can be found that generalizes the concept from the radio frequency to the optical range. We will give a number of examples and show the consequences of the general formalism for certain important application cases.

The design of an enhanced nanoantenna lies in the focus of Chapter IV. The starting geometry is a monomer rod or disc antenna. We analyze the localized mode with the adjoint modal framework and introduce a secondary structure whose modes increase the internal modal feedback of the monomer. In this way, we increase the quality factor of the antenna. We investigate the approach experimentally by using SNOM and multiphoton Photoemission Electron Microscopy (n-PEEM).

Chapter V investigates the coupling between a dielectric waveguide and plasmonic nanoparticles placed on top of it. A metasurface of particles covering the waveguide is producing a hybridization into a Waveguide Plasmon Polariton state which shows extreme dispersion characteristics such as superluminality or negative group velocity. We discuss this properties in the light of the adjoint modal formalism and discuss possible applications of the system.

It is not possible to do such a work alone. When implementing the aperiodic extension of the Fourier Modal Method (FMM) according to works of LALANNE and co-workers [167–172], I used the anisotropic core of the modesolver which T. PAUL, Institute of Condensed Matter Theory and Solid State Optics Jena, had implemented following the paper of NOPONEN and TURUNEN [173]. The rigorous simulation using the Finite Difference Time Domain (FDTD) method in Chapter IV was performed by J. QI from the same institute. The fabrication of the samples in Chapters IV and V was performed by M. STEINERT (Focused Ion Beam Milling) and C. HELGERT (electron beam lithography), respectively. Both are hosted at the Institute of Applied Physics, Jena. The SNOM experiments in Chapters IV and V have been performed together with A. KLEIN and S. DIZIAN at their setups in the same institute. The n-PEEM experiment was performed by M. FALKNER who also works at the Institute of Applied Physics in Jena.

II. Theoretical and computational concepts

In this chapter, we will lay the mathematical foundations for the adjoint modal framework. To present a complete picture, we derive all relevant quantities. The starting point is a formulation of MAXWELL's equations as eigenvalue problem and a discussion of the algebraic structure of the solutions when the HELMHOLTZ operator is non-Hermitian. As a consequence, modal decomposition must be performed with respect to the biorthogonal adjoint mode set. We clarify the nature of these modes and outline a numerical method used in this thesis to calculate them, namely the aperiodic Fourier Modal Method.

2.1. Electromagnetic wave propagation as mathematical eigenvalue problem

2.1.1. From Maxwell to Helmholtz

This thesis operates within the realm of classical electrodynamics. The theoretical description is based on MAXWELL's equations for the electromagnetic fields. For all considerations, we will need the macroscopic fields in matter. In time domain, the basic equations in their most general form read as [174]

$$\begin{aligned} \nabla \times \bar{\mathbf{E}}(\mathbf{r},t) &= -\frac{\partial \bar{\mathbf{B}}(\mathbf{r},t)}{\partial t} & \nabla \cdot \bar{\mathbf{D}}(\mathbf{r},t) &= \bar{\rho}(\mathbf{r},t) \\ \nabla \times \bar{\mathbf{H}}(\mathbf{r},t) &= \bar{\mathbf{j}}(\mathbf{r},t) + \frac{\partial \bar{\mathbf{D}}(\mathbf{r},t)}{\partial t} & \nabla \cdot \bar{\mathbf{B}}(\mathbf{r},t) &= 0. \end{aligned} \tag{2.1}$$

Quantities in the time domain will have a bar over the symbol. They will be used in the discussion considering the nonlinear Photoemission Electron Microscopy of a nanoantenna sample by the aid of ultrashort pluses. The temporal dependence is treated in the

slowly varying envelope approximation, which will be explained in more detail there.

Throughout the largest part of the thesis, we will look for stationary solutions of Eqs. (2.1) at a fixed frequency ω and most of the equations are in the FOURIER domain, which will have no special symbol decoration.

Throughout this thesis, we choose an $\exp[-i\omega t]$ time-dependence. In frequency domain, MAXWELL's equations will then take the form

$$\begin{aligned} \nabla \times \mathbf{E}(\mathbf{r},\omega) &= i\omega \cdot \mathbf{B}(\mathbf{r},\omega) & \nabla \cdot \mathbf{D}(\mathbf{r},\omega) &= \rho(\mathbf{r},\omega) \\ \nabla \times \mathbf{H}(\mathbf{r},\omega) &= \mathbf{j}(\mathbf{r},\omega) - i\omega \cdot \mathbf{D}(\mathbf{r},\omega) & \nabla \cdot \mathbf{B}(\mathbf{r},\omega) &= 0. \end{aligned} \tag{2.2}$$

We have to specify now the material model we will assume. The first assumption considers $\mathbf{B}$. Since this work considers the optical freqency range, we will assume all media to be non-magnetizable, *i. e.* $\mathbf{B}(\mathbf{r},\omega) = \mu_0 \cdot \mathbf{H}(\mathbf{r},\omega)$, which is a meaningful consideration from the point of view of solid state theory [175]. This assumption must not be mixed up with the occurrence of an *effective* magnetic response at optical frequencies which occurs for some optical »meta«materials, *e. g.* the cut-wire pair structure described in Sec. 5.1. This is an effect of the modal scattering properties and thus the geometric structure at the nanoscale, rather than the used materials themselves. This will be explained in more detail in Chapter V.

In a second assumption we have to model the response of the bound and free electrons in the materials we wish to consider. Throughout this thesis, we are interested in the linear material properties except for Sec. 4.2, where multiphoton-photoemission will play a role and is treated separately there. The electric displacement covers the response of the bound electrons to an external electric field by the polarization $\mathbf{P}(\mathbf{r},\omega)$ they create in the matter. We assume an isotropic medium, which can be modeled by a scalar function. The response to an electric field in frequency domain is described by the linear susceptibility $\chi(\mathbf{r},\omega)$ as

$$\mathbf{D}(\mathbf{r},\omega) = \epsilon_0 \mathbf{E}(\mathbf{r},\omega) + \mathbf{P}(\mathbf{r},\omega) = \epsilon_0 [1 + \chi(\mathbf{r},\omega)] \cdot \mathbf{E}(\mathbf{r},\omega). \tag{2.3}$$

For the contribution of the free electrons, we have to distinguish between charge flow due to external charges brought into the system (convective current $\mathbf{j}_{\text{conv}}$ due to an external charge density ρ_{ext}), and induced conductive currents $\mathbf{j}_{\text{cond}}$, which originate from the redistribution of free charges *within* the system due to electromagnetic fields. We assume the absence of external charges and yet also $\mathbf{j}_{\text{conv}} = 0$. Conductive currents redistribute

the existing charges in a globally neutral system and give rise to an induced charge density ρ_{ind}, which is linked to the conductive current $\mathbf{j}_{\text{cond}}$ by the continuity equation in frequency domain as [174, 176, 177]

$$\nabla \cdot \mathbf{j}_{\text{cond}}(\mathbf{r},\omega) - i\omega \cdot \rho_{\text{ind}}(\mathbf{r},\omega) = 0. \tag{2.4}$$

The response of the free electrons to an electric field is in the linear case modeled by OHM's law

$$\mathbf{j}_{\text{cond}}(\mathbf{r},\omega) = \sigma(\mathbf{r},\omega) \cdot \mathbf{E}(\mathbf{r},\omega) \tag{2.5}$$

with the conductivity $\sigma(\mathbf{r},\omega)$.

With these considerations, we can rewrite the two MAXWELL equations in (2.2) that have source terms as

$$\begin{aligned} \nabla \times \mathbf{H}(\mathbf{r},\omega) &= -i\omega\epsilon_0 \cdot \left[1 + \chi(\mathbf{r},\omega) + i \cdot \frac{\sigma(\mathbf{r},\omega)}{\omega\epsilon_0}\right] \cdot \mathbf{E}(\mathbf{r},\omega) \\ \nabla \cdot \left\{ \underbrace{\left[1 + \chi(\mathbf{r},\omega) + i \cdot \frac{\sigma(\mathbf{r},\omega)}{\omega\epsilon_0}\right]}_{\stackrel{def}{=} \varepsilon(\mathbf{r},\omega)} \mathbf{E}(\mathbf{r},\omega) \right\} &= 0. \end{aligned} \tag{2.6}$$

The »*complex permittivity*«

$$\varepsilon(\mathbf{r},\omega) = \varepsilon'(\mathbf{r},\omega) + i \cdot \varepsilon''(\mathbf{r},\omega) = 1 + \underbrace{\chi(\mathbf{r},\omega)}_{\text{bound charges}} + \underbrace{i \cdot \frac{\sigma(\mathbf{r},\omega)}{\omega\epsilon_0}}_{\text{free charges}} \tag{2.7}$$

covers the response of bound as well as free electrons. Some care should be taken when making use of this concept. The nomenclature can be misleading, since $\chi(\mathbf{r},\omega)$, being the FOURIER-Transform of a real-valued response function $\bar{R}(r,t)$, is already complex valued by itself

$$\bar{\mathbf{P}}(\mathbf{r},t) = \int_{-\infty}^{t} \bar{R}(\mathbf{r},t-t') \cdot \bar{\mathbf{E}}(\mathbf{r},t')\,\mathrm{d}t', \qquad \chi(\mathbf{r},\omega) = \frac{1}{2\pi}\int_{-\infty}^{\infty} \bar{R}(r,t) \cdot e^{-i\omega t}\,\mathrm{d}t. \tag{2.8}$$

Especially in the spectral region of electronic transitions, $\chi(\mathbf{r},\omega)$ has a significant ima-

ginary part as we will see in the next paragraph. There is a chance of mixing up the complex with the »classical« permittivity or »dielectric function« $1 + \chi(\mathbf{r}, \omega)$ from solid state physics, which is a purely dielectric property [178].

In summary, MAXWELL's equations in frequency domain will take the form

$$\begin{aligned} \nabla \times \mathbf{E}(\mathbf{r}, \omega) &= i\omega\mu_0 \cdot \mathbf{H}(\mathbf{r}, \omega) & \nabla \cdot \mathbf{E}(\mathbf{r}, \omega) &= -\frac{\nabla \cdot \varepsilon(\mathbf{r}, \omega)}{\varepsilon(\mathbf{r}, \omega)} \cdot \mathbf{E}(\mathbf{r}, \omega) \\ \nabla \times \mathbf{H}(\mathbf{r}, \omega) &= -i\omega\epsilon_0\varepsilon(\mathbf{r}, \omega) \cdot \mathbf{E}(\mathbf{r}, \omega) & \nabla \cdot \mathbf{H}(\mathbf{r}, \omega) &= 0 \end{aligned} \tag{2.9}$$

for our purpose.

The two curl equations in (2.9) can be decoupled by applying $\nabla\times$ and using the relations $c = [\epsilon_0\mu_0]^{-1/2}$ and $k_0 = \omega/c$. The speed of light in vacuum is denoted by c. This yields

$$\begin{aligned} \frac{1}{\varepsilon(\mathbf{r}, \omega)} \cdot \nabla \times \nabla \times \mathbf{E}(\mathbf{r}, \omega) &= k_0^2 \cdot \mathbf{E}(\mathbf{r}, \omega) \\ \nabla \times \frac{1}{\varepsilon(\mathbf{r}, \omega)} \cdot \nabla \times \mathbf{H}(\mathbf{r}, \omega) &= k_0^2 \cdot \mathbf{H}(\mathbf{r}, \omega). \end{aligned} \tag{2.10}$$

The inverse of the permittivity ε is called »impermittivity« in the literature. Eqs. (2.10) are sometimes called the »generalized HELMHOLTZ equations« [177]. If we concatenate the electromagnetic fields into a single field vector

$$\mathbf{F}(\mathbf{r}, \omega) = \begin{bmatrix} \mathbf{E}(\mathbf{r}, \omega) \\ \mathbf{H}(\mathbf{r}, \omega) \end{bmatrix}, \tag{2.11}$$

one can concisely rewrite Eqs. (2.10) with a linear »HELMHOLTZ operator« $\hat{H}$ which yields

$$\hat{H}\,\mathbf{F}(\mathbf{r}, \omega) = k_0^2 \cdot \mathbf{F}(\mathbf{r}, \omega), \qquad \hat{H} = \begin{bmatrix} \varepsilon^{-1}(\mathbf{r}, \omega) \cdot \nabla \times \nabla \times & 0 \\ 0 & \nabla \times \varepsilon^{-1}(\mathbf{r}, \omega) \cdot \nabla \times \end{bmatrix}. \tag{2.12}$$

Now, we have shown that the HELMHOLTZ equation is equivalent to an eigenvalue problem with eigenvalues k_0^2. From the mathematical point of view, the spectral properties[1] of $\hat{H}$ determine the solution, which must still fulfill the divergence conditions in Eqs. (2.9). Especially questions of symmetry will play an important role, as will be dis-

[1] »Spectral« means from the point of view of spectral theory of linear operators in functional analysis here. An excellent discussion for physicists is found in [7].

cussed later. A powerful strategy to solve a particular problem is to *expand* the solution into its eigenmodes and begin the analysis and design there, which is at the heart of this thesis.

A significant simplification is achieved, when the problem is homogeneous or at least piece-wise homogeneous. This case is of great importance for us in what follows. The fields become divergence-free as is evident from Eqs. (2.9). By using the vector identity $\nabla \times \nabla \times \mathbf{F} = \nabla \cdot \nabla \mathbf{F} - \Delta \mathbf{F}$, we then arrive at the classical HELMHOLTZ equation for the electromagnetic fields

$$\left[\Delta + k_0^2\, \varepsilon(\omega)\right] \cdot \mathbf{F}(\mathbf{r}, \omega) = 0. \tag{2.13}$$

Since $\hat{H}$ is a diagonal operator in the generalized Eq. (2.12) as well as in the homogeneous form (2.13), we have decoupled the problem for the magnetic as well as the electric field into two independent eigenvalue problems. This opens the possibility to solve for one field and find the other from the respective MAXWELL equation. The magnetic part of $\hat{H}$ in Eq. (2.12) has the advantage of being hermitian when $\varepsilon(\mathbf{r}, \omega)$ is real [177], which significantly simplifies the computational effort to solve the equation [179], *e. g.* for dielectric photonic crystal structures. However, since we want to consider lossy metallic ingredients throughout this thesis, this leads to a non-hermitian problem anyway.

Boundary conditions. When describing piece-wise homogeneous structures which are typical for optics, the transition of the fields at the interface between two different media with permitivities $\varepsilon_1(\mathbf{r}, \omega)$ and $\varepsilon_2(\mathbf{r}, \omega)$ has to be considered. These boundary conditions follow directly by applying GAUSS' and STOKES' theorem to the MAXWELL's equations (2.2)[2]. They read as

$$\begin{aligned} \mathbf{n} \times [\mathbf{E}_2(\mathbf{r}, \omega) - \mathbf{E}_1(\mathbf{r}, \omega)] &= 0 \qquad & \mathbf{n} \times [\mathbf{H}_2(\mathbf{r}, \omega) - \mathbf{H}_1(\mathbf{r}, \omega)] &= 0 \\ \mathbf{n} \cdot [\varepsilon_2(\mathbf{r}, \omega) \cdot \mathbf{E}_2(\mathbf{r}, \omega) - \varepsilon_1(\mathbf{r}, \omega) \cdot \mathbf{E}_1(\mathbf{r}, \omega)] &= 0 \qquad & \mathbf{n} \cdot [\mathbf{H}_2(\mathbf{r}, \omega) - \mathbf{H}_1(\mathbf{r}, \omega)] &= 0, \end{aligned} \tag{2.14}$$

where $\mathbf{n}$ denotes the normal vector of the interface between the two media. The magnetic field is continuous as well as the tangential components of the electric field. The normal component of the electric field has a discontinuity which is characterized by the different permitivities.

[2] This standard derivation is found in many texts on elementary electrodynamics like [174, 176].

Material response model. We have summarized the contributions from bound and free carriers in the complex permittivity. How does its spectral behavior look like in a genuinely homogeneous material? The answer can be developed from two simple models, which are known as the LORENTZ (bound electrons) and DRUDE (free electrons) model. We will use subscripts b and f for the different contributions.

The response of bound electrons can be assumed as a driven harmonic oscillator. The differential equation for the displacement $\bar{\mathbf{s}}(\mathbf{r},t)$ of the electrons reads as

$$\frac{\partial^2 \bar{\mathbf{s}}_b(\mathbf{r},t)}{\partial t^2} + \gamma_b \cdot \frac{\partial \bar{\mathbf{s}}_b(\mathbf{r},t)}{\partial t} + \omega_0^2 \bar{\mathbf{s}}_b(\mathbf{r},t) = -\frac{e}{m_e} \cdot \bar{\mathbf{E}}(\mathbf{r},t), \tag{2.15}$$

where γ_b is a generic damping constant of the bound electrons' oscillation, ω_0 is their eigenfrequency, e the elementary charge and m_e the electron mass. The polarization $\bar{\mathbf{P}}(\mathbf{r},t)$ is directly related to the collective dipole moments via

$$\bar{\mathbf{P}}(\mathbf{r},t) = -N_b e \cdot \bar{\mathbf{s}}(\mathbf{r},t), \qquad N_b \text{ – number of bound charges.} \tag{2.16}$$

If we FOURIER transform and combine the two relations, we find an expression for the frequency dependent susceptibility

$$\chi(\omega) = \frac{f}{\omega_0^2 - \omega^2 - i\omega\gamma_b}, \tag{2.17}$$

where

$$f = \frac{1}{\epsilon_0} \cdot \frac{N_b e^2}{m_e} \tag{2.18}$$

is called the oscillator strength.

The movement of free electrons can be modeled without restoring force as

$$\frac{\partial^2 \bar{\mathbf{s}}_f(\mathbf{r},t)}{\partial t^2} + \gamma_f \cdot \frac{\partial \bar{\mathbf{s}}_f(\mathbf{r},t)}{\partial t} = -\frac{e}{m_e} \cdot \bar{\mathbf{E}}(\mathbf{r},t). \tag{2.19}$$

The conductive current is given by

$$\bar{\mathbf{j}}_{cond}(\mathbf{r},t) = -N_f \cdot e \cdot \frac{\partial \bar{\mathbf{s}}_f(\mathbf{r},t)}{\partial t}, \qquad N_f \text{ – number of free charges.} \tag{2.20}$$

If we abbreviate the equation by introducing the »plasma frequency«[3]

$$\omega_p^2 = \frac{1}{\epsilon_0} \cdot \frac{N_f e^2}{m_e} \tag{2.21}$$

and FOURIER transform the differential equation, we find the expression for the frequency dependent conductivity to be

$$\sigma(\omega) = \epsilon_0 \cdot \frac{\omega_p^2}{\gamma_f - i\omega}. \tag{2.22}$$

A particular material has a multitude of electronic transitions between bound states, giving rise to multiple resonant frequencies $\omega_{0,l} = \Delta E_l/\hbar$, where ΔE_l is an energy difference between two molecular energy levels and $\hbar$ is PLANCK's constant. The combined complex permittivity is thus found as

$$\varepsilon(\omega) = 1 + \left\{ \sum_l \underbrace{\frac{f_l}{\omega_{0,l}^2 - \omega^2 - i\omega\gamma_{b,l}}}_{\text{LORENTZ}} \right\} - \underbrace{\frac{\omega_p^2}{\omega^2 + i\omega\gamma_f}}_{\text{DRUDE}}. \tag{2.23}$$

It summarizes the contributions from bound and free electrons. An important limiting case are dielectrics for an excitation frequency in the transparency region which lies in between two energy transitions $\omega_{0,1}$ and $\omega_{0,2}$. Without contributions from free charges ($\omega_p = 0$), this is a spectral region where the real part of the permittivity usually grows with frequency (»normal dispersion«. The imaginary part of the permittivity is negligible there and loss can be treated perturbativly from the loss-less solutions. The absence of dissipation guarantees that the HELMHOLTZ operator in Eq. (2.10) is hermitian, *i. e.* all eigenvalues are real. This assumption applies to most glasses and other dielectrics used in traditional optics.

Another important case are metals at optical frequencies, where free electrons play the most important role. If we summarize the dielectric background contributions with ε_∞, one arrives at the DRUDE formula for the metal's permittivity in the case of an undamped

[3] The name originates from the fact that ω_p appears as the eigenfrequency of the oscillating charge density $\rho(\mathbf{r}, t)$, which can be viewed as an oscillating plasma.

electron motion ($\gamma_f = 0$)

$$\varepsilon_{metal} = \varepsilon_\infty - \frac{\omega_p^2}{\omega^2}. \tag{2.24}$$

For frequencies lower than ω_p, the permittivity is negative. In this frequency range, a special modal solution of Eq. (2.10) exists, which is at the heart of contemporary nanooptics, namely the Surface Plasmon Porlariton. We will derive this mode and discuss its beneficial properties in the next section.

Nanooptics is all about spatially structuring $\varepsilon(\mathbf{r}, \omega)$ on a length scale smaller than the wavelength of the used light. This can be done by manipulating the geometry of an otherwise monolithic material, or by putting together materials which differ strongly in their optical properties, such as dielectrics and a metals. We will discuss an antenna for visible light, made entirely of gold as a representative of the first approach in Chapter IV, and dielectric waveguides with incorporated plasmonic nanostructures as an example for the second approach in Chapter V.

Since the light cannot fully »resolve« structural changes on such a small scale, it is possible to influence the way how light behaves in these structures. Under certain prerequisites, such a nanostructured medium can be described by an »effective« response ε_{eff}, which replaces the solid-state theory based material model. Even an effective magnetic response μ_{eff} is possible, although all underlying materials are non-magnetizable. This leads to the effect of *negative refraction* [180]. However, it turns out that the conditions for such true »meta«materials are very hard to fulfill in reality [29, 30, 33, 181].

2.1.2. Modal methods for the Helmholtz equation

The HELMHOLTZ equation (2.12) is formulated as an eigenvalue problem for k_0^2. One finds eigenfrequencies ω of the system, which are in general complex. The imaginary part of ω is associated to the damping of the system. This form is well suited for finding *localized* solutions, *e. g.* for resonators, which constitute a cavity.

Within this thesis, we are interested in *propagating* solutions for a particular given real frequency ω. We therefore choose our coordinate system in such a way that z defines a *propagation direction*[4]. Every solution to Eq. (2.12) can then be *expanded* into eigenmodes

[4] We will deal with cylindrical symmetric structures in Sec. 4.1 so that the radial direction will play that role there.

as

$$\mathbf{F}(\mathbf{r},\omega) = \sum\!\!\!\!\!\!\int_l a_l \cdot \mathbf{F}_l^+(\mathbf{r},\omega) + \sum\!\!\!\!\!\!\int_l b_l \cdot \mathbf{F}_l^-(\mathbf{r},\omega), \tag{2.25}$$

which fundamentally distinguishes *forward* (+) and *backward* (−) propagating modes with respect to z. The specific modal solutions $\mathbf{F}_l^{\pm}(\mathbf{r},\omega)$ can then be further categorized according to the symmetry properties of $\varepsilon(\mathbf{r},\omega)$. The modal parameter l can especially be discrete, continuous or a mixture of both, which is indicated by summation sign superimposed by an integral. We outline the three most important cases with relevance to this thesis in the following.

Plane waves. The most simple symmetry is homogeneity, *i. e.* a continuous translational invariance of $\varepsilon(\mathbf{r},\omega)$ in all three dimensions. $\hat{H}$ commutes with the unitary three-dimensional translation operator. Both operators have joint eigenfunctions in this case [7], which can be written as a complex exponential

$$\mathbf{F}_\mathbf{k} \cdot \exp(i\mathbf{kr}), \tag{2.26}$$

where $\mathbf{F}_\mathbf{k}$ is a constant. This defines *plane waves*, the eigenfunctions of homogeneous space. They present a generic complete functional basis, which will play an important role for the numerical techniques described in the next section. The *wavevector* $\mathbf{k}$ characterizes the eigenfunction as a continuous parameter and depends on ω as

$$\mathbf{k}^2 = k_x^2 + k_y^2 + k_z^2 = \varepsilon(\omega) \cdot \frac{\omega^2}{c^2}. \tag{2.27}$$

This is the *dispersion relation* of plane waves.

Waveguide modes, stratified media. An important symmetry class, which is relevant for waveguiding devices, is a continuous translational invariance only in the propagation direction z. The symmetry demands a form $\mathbf{F}_\beta(x,y)\cdot\exp(i\beta(\omega)z)$ for the eigenfunctions. The role of k_z is played by the »*propagation constant*«, which is traditionally called $\beta(\omega)$ in the waveguide literature. We want to follow this tradition for readability. Eq. (2.13)

can be adapted to form a new eigenvalue problem that depends parametrically on ω as

$$\left[\Delta_\perp + \frac{\omega^2}{c^2}\varepsilon(x,y,\omega)\right]\mathbf{F}_\beta(x,y,\omega) = \beta^2(\omega)\cdot\mathbf{F}_\beta(x,y,\omega), \tag{2.28}$$

where $\Delta_\perp = \partial^2/\partial x^2 + \partial^2/\partial y^2$ is the transverse LAPLACE operator. The permittivity may exhibit additional symmetries in the transverse direction, which further classifies the solution. Since $\pm\beta(\omega)$ belong to the same eigenvalue, the solutions split into two subspectra for forward and backward propagating modes. Later in this chapter, we will identify them as the adjoint mode pairs and analyze their properties thoroughly.

Especially stratified structures composed of layers of piecewise homogeneous materials play an important role in optics and for the following chapters of this thesis. The modal solutions can be found analytically. Consider a structure which is composed of S layers in x-direction. We want to count them by the index $m \in [1\ldots S]$. The structure has a translational symmetry in y and z-directions. We are looking for solutions which are invariant in y, so that $(\partial/\partial y = 0)$. The solutions split into two classes. The first has only one non-zero electric field component $E_y(x,z,\omega)$ (TE polarization) while the other has only one non-zero magnetic field component $H_y(x,z,\omega)$ (TM polarization). The symmetry of MAXWELL's curl equations allows us to treat both simultaneously [182] if we renormalize the magnetic field by $\mathbf{H}(\mathbf{r},\omega) \mapsto i[\mu_0/\epsilon_0]^{1/2}\,\mathbf{H}(\mathbf{r},\omega)$. We will only refer to a »principal« field component $F_y(x,z,\omega)$ which represents both cases.

Since every layer is locally homogeneous, we can expand the principal component in every layer into plane waves[5]

$$F_y^m(x,z,\omega) = \left[a_m\cdot e^{ik_m x} + b_m\cdot e^{-ik_m x}\right]\cdot e^{i\beta(\omega)z} \tag{2.29}$$

with the local dispersion relation

$$k_m^2 + \beta^2(\omega) = \varepsilon_m(\omega)\cdot k_0^2. \tag{2.30}$$

The boundary conditions (2.14) demand the continuity of the tangential components at the interfaces between the different media

$$\begin{aligned} F_y^m(x_m,z,\omega) &= F_y^{m+1}(x_m,z,\omega)\\ F_z^m(x_m,z,\omega) &= F_z^{m+1}(x_m,z,\omega). \end{aligned} \tag{2.31}$$

[5] Since we have excluded solutions with $k_y \neq 0$, only two plane waves remain in the expansion.

The z-component is found from MAXWELL's curl equations to be

$$F_z^m(x,z,\omega) = \frac{q_i}{k_0} \cdot \frac{\partial F_y(x,z,\omega)}{\partial x} \qquad q_m = \begin{cases} 1 & \text{(TE)} \\ \frac{1}{\varepsilon_m(\omega)} & \text{(TM)} \end{cases}. \tag{2.32}$$

Inserting Eq. (2.29) and (2.32) into (2.31) yields a system of equations for the plane wave amplitudes a_m and b_m

$$\begin{aligned} a_m \cdot e^{ik_m x_m} + b_m \cdot e^{-ik_m x_m} &= a_{m+1} \cdot e^{ik_{m+1} x_m} + b_{m+1} \cdot e^{-ik_{m+1} x_m} \\ q_m a_m k_m \cdot e^{ik_m x_m} - q_m b_m k_m \cdot e^{-ik_m x_m} &= q_{m+1} a_{m+1} k_{m+1} \cdot e^{ik_{m+1} x_m} - q_{m+1} b_{m+1} k_{m+1} \cdot e^{-ik_{m+1} x_m}. \end{aligned} \tag{2.33}$$

It has the form

$$\hat{M} \cdot \begin{bmatrix} \mathbf{a} \\ \mathbf{b} \end{bmatrix} = 0, \tag{2.34}$$

with a sparse system matrix $\hat{M}$. We set $a_1 = 0$ and $b_S = 0$ (no impinging radiation) in order to solve for the self-consistent modal solutions, which are found from the condition $\det \hat{M} = 0$. We explicitly solve the $S = 2$ (single interface) and the $S = 3$ (slab waveguide) case here due to their importance for later discussions.

$S = 2$: Single interface. The Surface Plasmon Polariton. The system of equations for an interface at $x_1 = 0$ reads as

$$\begin{bmatrix} -1 & 1 \\ -q_2 k_2 & -q_1 k_1 \end{bmatrix} \cdot \begin{bmatrix} a_2 \\ b_1 \end{bmatrix} = 0, \tag{2.35}$$

and $\det \hat{M} = 0$ yields

$$q_1 k_1 + q_2 k_2 = 0. \tag{2.36}$$

Inserting the local dispersion relation Eq. (2.30) and solving for $\beta(\omega)$ yields

$$\beta(\omega) = k_0 \cdot \left[\frac{q_2^2 \varepsilon_2(\omega) - q_1^2 \varepsilon_1(\omega)}{q_2^2 - q_1^2} \right]^{\frac{1}{2}}. \tag{2.37}$$

No solution exists for TE polarization, while the TM solution reads as

$$\beta(\omega) = k_0 \left[\frac{\varepsilon_1(\omega) \cdot \varepsilon_2(\omega)}{\varepsilon_1(\omega) + \varepsilon_2(\omega)} \right]^{\frac{1}{2}}, \tag{2.38}$$

and represents the dispersion relation of a surface wave. If one assumes a DRUDE-type metal Eq. (2.24) and air as cladding, this specifies to

$$\beta(\omega) = \frac{\omega}{c} \cdot \left[\frac{\omega^2 - \omega_p^2}{2\omega^2 - \omega_p^2} \right]^{\frac{1}{2}}. \tag{2.39}$$

There are three regions which are characteristic for all problems involving waveguide eigenmodes:

- $\omega < \omega_p/\sqrt{2}$: The propagation constant $\beta(\omega)$ is purely real while the $k_{1,2}$ are purely imaginary. The energy is exclusively transported in z-direction and called a »truly bound« mode. In the case of a metal surface, this is the Surface Plasmon Polariton (SPP) mode.

- $\omega_p/\sqrt{2} < \omega < \omega_p$: $\beta(\omega)$ is purely imaginary and does not transport energy in the z-direction, the mode is »evanescent«.

- $\omega > \omega_p$: $\beta(\omega)$ is purely real, as well as k_2. The mode transports energy through the cladding towards infinity and is thus called »leaky«. A mode which is leaky to both the substrate and the cladding is commonly called »radiative«.

Especially the SPP mode has attracted much attention in nanooptics, since its $\beta(\omega)$ diverges for $\omega \to \omega_p/\sqrt{2}$. This means that the effective wavelength $\lambda_0/n_{\text{eff}}(\omega)$ tends to zero. $n_{\text{eff}}(\omega) = \beta(\omega)/k_0$ is the »effective index« of a mode and allows for an easy comparison to the *refractive index* $n(\omega) = [\varepsilon(\omega)]^{1/2}$ of genuinely homogeneous materials.

When loss comes into play, the simple classification into the three categories breaks down and $\beta(\omega)$ becomes a mixed-complex quantity for every frequency. Mode loss is then distinguished as intrinsic (due to absorption / dissipation) or radiative (due to energy transport). Both mechanisms can take place for a mode at the same time.

S = 3: Slab structure. If we define $x_1 = 0$ and $x_2 = d$, with d being the thickness of the slab, the system reads as

$$\begin{bmatrix} -1 & 0 & 1 & -1 \\ e^{ik_2 d} & -e^{-k_3 d} & 0 & e^{-ik_2 d} \\ -q_2 k_2 & 0 & -q_1 k_1 & q_2 k_2 \\ q_2 k_2 \cdot e^{ik_2 d} & -q_3 k_3 \cdot e^{ik_3 d} & 0 & -q_2 k_2 \cdot e^{ik_2 d} \end{bmatrix} \cdot \begin{bmatrix} a_2 \\ a_3 \\ b_1 \\ b_2 \end{bmatrix} = 0. \tag{2.40}$$

The requirement $\det \hat{M} = 0$ leads after some manipulation to

$$e^{-2ik_2 d} = \frac{q_2 k_2 + q_1 k_1}{q_2 k_2 - q_1 k_1} \cdot \frac{q_2 k_2 + q_3 k_3}{q_2 k_2 - q_3 k_3}. \tag{2.41a}$$

A more favorable form for numerical solution of this equation introduces the mode index $n = 0, 1, \ldots$ and reads [182]

$$\tan(k_2 d + n \cdot \pi) - i \cdot \frac{q_2 k_2 (q_1 k_1 + q_3 k_3)}{q_2^2 k_2^2 + q_1 q_3 k_1 k_3} = 0. \tag{2.41b}$$

A countable set of bound solutions exists for both polarizations, as well as a continuum of leaky and evanescent modes. The number of bound modes depends on d and the $\varepsilon_m(\omega)$, and can also be zero (waveguide at cut-off). This will be discussed in detail in Sec. 5.1.

Periodic structures, Bloch modes. An important class of photonic structures possesses a *discrete* translational invariance, *i. e.* periodicity. This has profound implications for the solutions of the underlying differential equations, first summarized by FLOQUET [183] and later successfully applied by BLOCH [184] to describe electrons in a periodic potential by SCHRÖDINGER's equation. Its two-dimensional version [178] is formally identical to Eq. (2.28), with $\varepsilon(x, y, \omega)$ serving as the »potential« and $\beta^2(\omega)$ as the »energy« eigenvalue. This fact allows to extend the powerful concepts developed in quantum mechanics to our problem, especially the concepts of *bands*, but also tools from the mathematical apparatus, such as the concept of a HILBERT space with an inner product or the DIRAC notation. We will make extensive use of these concepts throughout this thesis.

The BLOCH theorem states that the eigensolutions of a structure which is periodic in the z-direction with a period p are »quasi-periodic« and obey the form

$$\mathbf{F}_{\beta_b}(\mathbf{r}, \omega) = e^{i\beta_b(\omega) z} \cdot \mathbf{B}_{\beta_b}(\mathbf{r}, \omega), \tag{2.42}$$

where $\mathbf{B}_{\beta_b}(x,y,z+p,\omega) = \mathbf{B}_{\beta_b}(x,y,z,\omega)$ is the truly periodic »BLOCH function«. The permittivity may possess additional periodicity also in the other directions, leading to the theory of photonic crystals (3D periodicity) or photonic crystal waveguides (2D periodicity) [19], where transverse Bloch wavevector components represent an additional degree of freedom to parameterize the eigenfunctions. We keep the notation general and just demand periodicity in the propagation direction here. The propagation constant $\beta_b(\omega)$ parameterizes the eigenfunctions which are not unambiguous since $\beta(\omega) + n \cdot 2\pi/p, n \in \mathbb{Z}$ leads to the same mode. One thus limits its values to the first BRILLOUIN zone in reciprocal space $\beta_b(\omega) \in [-\pi/p, \pi/p]$ [19, 177, 178]. The exponential prefactor modulates the truly periodic BLOCH function when the mode advances from one unit cell to the next. Strong effects from the periodicity can generally be anticipated, when $\beta_b(\omega)$ is near the center or the edge of the band diagram, especially due to the coupling of forward and backward propagating modes. This will play a crucial role for the nanoantenna design in Chapter IV.

The strength of the modal expansion technique lies in its ability to break down a physical phenomenon into its mathematical key ingredients. In quantum physics, this is of utmost importance since the structure of the used operators define what is »observable« at all in the sense of a measurement. The physics is understood by the properties of the eigenfunctions of the operators. We wish to exploit much of this concept for the understanding and design of nanophotonic structures in this thesis. From the mathematical apparatus, the most important thing is an *inner product* between mode functions and the *orthogonality* property, which we will derive now. This task is surprisingly subtle for optics, as we will see in the following. Especially the presence of loss, which is inherent to plasmonics, turns out to be a true game changer from the point of view of the underlying theory.

Reciprocity. Conjugated, unconjugated, adjoint formulation. Mode orthogonality and completeness. Besides the derivation of the HELMHOLTZ equation, the two curl equations in Eqs. (2.2) allow for a second powerful theorem known as LORENTZ reciprocity. We consider two electromagnetic field solutions of MAXWELL's equations $\mathbf{F}_1(\mathbf{r},\omega_1)$ and $\mathbf{F}_2(\mathbf{r},\omega_2)$ for the same geometry, *i. e.* $\varepsilon_1(\mathbf{r},\omega) = \varepsilon_2(\mathbf{r},\omega) = \varepsilon(\mathbf{r},\omega)$. By using the vector identity $\nabla\cdot(\mathbf{a}\times\mathbf{b}) = \mathbf{b}\cdot(\nabla\times\mathbf{a}) - \mathbf{a}\cdot(\nabla\times\mathbf{b})$ as well as the complex conjugate of Eqs. (2.2),

we can deduce

$$\nabla \cdot \left[\mathbf{E}_1(\mathbf{r},\omega_1) \times \mathbf{H}_2^*(\mathbf{r},\omega_2) + \mathbf{E}_2^*(\mathbf{r},\omega_2) \times \mathbf{H}_1(\mathbf{r},\omega_1)\right] = \\ \frac{i}{c}(\omega_1 - \omega_2)\cdot\mathbf{H}_1(\mathbf{r},\omega_1)\cdot\mathbf{H}_2^*(\mathbf{r},\omega_2) + \frac{i}{c}\sqrt{\frac{\epsilon_0}{\mu_0}}\left[\omega_1\varepsilon(\omega_1) - \omega_2\varepsilon^*(\omega_2)\right]\cdot\mathbf{E}_1(\mathbf{r},\omega_1)\cdot\mathbf{E}_2^*(\mathbf{r},\omega_2) \tag{2.43}$$

For identical fields at the same frequency, this expresses the local energy balance since the LHS is proportional to the time averaged POYNTING vector $\langle \mathbf{S}(\mathbf{r}) \rangle = 1/4 \cdot (\mathbf{E}(\mathbf{r},\omega) \times \mathbf{H}^*(\mathbf{r},\omega) + c.c.)$, while the RHS represents the loss in energy characterized by $\varepsilon(\omega) - \varepsilon^*(\omega) = 2\varepsilon''(\omega)$, *i. e.* the imaginary part of $\varepsilon(\omega)$.

If a structure is *lossless*, the permittivity is real and the RHS of the equation vanishes, if two solutions at the same frequency $\omega_1 = \omega_2 = \omega$ are considered. We want to investigate this case and focus our attention on the modal fields in a plane $z = z_0 = const.$, where z is the propagation direction. Now and in what follows, we leave out the explicit dependence of the fields on $(\mathbf{r},\omega)$ for readability. The indices now simply denote different solutions to the same electromagnetic problem at the same frequency. When we apply the modified version of the GAUSS theorem for an arbitrary vector $\mathbf{A}$[6]

$$\iint\limits_{(x,y)\in\mathbb{R}^2} \nabla \cdot \mathbf{A}\, \mathrm{d}S = \frac{\partial}{\partial z}\left[\iint\limits_{(x,y)\in\mathbb{R}^2} \mathbf{A}\cdot\mathbf{e}_z\, \mathrm{d}S\right] \tag{2.44}$$

to Eq. (2.43) we get

$$\frac{\partial}{\partial z}\underbrace{\iint_{\perp}\left(\mathbf{E}_1 \times \mathbf{H}_2^* + \mathbf{E}_2^* \times \mathbf{H}_1\right)\cdot\mathbf{e}_z\, \mathrm{d}S}_{\stackrel{def}{=}\mathscr{C}(\mathbf{F}_1,\mathbf{F}_2)} = 0. \tag{2.45}$$

In the following, the $\perp$ sign will refer to the transverse (x,y)-plane with $\mathbf{e}_z$ as normal vector, the transverse components of a vector, and so on. Eq. (2.45) is often referred to as »the« LORENTZ reciprocity theorem although we will see that it just represents the *conjugated formulation* build on a bilinear form $\mathscr{C}(\mathbf{F}_1,\mathbf{F}_2)$ making use of conjugate fields. It allows to derive the *orthogonality relation* of the components in the modal expan-

[6] This equation is quite central in the argumentation and used in [185] without explicit derivation. We therefore give this derivation from a variational principle in the appendix Sec. A1 and show its applicability to *all* modal solutions including radiating ones.

sion Eq. (2.25). If we consider z-invariant waveguides where the modal fields vary as $\exp(i\beta z)$, application of Eq. (2.45) reads

$$(\beta_m - \beta_n) \iint_{\perp} \left(\mathbf{E}_{\beta_m} \times \mathbf{H}^*_{\beta_n} + \mathbf{E}^*_{\beta_n} \times \mathbf{H}_{\beta_m} \right) \cdot \mathbf{e}_z \, \mathrm{d}S = 0, \tag{2.46}$$

which implies

$$\iint_{\perp} \left(\mathbf{E}_{\beta_m} \times \mathbf{H}^*_{\beta_m} + \mathbf{E}^*_{\beta_m} \times \mathbf{H}_{\beta_m} \right) \cdot \mathbf{e}_z \, \mathrm{d}S = \mathscr{C}(\mathbf{F}_{\beta_1}, \mathbf{F}_{\beta_2}) = 4 \cdot S_m \delta_{mn}, \tag{2.47}$$

where δ_{mn} is the KRONECKER symbol and S_m is the modal POYNTING flux, which constitutes a mode-dependent constant. This property is the key for the modal expansion method to be so powerful since we can immediately draw the following conclusions:

- Every forward mode is orthogonal to any backward mode.
- A particular mode in a given direction is orthogonal to all other modes in that direction, except to itself. This holds also in the case of degeneracy [TK2009, TK2010]. The constant modal POYNTING flux S_m can be used for normalization.
- Since the HELMHOLTZ operator in Eq. (2.28) is trivially hermitian when $\varepsilon(x, y, \omega)$ is real, the completeness of a basis from its eigenmodes is algebraically ensured.
- Since β^2 appears as the eigenvalue in Eq. (2.28), the for- and backward modes with $\pm\beta$ form a complete set each and an orthonormal basis in a HILBERT space formed by all electromagnetic field solutions to the lossless HELMHOLTZ problem with the inner product $\mathscr{C}(\mathbf{F}_{\beta_m}, \mathbf{F}_{\beta_n})$.
- When the modes are normalized ($S_m = 1$), completeness implies for the modal expansion coefficients in Eq. (2.25)

  $$\sum_l |a_l|^2 = \sum_l |b_l|^2 = 1. \tag{2.48}$$

  The quantity $|a_l|^2$ and $|b_l|^2$, respectively, represents the fraction of intensity carried by the l^{th} mode $\mathbf{F}^{\pm}_{\beta_l}$ into the for- or backward direction.
- The complex modal expansion coefficients are simply given by the projection of the

solution on the orthonormal basis using the inner product

$$a_l = \mathscr{C}(\mathbf{F}, \mathbf{F}^+_{\beta_l}), \qquad b_l = \mathscr{C}(\mathbf{F}, \mathbf{F}^-_{\beta_l}). \tag{2.49}$$

These powerful conclusions have made the modal expansion a method of choice for many electromagnetic problems, especially in the waveguide community [185, 186]. Its applicability to the BLOCH modes of lossless photonic crystals and -waveguides has also been shown [187]. Equipped with this mathematical framework, one can solve a large number of photonic problems by »modally decomposing« them. Where different systems interact, coupled mode equations are derived from the conjugated energy balance (2.43) [177, 182, 185] and everything is broken down to z-dependent expansion coefficients which are projections of the modes onto each other, *i. e.* »overlap« integrals which have an intuitive physical interpretation of an energy redistribution among the modes according to their spatial overlap.

The modal expansion method using conjugated reciprocity has become so common in optics that the prerequisites for its applicability have almost been forgotten: It just holds for *lossless* systems! Any non-zero imaginary part of $\varepsilon(\omega)$, may it be loss or gain, will render it invalid. While *small* losses have successfully been treated as a perturbation [185], the strong metal loss at optical frequencies in plasmonics asks for an entirely renewed mathematical framework. The problem appeared first in the analysis of open laser resonators back in the 1970s [8, 188, 189]. Since the HELMHOLTZ operator looses its self-adjoint property, non of the conclusions given above is true any more. Modes are simply not orthogonal in the sense of $\mathscr{C}(\mathbf{F}_{\beta_m}, \mathbf{F}_{\beta_n})$. Authors like SIEGMAN argue enthusiastically that this issue is much too less reflected in the community and even renders the whole concept of »photons« questionable [10]. The nature of classical electromagnetism, as it presents itself to us today, is, however, so mathematically »well-behaved« [190] that an escape route exists, although it is much less paved and convenient.

Starting once again with two solutions to MAXWELL's equations with a slightly different ansatz, we can obtain the relation

$$\nabla \cdot (\mathbf{E}_1 \times \mathbf{H}_2 - \mathbf{E}_2 \times \mathbf{H}_1) = \frac{i}{c}(\omega_1 - \omega_2) \cdot \left(\mathbf{H}_1 \cdot \mathbf{H}_2 - \varepsilon(\omega) \sqrt{\frac{\mu_0}{\epsilon_0}}\, \mathbf{E}_1 \cdot \mathbf{E}_2 \right). \tag{2.50}$$

For two solutions at the same frequency ω, the RHS is *always* zero. If we apply again

Eq. (2.44), this yields

$$\frac{\partial}{\partial z} \underbrace{\iint_{\perp} (\mathbf{E}_1 \times \mathbf{H}_2 - \mathbf{E}_2 \times \mathbf{H}_1) \cdot \mathbf{e}_z \, \mathrm{d}S}_{\stackrel{def}{=} \mathscr{U}(\mathbf{F}_1, \mathbf{F}_2)} = 0, \tag{2.51}$$

and if we again insert two modal solutions of a waveguide problem

$$(\beta_m + \beta_n) \iint_{\perp} \left(\mathbf{E}_{\beta_m} \times \mathbf{H}_{\beta_n} - \mathbf{E}_{\beta_n} \times \mathbf{H}_{\beta_m} \right) \cdot \mathbf{e}_z \, \mathrm{d}S = 0, \tag{2.52}$$

which is called the *unconjugated* formulation of LORENTZ reciprocity [172, 185] using the inner product $\mathscr{U}(\mathbf{F}_{\beta_m}, \mathbf{F}_{\beta_n})$.

This relation seems entirely useless at the first glance. It implies that modes are orthogonal on themselves and all other modes propagating in the same direction. This spoils all intuitive properties of the conjugated modal framework listed above.

However, an interesting case is obviously given, when $\beta_n = -\beta_m$. Let us denote by $\hat{H}_\omega$ the HELMHOLTZ operator in Eq. (2.28) which is parameterized by a real ω. Let us further assume we have found a particular solution to the eigenvalue problem

$$\hat{H}_\omega \mathbf{F}_\beta = \beta^2 \cdot \mathbf{F}_\beta, \tag{2.53}$$

with a non-degenerate eigenvalue β^2. We have thus automatically found *two* solutions for our modal ansatz in the propagation directions $\pm z$, which belong to the *same non-degenerate* eigenvalue! Physically, we of course interpret them as forward or backward propagating modes. Since they belong to the same eigenvalue, do their electromagnetic fields have to be exactly equal? The answer is no. For a scalar eigenvalue problem like SCHRÖDINGER's equation in quantum mechanics any multiplication of the eigenfunction with a complex constant yields the same eigenvalue and belongs to the *same* vector in HILBERT space. This is also true here, but the possibilities for symmetry operations on the vectorial electromagnetic field are richer than in the scalar case and link for- and backward propagating fields. Mathematically, one can define the »adjoint« to the problem in Eq. (2.53) in dual space [7], which formally reads as

$$\hat{H}^\dagger_\omega \mathbf{F}^\dagger_\beta = \left(\beta^\dagger\right)^2 \cdot \mathbf{F}^\dagger_\beta. \tag{2.54}$$

The adjoint operator is defined as the operator fulfilling the relation [191]

$$\mathscr{U}\left(\hat{H}_\omega \mathbf{F}_\beta, \mathbf{F}_\beta^\dagger\right) = \mathscr{U}\left(\mathbf{F}_\beta, \hat{H}_\omega^\dagger \mathbf{F}_\beta^\dagger\right). \tag{2.55}$$

As stated before, $\hat{H}_\omega \neq \hat{H}_\omega^\dagger$ is not self-adjoint when $\varepsilon''(\omega) \neq 0$. The physical interpretation is that the adjoint modes are given by the backward modes of the system, *i. e.* $\beta^\dagger = -\beta$. By linking them together, forward exponential decay is compensated by backward exponential decay, which means forward exponential increase. We can than proceed to derive an orthogonality relation from Eq. (2.52) as

$$\underbrace{\iint_\perp \left(\mathbf{E}_{\beta_m} \times \mathbf{H}_{\beta_n}^\dagger - \mathbf{E}_{\beta_n}^\dagger \times \mathbf{H}_{\beta_m}\right) \cdot \mathbf{e}_z \,\mathrm{d}S}_{\stackrel{def}{=} \mathscr{A}\left(\mathbf{F}_{\beta_m}, \mathbf{F}_{\beta_n}\right)} = 4F_m \cdot \delta_{mn}, \tag{2.56}$$

This is the *adjoint* formulation [32, 192]. While S_m is the POYNTING flux of mode m, F_m is its generalization, the »adjoint flux« [192–194], which is not related to energy considerations. While energy is not preserved throughout propagation, adjoint flux is.

Eq. (2.56) is called a *biorthogonality* relation in functional analysis. The completeness of the mode set $\{\mathbf{F}_m, \mathbf{F}_m^\dagger\}$ can mathematically be shown [7, 195–198], so that we can rescue many of the appealing consequences of the conjugated lossless formalism. The main difference is that the subspace of modes propagating in only one direction is incomplete without considering their adjoints, *i. e.* modes in the opposite direction. In many cases, these modes do not need to be calculated separately, but can be found by symmetry relations. Note that only transverse field components enter the inner products. For z-invariant structures and BLOCH modes with a unit cell which is mirror symmetric in z, they are found by the transformation properties of the electromagnetic field as a vector or pseudovector, respectively [174]. This yields

$$\{\mathbf{E}_\perp^\dagger(x,y,z,\omega), \mathbf{H}_\perp^\dagger(x,y,z,\omega)\} = \{-\mathbf{E}_\perp(x,y,-z,\omega), \mathbf{H}_\perp(x,y,-z,\omega)\} \tag{2.57}$$

or

$$\begin{aligned}\{\mathbf{E}_\perp^\dagger(x,y,z,\omega), \mathbf{H}_\perp^\dagger(x,y,z,\omega)\} &= \{\mathbf{E}_\perp^*(x,y,z,-\omega), -\mathbf{H}_\perp^*(x,y,z,-\omega)\} \\ &= \{\mathbf{E}_\perp(x,y,z,\omega), -\mathbf{H}_\perp(x,y,z,\omega)\}.\end{aligned} \tag{2.58}$$

The latter possibility is motivated by the fact that the electromagnetic fields in frequency domain are the FOURIER transform of real physical fields in the spatio-temporal domain

and must thus obey

$$\mathbf{F}(-\omega) = \mathbf{F}^*(\omega). \tag{2.59}$$

Some authors prefer the first convention [192], while others use the second [32, 172, 185, 193, 194]. They are equivalent and correspond to the two physical possibilities of mode reversal by mirroring or phase-conjugation. In the case of a lossless system, all three formulations of reciprocity become equivalent

$$\mathscr{A}\left(\mathbf{F}_{\beta_m}, \mathbf{F}^*_{\beta_n}\right) = \mathscr{U}\left(\mathbf{F}_{\beta_m}, \left(\mathbf{F}^*_{\beta_n}\right)^\dagger\right) = \mathscr{C}\left(\mathbf{F}_{\beta_m}, \mathbf{F}_{\beta_n}\right). \tag{2.60}$$

In the following parts of the thesis, we will increase readability by introducing DIRAC's notation of the inner product. In order to keep the reader constantly reminded that adjoint modes have to be used and prevent unclarities, we use the conjugate formulation (where a mode has to be specifically »marked« as being adjoint). However, instead of the formal † symbol, we use + and − for for- and backward propagating modes to reestablish a physical intuition. Let thus be $\left|\psi_l^+\right\rangle = (\mathbf{E}^+_{\perp,\beta_l}, \mathbf{H}^+_{\perp,\beta_l})$ a ket vector in HILBERT space with the concatenated transverse field components of the forward mode $\mathbf{F}^+_{\beta_l}$, $\langle\psi_l^-|$ its associated bra and $\left\langle\psi_m^- \middle| \psi_n^+\right\rangle = \mathscr{U}(\mathbf{F}^-_{\beta_m}, \mathbf{F}^+_{\beta_n})$ the inner product in this space. Then, the biorthogonality relation reads as

$$\left\langle\psi_m^\pm \middle| \psi_n^\pm\right\rangle = 0, \qquad \left\langle\psi_m^\pm \middle| \psi_n^\mp\right\rangle = \mp A_m \cdot \delta_{mn}. \tag{2.61}$$

Decomposition of a general field solution $|F\rangle$ reads as

$$|F\rangle = \sum\!\!\!\!\!\!\int_l a_l \cdot \left|\psi_l^+\right\rangle + \sum\!\!\!\!\!\!\int_l b_l \cdot \left|\psi_l^-\right\rangle, \tag{2.62}$$

where the expansion coefficients are given by the projections

$$a_l = \left\langle\psi_l^- \middle| F\right\rangle, \qquad b_l = -\left\langle\psi_l^+ \middle| F\right\rangle, \tag{2.63}$$

if the modes are normalized according to $A_m = 1$. Equipped with this framework, we are ready to apply the adjoint modal formalism to nanooptical problems.

2.2. Numerical Computations: Aperiodic Fourier Modal Method

There are few cases, where the basis functions and the decomposition can be calculated analytically. Examples are MIE-theory [121] and to some extent the multipole expansion technique [148, 199, 200]. For the vast number of problems, modes and inner products have to be calculated numerically. Common strategies for this purpose are finite-elements or finite-difference mode solvers and especially for periodic media the use of a FOURIER series expansion techniques. We will use the latter. An advantage of this approach is that the plane wave basis used for a FOURIER expansion is guaranteed to be a complete, orthonormal set. One can think of the method as using an auxiliary basis to express the original eigenfunctions.

If we denote by $|\varphi_m\rangle$ a vector containing the transverse electromagnetic field components of plane-wave basis function $\mathbf{F}_{\mathbf{k}_m} \cdot \exp(ik_{x,m}x + ik_{y,m}y)$ and by $|\varphi_m\rangle\langle\varphi_m|$ the projection operator onto itself, we find from Eq. (2.62)

$$\sum_m \langle\varphi_m|F\rangle \cdot |\varphi_m\rangle = \sum_m \sum_l a_l \cdot \left\langle \varphi_m \middle| \psi_l^+ \right\rangle \cdot |\varphi_m\rangle + \sum_m \sum_l b_l \cdot \left\langle \varphi_m \middle| \psi_l^- \right\rangle \cdot |\varphi_m\rangle \quad (2.64)$$

The LHS is of course just the FOURIER representation of $|F\rangle$ in a more formal framework. A FOURIER mode solver now has the purpose to calculate the $\left\langle \varphi_m \middle| \psi_l^\pm \right\rangle$.

This *Fourier Modal Method* has its origins in the rigorous calculation of diffraction from layered gratings [173, 201–204]. It generally treats the problem shown in Fig. 2.1 by the following strategy: The three-dimensional space is divided into S regions or »slices«, denoted by superscript $(s) = 0 \ldots S$, where $\varepsilon^{(s)}(x, y, \omega)$ is z-invariant in each slice. One finds the $\left\langle \varphi_m \middle| \psi_l^{\pm,(s)} \right\rangle$ within each slice with a FOURIER mode solver algorithm, which is just the FOURIER representation of the HELMHOLTZ problem and reads as

$$\sum_m \langle\varphi_m|\hat{H}_\omega^{(s)}|\psi_l^{(s)}\rangle \cdot |\varphi_m\rangle = \left(\beta_l^{(s)}\right)^2 \cdot \sum_m \langle\varphi_m|\psi_l^{(s)}\rangle \cdot |\varphi_m\rangle \,. \quad (2.65)$$

This is an algebraic eigenvalue equation for the FOURIER coefficients $\langle\varphi_m|\psi_l^{(s)}\rangle$ of the mode l in slice s. The FOURIER representation of the HELMHOLTZ operator $\langle\varphi_m|\hat{H}_\omega^{(s)}$ is a TOEPLITZ matrix with the FOURIER coefficients of each slices' permittivity distribution $\varepsilon^{(s)}(x, y, \omega)$. Efficient implementations to solve algebraic eigenvalue equations are at hand [205].

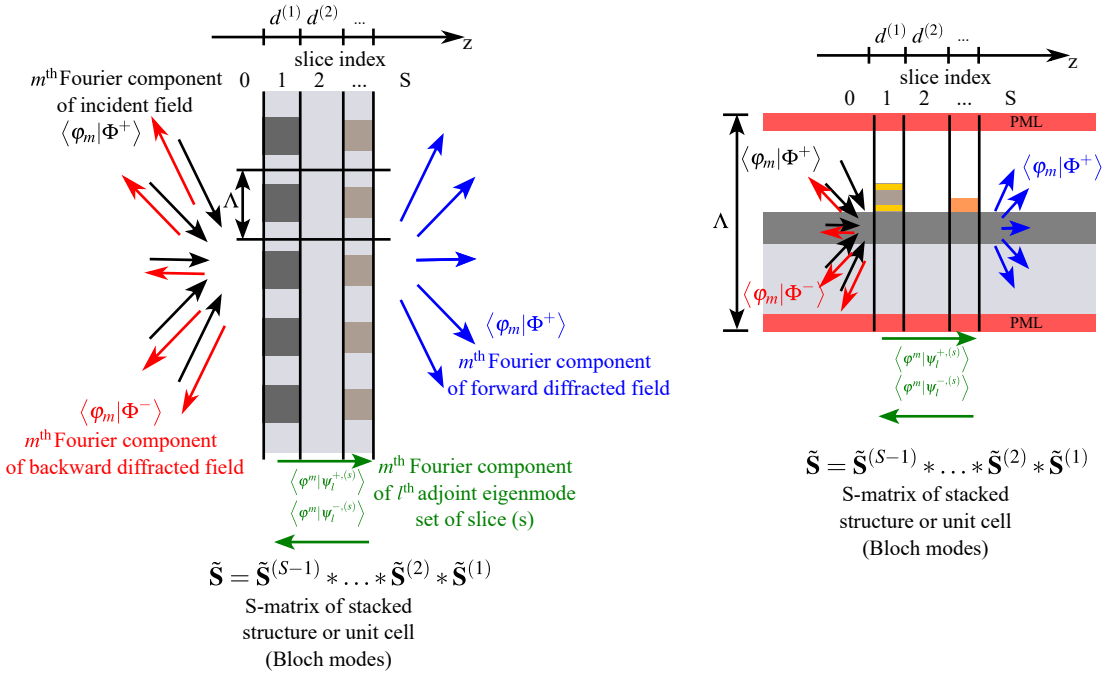

Figure 2.1. (left) Basic scheme of the Fourier Modal Method. All relevant modes are expressed in a transverse FOURIER basis, *i. e.* projected with $\langle\varphi_m|$. The diffraction problem is solved by successively iterating the modal amplitudes in every slice (s) by the $\tilde{\mathbf{S}}$-matrix algorithm. (right) Aperiodic extension of the Fourier Modal Method to treat *e. g.* waveguide problems. The basic scheme is unaltered, however, the transverse period Λ can now be chosen arbitrarily. Perfectly Matched Layers (PMLs) ensure the electromagnetic isolation of the computation cell.

The second step solves the diffraction problem and finds the $\{a_l^{(s)}, b_l^{(s)}\}$ from the $S-1$ interface boundary conditions, *i. e.* the continuity of the tangential field components. At the interface between slice $s-1$ and s, this reads

$$\begin{aligned}\left|F^{(s-1)}\right\rangle = \left|F^{(s)}\right\rangle &\Rightarrow \sum_m \left\langle\varphi_m \middle| F^{(s-1)}\right\rangle \cdot |\varphi_m\rangle = \sum_m \left\langle\varphi_m \middle| F^{(s)}\right\rangle \cdot |\varphi_m\rangle \\ &\Rightarrow \left\langle\varphi_m \middle| F^{(s-1)}\right\rangle = \left\langle\varphi_m \middle| F^{(s)}\right\rangle . \end{aligned} \tag{2.66}$$

This equation expresses just the well-known continuity of the tangential field components in FOURIER space. If we insert the modal decomposition Eq. (2.62), we get

$$\begin{aligned}\sum_l a_l^{(s-1)} \cdot \left\langle\varphi_m \middle| \psi_l^{+,(s-1)}\right\rangle + \sum_l b_l^{(s-1)} \cdot \left\langle\varphi_m \middle| \psi_l^{-,(s-1)}\right\rangle = \\ \sum_l a_l^{(s)} \cdot \left\langle\varphi_m \middle| \psi_l^{+,(s)}\right\rangle + \sum_l b_l^{(s)} \cdot \left\langle\varphi_m \middle| \psi_l^{-,(s)}\right\rangle . \end{aligned} \tag{2.67}$$

We also have to consider the initial conditions, *i. e.* the known incoming wave amplitudes $\{a_l^{(0)}, b_l^{(S)}\}$. The propagation of each mode through the z-invariant slice s with thickness $d^{(s)}$ is analytically known

$$|\psi_l^{+,(s)}(z+d^{(s)})\rangle = e^{i\beta_l d^{(s)}} \cdot |\psi_l^{+,(s)}(z)\rangle\,, \qquad \text{and} \qquad |\psi_l^{-,(s)}(z-d^{(s)})\rangle = e^{-i\beta_l d^{(s)}} \cdot |\psi_l^{+,(s)}(z)\rangle\,. \tag{2.68}$$

One can rewrite these equations in a block matrix form

$$\begin{bmatrix} \mathbf{a}^{(s)} \\ \mathbf{b}^{(s)} \end{bmatrix} = \begin{bmatrix} \tilde{\mathbf{T}}_{11}^{(s)} & \tilde{\mathbf{T}}_{12}^{(s)} \\ \tilde{\mathbf{T}}_{21}^{(s)} & \tilde{\mathbf{T}}_{22}^{(s)} \end{bmatrix} \begin{bmatrix} \mathbf{a}^{(s-1)} \\ \mathbf{b}^{(s-1)} \end{bmatrix}, \tag{2.69}$$

with a modal block transfer matrix $\tilde{\mathbf{T}}^{(s)}$. The whole layered stack is solved iteratively as

$$\begin{bmatrix} \mathbf{a}^{(S)} \\ \mathbf{b}^{(S)} \end{bmatrix} = \tilde{\mathbf{T}}^{(S)} \cdot \tilde{\mathbf{T}}^{(S-1)} \cdot \ldots\ldots \cdot \tilde{\mathbf{T}}^{(2)} \cdot \tilde{\mathbf{T}}^{(1)} \cdot \begin{bmatrix} \mathbf{a}^{(0)} \\ \mathbf{b}^{(0)} \end{bmatrix} = \tilde{\mathbf{T}} \cdot \begin{bmatrix} \mathbf{a}^{(0)} \\ \mathbf{b}^{(0)} \end{bmatrix}. \tag{2.70}$$

With the knowledge of the incoming modal amplitudes $\{\mathbf{a}^{(0)}, \mathbf{b}^{(S)}\}$, the diffraction problem is thus fully solved. The »classical« FMM [173, 201, 203] treats gratings which have homogeneous half-spaces adjacent to the grating structure, so that the $|\psi_l^{+,(s)}\rangle$ are identical to the $|\varphi_m\rangle$ in the first and last stack. The method itself is, however, in no way limited to this case and can successfully be applied to cases where the adjacent media are photonic crystals or metamaterials [32].

The equations above are given in a manner where convergence, uniqueness and exactness of the solution are algebraically ensured by the functional theoretical arguments stated earlier [7], especially the completeness of the mode set under adjoint biorthogonality [195, 196]. This is reflected by the $\sum\!\!\!\!\!\!\int$ signs, which cover the complete HILBERT space for discrete (bound) and continuous (radiating, leaky) modes. To find an approximative solution on a computer, all quantities need to be discretized and truncated. The FMM as a numerical routine requires periodicity in the transverse (x, y) directions with periods Λ_x and Λ_y. The functions can then be represented by a FOURIER *series* expansion instead of a FOURIER *transform*. In this way, the otherwise continuous generic parameter m becomes countable and the transverse wavevector components reduce to $k_{x,m} = m \cdot 2\pi/\Lambda_x$ and $k_{y,m} = m \cdot 2\pi/\Lambda_y$. In the algorithm, m is truncated to a number where a certain level of convergence is reached.

The specific implementation of an FMM algorithm can have a number of numerical pitfalls, which need to be considered. It took several years in the 1990s until the problems were properly analyzed and overcome. Even in recent years, LI discovered some rare geometries, where field singularities prevent the numerical FOURIER series expansion from converging at all [206]. Nevertheless, after several drastic improvements, the FMM has become a stable and reliable work horse in the rigorous computation of periodic media.

The method has two principal ingredients: a FOURIER eigenmode solver plus a recursive solver for the boundary conditions. The first problems occur in the eigenmode solver. The eigenvalue problem needs to be formulated in a way, which is adequate when numerical convergence is considered [203], otherwise it converges slow in TM polarization. The same is true for the FOURIER factorization of $\varepsilon^{(s)}(x, y, \omega)$ [207].

A second problem considers the matching of boundary conditions. Since the $\tilde{\mathbf{T}}$ matrix contains exponentially growing factors which potentially cause overflow, the recursion is not unconditionally stable. This problem was overcome by the use of scattering or $\tilde{\mathbf{S}}$ matrices instead, which are defined by

$$\begin{bmatrix} \mathbf{a}^{(s)} \\ \mathbf{b}^{(s-1)} \end{bmatrix} = \begin{bmatrix} \tilde{\mathbf{S}}_{11}^{(s)} & \tilde{\mathbf{S}}_{12}^{(s)} \\ \tilde{\mathbf{S}}_{21}^{(s)} & \tilde{\mathbf{S}}_{22}^{(s)} \end{bmatrix} \begin{bmatrix} \mathbf{a}^{(s-1)} \\ \mathbf{b}^{(s)} \end{bmatrix}. \tag{2.71}$$

They link »input« fields to »output« fields, contain no exponentially growing factors and their recursion is therefore unconditionally stable. The $\tilde{\mathbf{S}}$ matrices of different layers can, however, not be multiplied in the classical sense to obtain the system $\tilde{\mathbf{S}}$ matrix, but need to undergo the »star product« $\tilde{\mathbf{S}} = \tilde{\mathbf{S}}^{(S)} * \tilde{\mathbf{S}}^{(S-1)} * \cdots \star \tilde{\mathbf{S}}^{(2)} * \tilde{\mathbf{S}}^{(1)}$. The whole algorithm and its relation to the $\tilde{\mathbf{T}}$ matrix, as well as the definition of the star product is given in [208].

The approach can also be used to calculate the band structure and BLOCH modes of systems which possess a periodicity in z-direction with period p. The stack of FMM slices represents the unit cell in that case. The pseudo-periodic BLOCH boundary conditions then yield a generalized eigenproblem for the expansion coefficients of the BLOCH modes in each slice [169, 209, 210]. In a numerically favorable form, it reads

$$\begin{bmatrix} \mathbb{1} & -\tilde{\mathbf{S}}_{12}^{(s)} \\ 0 & \tilde{\mathbf{S}}_{22}^{(s)} \end{bmatrix} \cdot \begin{bmatrix} \mathbf{a}^{(s)} \\ \mathbf{b}^{(s)} \end{bmatrix} = \frac{1}{1 + e^{i\beta_b(\omega)p}} \begin{bmatrix} \mathbb{1} + \tilde{\mathbf{S}}_{11}^{(s)} & -\tilde{\mathbf{S}}_{12}^{(s)} \\ \tilde{\mathbf{S}}_{21}^{(s)} & -\mathbb{1} - \tilde{\mathbf{S}}_{22}^{(s)} \end{bmatrix} \cdot \begin{bmatrix} \mathbf{a}^{(s)} \\ \mathbf{b}^{(s)} \end{bmatrix}, \tag{2.72}$$

and yields the BLOCH wavevectors $\beta_b(\omega)$ as well as the expansion coefficients $\{\mathbf{a}^{(s)}, \mathbf{b}^{(s)}\}$ of

the BLOCH function in every slice. Thus, the full BLOCH mode is known. We will see in the following parts of this thesis, however, that only the BLOCH mode profile at the entrance facet of the unit cell is important for mode coupling, provided that the cut-plane has been chosen in a way that preserves the intrinsic symmetry of the system.

Aperiodic extension of the FMM. The use of FOURIER series appears as a logical step in the numerical analysis of periodic media. LALANNE and co-workers showed, however, that the method can as well be advantageously applied to *aperiodic* systems like waveguides, which lack transverse periodicity [167, 168, 170]. The FOURIER series expansion is performed by introducing a virtual transverse periodicity. Instead of an isolated waveguide, one calculates a periodic array of identical waveguides. Such a calculation would not be correct for the single waveguide case due to the electromagnetic interaction between the computational cells under BLOCH periodic boundary conditions. The second ingredient of the method are thus artificial absorbers, which isolate adjacent cells from each other, so-called *Perfectly Matched Layers* (PMLs) [211, 212]. They have to fulfill two tasks: absorbing outgoing radiation so that it cannot interact with neighboring cells while also not reflecting such radiation back into the original cell, which would disturb the field solution there. It has been shown that the interface between an anisotropic and magnetic artificial medium $(\mu^{(2)}, \hat{\varepsilon}^{(2)})$ and a non-magnetic isotropic medium with permittivity $\varepsilon^{(1)}$ can be reflection-less under all angles of incidents in our coordinate definition, when the following conditions hold [168, 211]

$$\varepsilon^{(1)} = \frac{\varepsilon_{zz}^{(2)}}{\mu^{(2)}}, \qquad \varepsilon_{xx}^{(2)} \cdot \varepsilon_{zz}^{(2)} = \left[\varepsilon^{(1)}\right]^2. \tag{2.73}$$

By introducing a positive imaginary part, the »PML medium« becomes lossy and so fulfills both requirements. The introduction of PMLs can be seen as introducing a coordinate transform region which maps the infinite transverse space onto the finite computational interval [171], and preserves the orthonormal properties of modes. Their numerical representation, especially in the case of leaky and radiating modes, are therefore called *Quasi-Normal Bloch Modes* [172].

With the aperiodic Fourier Modal Method (a-FMM), we have thus found the computational method of choice for using the modal formalism from above. It ensures the correctness of the overlap integrals although the computational domain has only a finite size. The calculated field profiles of bound modes are unaffected by the PMLs as long as

a proper choice of the cell size and PML thickness was made, since their field is localized in close vicinity of the waveguiding structure.

The implementation of the method requires a formulation of the FMM which accounts for anisotropic media. The necessary modifications to the scheme above are minor and just need to allow for a tensorial permittivity $\tilde{\varepsilon}(\omega)$, as well as a non-zero permeability $\mu(\omega)$. Since the principal scheme and arguments outlined above stay unaltered, we do not repeat the explicit anisotropic formulation of the FMM here, but refer to the literature [167, 168, 213].

We have implemented the method outlined above in order to calculate the necessary modal quantities throughout this thesis rigorously, with a particular focus on:

- the dispersion relation $\beta(\omega)$ and field profiles $\mathbf{F}_\beta(\mathbf{r}, \omega)$ of waveguide modes, especially bound ones (Chaps. III, IV & V).
- the band diagram $\beta_b(\omega)$ and BLOCH mode profiles $\mathbf{B}_{\beta_b}(\mathbf{r}, \omega)$ of periodic systems like waveguide gratings (Chap. IV) and waveguides hybridized with periodic arrays of nanoparticles (Chap. V).
- the modal expansion coefficients $\{a_l, b_l\}$, especially the modally resolved scattering parameters reflection and transmission at the interfaces between different structures (Chaps. III & IV).

The classification into *bound* or *leaky/radiative* modes needs more care when loss and metals are present, since $\beta(\omega)$ will always be a mixed complex (neither purely real nor purely imaginary) quantity. Therefore, we additionally evaluate the transverse POYNTING vector of the field solutions close to the PML regions in our code to determine whether a mode radiates energy towards either of the substrate or cladding directions.

III. Generalization of the impedance using the adjoint eigenmode framework

The impedance is of utmost importance for the design of electronic circuits. However, it is not clear how a rigorous generalization for nanooptical structures is possible. In this Chapter, we derive such a generalization based on the adjoint modal framework. From the general expression, we show that modal symmetry properties lead to the classical formulas for genuinely homogeneous materials and waveguides in the radio frequency range, such as a coaxial wire. We will also discuss the role of the »BLOCH impedance« for metamaterials and the possibilities to find the impedance of (plasmonic) waveguides and other sophisticated structures.

3.1. Generalized impedance definition from the adjoint mode framework

One can derive from the MAXWELL curl equation in vacuum

$$\nabla \times \bar{\mathbf{E}}(\mathbf{r}, t) = -\frac{\partial \bar{\mathbf{B}}(\mathbf{r}, t)}{\partial t} \tag{3.1}$$

that, after a FOURIER transform over space and time[1],

$$\mathbf{k} \times \tilde{\mathbf{E}}(\mathbf{k}, \omega) = \omega \cdot \tilde{\mathbf{B}}(\mathbf{k}, \omega). \tag{3.2}$$

We will decorate functions in the spatio-temporal FOURIER domain with a tilde sign on top. Since $\tilde{\mathbf{B}}(\mathbf{k}, \omega) = \mu_0 \cdot \tilde{\mathbf{H}}(\mathbf{k}, \omega)$ and $\mathbf{k} = \mathbf{u} \cdot \omega / c$ for plane waves in vacuum with $\mathbf{u} = \mathbf{k}/k$

[1] The derivative operators behave under FOURIER transform as $\frac{\partial}{\partial t} \to -i\omega$ and $\nabla \to i\mathbf{k}$.

and c being the speed of light in vacuum, we have

$$\mathbf{u} \times \tilde{\mathbf{E}}(\mathbf{k}, \omega) = c\mu_0 \cdot \tilde{\mathbf{H}}(\mathbf{k}, \omega). \tag{3.3}$$

If we use the fact that $c = [\varepsilon_0 \mu_0]^{-1/2}$, we arrive at the result that

$$\mathbf{u} \times \tilde{\mathbf{E}}(\mathbf{k}, \omega) = Z_0 \cdot \tilde{\mathbf{H}}(\mathbf{k}, \omega), \tag{3.4}$$

with $Z_0 = c\mu_0 = [\mu_0/\varepsilon_0]^{1/2} \approx 376.73\,\Omega$, which is typically termed »the« impedance of free space[2]. This important result states the orthogonal nature of every spatio-temporal FOURIER component of the electric and magnetic field. The fact that their ratio is a real-valued constant means that both fields are in phase.

In a genuinely homogeneous and non-magnetic medium, the speed of light is smaller by a factor of $n = (\varepsilon)^{-1/2}$. The quantity n is called the *refractive index* of the medium. It is often regarded as a material constant, although it actually describes the propagation of a wave. One usually defines the »*intrinsic impedance*« of the medium as $Z = Z_0/n$ in this case. We will come back to this point later, when we introduce the adjoint eigenmode analysis.

It is instructive to write Eq. (3.4) component-wise, using the antisymmetric LEVI-CIVITA tensor $\tilde{\epsilon}$ [214]. This yields

$$Z_0 = \frac{1}{\tilde{H}_l(\mathbf{k}, \omega)} \sum_{m,n} \epsilon_{lmn} u_m \tilde{E}_n(\mathbf{k}, \omega) \tag{3.5}$$

and expresses magnitude, phase and *handedness* of the relation between the electric and magnetic field components of a plane wave going into an arbitrary unit direction $\mathbf{u}$. If we consider for instance a plane wave going in z direction, we have

$$\mathbf{u} = [0, 0, 1] \quad \Longrightarrow \quad Z_0 = +\frac{\tilde{E}_x(\mathbf{k}, \omega)}{\tilde{H}_y(\mathbf{k}, \omega)} = -\frac{\tilde{E}_y(\mathbf{k}, \omega)}{\tilde{H}_x(\mathbf{k}, \omega)}. \tag{3.6}$$

The signs express the right-handedness of the wave in vacuum or ordinary matter, a property which can be altered in certain left-handed photonic »meta«materials [20, 215].

[2] Since μ_0 and c have definite and fixed values in the SI system of units, so has Z_0.

However, it is also possible to think just of the magnitudes of the fields for which we find

$$\sum_l \tilde{H}_l(\mathbf{k},\omega)\cdot\tilde{H}_l^*(\mathbf{k},\omega) = \left|\tilde{\mathbf{H}}(\mathbf{k},\omega)\right|^2 = \frac{1}{Z_0^2}\sum_{l,m,n,p,q} \underbrace{\epsilon_{lmn}\epsilon_{lpq}}_{\delta_{mp}\delta_{nq}-\delta_{mq}\delta_{np}} u_m u_p \tilde{E}_n(\mathbf{k},\omega)\cdot\tilde{E}_q^*(\mathbf{k},\omega)$$
$$= \frac{1}{Z_0^2}\left[\sum_m u_m^2 \cdot \sum_n \tilde{E}_n(\mathbf{k},\omega)\cdot\tilde{E}_n^*(\mathbf{k},\omega) - \sum_m u_m\tilde{E}_m(\mathbf{k},\omega)\cdot\sum_n u_n\tilde{E}_n^*(\mathbf{k},\omega)\right]. \quad (3.7)$$

Since the last term vanishes due to MAXWELL's divergence theorem[3] and $\sum_m u_m^2 = 1$ due to normalization, we find

$$Z_0 = \frac{\left|\tilde{\mathbf{E}}(\mathbf{k},\omega)\right|}{\left|\tilde{\mathbf{H}}(\mathbf{k},\omega)\right|}. \quad (3.8)$$

It is important to remember that the interchangeable possibilities to define Z_0 resulted from the very specific properties of the eigenmodes of free-space, namely *homogenity, transversality* and *right-handedness*. Another important fact is that the system is *loss-free*. It is neither trivial nor guaranteed that the simple interpretation of the impedance will still hold when we give up any of those properties.

Phenomenological introduction of the impedance using the adjoint modal framework. We want to find a more general impedance definition for nanooptical structures now. The starting point of our derivation should be the expectation, what an impedance should actually *describe*. We have already seen that the usual field-ratio-based understanding just makes sense for plane waves or other waves with specific symmetry and makes it unpractical for *e. g.* a waveguide.

An experimentally and practically relevant impedance definition must correctly describe the *behavior* of a structure in the same way it does for electronics. We must thus not only consider intrinsic, but also *extrinsic* parameters of a photonic structure, namely how it couples to its surrounding.

It has been pointed out by HECHT and co-workers [51, 85] that such a definition would correctly reproduce the reflection that occurs at the interface between *two different* struc-

[3] Maxwell's equation $\nabla\cdot\bar{\mathbf{D}}(\mathbf{r},t) = 0$ in (source-) free space implies $\sum_m u_m\tilde{E}_m(\mathbf{k},\omega) = 0$ for any medium which is homogeneous and isotropic.

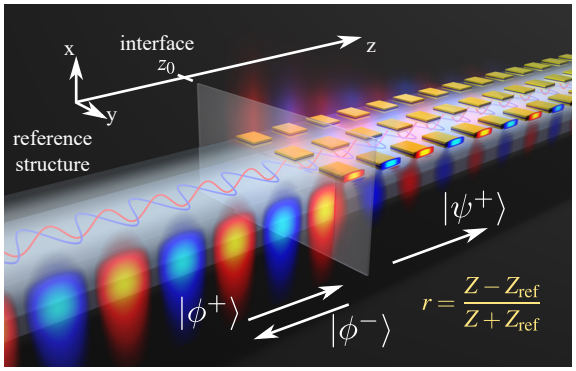

Figure 3.1. Basic scheme of this Chapter. A forward mode of a reference structure $|\phi^+\rangle$ is impinging at an interface to a structure under consideration with a forward mode $|\psi^+\rangle$ at $z = z_0$. The sketch shows the structures analyzed in Chapter V (reference = dielectric slab waveguide, analyzed structure = metasurface covered waveguide). However, this basic scheme is independent of the specific structures for the considerations of this Chapter. The discontinuity leads to a coupling into the backward mode $|\phi^-\rangle$, characterized by the modal reflection coefficient r. On this coefficient, we wish to build a rigorous impedance definition.

tures with the well-known formula

$$r = \frac{Z - Z_{\mathrm{ref}}}{Z + Z_{\mathrm{ref}}} \tag{3.9}$$

for the complex reflection coefficient r. Here and in what follows, we will understand Z as the impedance of the structure we want to analyze and Z_{ref} as the impedance of a reference system, from which we wish to couple light to the structure under consideration. This can for instance be free-space, if we illuminate our structure with a plane wave, a waveguide from which we couple light to our structure, a nanoantenna we use for light localization, or also any other photonic structure which is used for excitation. A basic sketch of the problem we want to analyze is shown in Fig. 3.1.

In order to find a reasonable definition, we will now invert the problem and ask, which impedance definition would fulfill Eq. (3.9)? Obviously, we have to consider impedances for which the relation

$$Z = Z_{\mathrm{ref}} \cdot \frac{1 + r}{1 - r} \tag{3.10a}$$

holds. We encounter a point here which is as trivial as important, namely that the reflection from an interface of impedance discontinuity does solely depend on the *ratio* of the impedances but not their absolute values. This gives us a certain freedom – and also requires us – to choose a proper reference frame which we compare any impedance value against. In literature, even though the reference frame is rarely explicitly mentioned, it is usually the impedance of a plane wave in free-space Z_0, as it was introduced above.

We will consequently concentrate our efforts on finding the *relative* impedance of the

two structures under consideration

$$\frac{Z}{Z_{\mathrm{ref}}} = \frac{1+r}{1-r}. \tag{3.10b}$$

The problem is now conceptually shifted to finding a rigorous expression for the complex reflection coefficient at the interface between two (arbitrary) structures. This very general task requires very general means and we will show that the adjoint modal framework will provide the necessary answers.

We must first understand, what we mean by a »reflection coefficient«. Intuitively, one may think of the total energy that is scattered from the interface into the backward direction. However, since r is complex, we rather want to describe the *strength* and *phase* of the *field* that is moving in backward direction. This field is composed of modal components that are the generic eigenmodes of the reference structure. Every backward eigenmode has its own strength and phase encoded in a complex expansion coefficient b_l in Eq. (2.25). Thus, we need to relate r to the multitude of backward expansion coefficients b_l.

We introduce the adjoint modal framework from Chap. II to describe the MAXWELL boundary conditions at the interface between the two structures. Unfortunately, we need some space for numeration of the modes and the declaration as forward or backward. By the Greek letter ϕ, we will now understand modes of the *reference* structure whereas ψ refers to the structure under consideration. The continuity of the tangential field components thus reads

$$|\Phi^+\rangle + |\Phi^-\rangle = |\Psi^+\rangle\,. \tag{3.11}$$

The total field in the reference structure $|\Phi\rangle = |\Phi^+\rangle + |\Phi^-\rangle$ is composed of the forward propagating incident field $|\Phi^+\rangle$ and the backward propagating reflected field $|\Phi^-\rangle$, whereas the transmitted field in the structure of interest $|\Psi^+\rangle$ is purely forward propagating[4].

We will now perform the modal decomposition of all fields. We denote the forward propagating eigenmodes of the reference structure as $\left|\phi_n^+\right\rangle$ and write

$$|\Phi^+\rangle = \sum_n c_n \left|\phi_n^+\right\rangle \tag{3.12}$$

with complex expansion coefficients c_n. If we follow the same strategy for modal expan-

[4]We do not want to consider the case where fields are coherently incident from *both* sides here.

sion for all other fields, we can rewrite Eq. (3.11) as

$$\sum_n c_n \left|\phi_n^+\right\rangle + \sum_n r_n \left|\phi_n^-\right\rangle = \sum_n t_n \left|\psi_n^+\right\rangle. \tag{3.13}$$

The modal expansion coefficients now must be interpreted in a way that r_n denotes the complex excitation coefficient for reflection into the n^{th} backward mode of the reference structure and t_n describes the transmission into the n^{th} forward mode of the structure under consideration.

The next step in order to solve Eq. (3.13) for the reflection coefficients is to make use of the biorthogonality relations Eqs. (2.61). By applying a projecting of the equation onto modes $\left\langle\psi_m^+\right|$ we arrive at

$$\sum_n c_n \left\langle\psi_m^+ \middle| \phi_n^+\right\rangle + \sum_n r_n \left\langle\psi_m^+ \middle| \phi_n^-\right\rangle = \sum_n t_n \left\langle\psi_m^+ \middle| \psi_n^+\right\rangle. \tag{3.14}$$

The RHS of the equation vanishes due to the biorthogonality relations (2.61). Introducing an algebraic notation yields

$$\begin{bmatrix} \left\langle\psi_1^+ \middle| \phi_1^-\right\rangle & \left\langle\psi_1^+ \middle| \phi_2^-\right\rangle & \cdots \\ \left\langle\psi_2^+ \middle| \phi_1^-\right\rangle & \left\langle\psi_2^+ \middle| \phi_2^-\right\rangle & \cdots \\ \vdots & \vdots & \ddots \end{bmatrix} \begin{bmatrix} r_1 \\ r_2 \\ \vdots \end{bmatrix} = - \begin{bmatrix} \left\langle\psi_1^+ \middle| \phi_1^+\right\rangle & \left\langle\psi_1^+ \middle| \phi_2^+\right\rangle & \cdots \\ \left\langle\psi_2^+ \middle| \phi_1^+\right\rangle & \left\langle\psi_2^+ \middle| \phi_2^+\right\rangle & \cdots \\ \vdots & \vdots & \ddots \end{bmatrix} \begin{bmatrix} c_1 \\ c_2 \\ \vdots \end{bmatrix} \tag{3.15a}$$

or in a short matrix notation

$$\tilde{\mathbf{P}} \cdot \mathbf{r} = -\tilde{\mathbf{Q}} \cdot \mathbf{c}, \tag{3.15b}$$

with

$$\begin{aligned} P_{mn} &= \left\langle\psi_m^+ \middle| \phi_n^-\right\rangle, \quad r_m = [r_1, r_2, \ldots]^T, \\ Q_{mn} &= \left\langle\psi_m^+ \middle| \phi_n^+\right\rangle, \quad c_m = [c_1, c_2, \ldots]^T. \end{aligned} \tag{3.15c}$$

By multiplying from the left with the inverse[5] of $\tilde{\mathbf{P}}$ we get a preliminary result

$$\mathbf{r} = -\tilde{\mathbf{P}}^{-1} \cdot \tilde{\mathbf{Q}} \cdot \mathbf{c} \tag{3.16a}$$

[5] The existence of the inverse is ensured by the biorthogonality relations (non-zero overlap integrals of for- and backward modes). Even if both structures were identical, $\mathbf{P}$ would be diagonal, *i. e.* of full rank.

or in components

$$r_m = -\sum_{l,n} P^{-1}_{ml} Q_{ln} c_n. \tag{3.16b}$$

To check for consistency, we imagine both structures to be identical. The biorthogonality relations (2.61) imply that $\tilde{\mathbf{Q}}$ is a null matrix in this case whereas $\tilde{\mathbf{P}} = \mathbb{1}$ becomes the unit matrix. Consequently, $\mathbf{r}$ vanishes for every modal excitation spectrum $\mathbf{c}$. As expected, no reflection occurs at the interface in that case, regardless of the specific illumination.

It is interesting to examine Eq. (3.16) a little closer with respect to our initial question. The formula for the modal reflection coefficients consists of two parts. The first part is the product $-\tilde{\mathbf{P}}^{-1}\tilde{\mathbf{Q}}$, which consists only of mutual overlap integrals between the eigenmodes of the two structures and describes how the *coupling* between the different modes happens. It is a property which is inherent to the interface and just depends on the structures themselves. The second part is the modal spectrum of the illumination, which is simply multiplied algebraically and »selects« a specific physical situation out of the general term. If we wanted to build our impedance generalization on r_m, we would arrive at a situation where the impedance becomes dependent on the illumination, which is of course highly unwanted.

Instead, we can overcome this drawback by just making use of the first part. We define an intermodal reflection matrix

$$\tilde{\mathbf{r}} = -\tilde{\mathbf{P}} \cdot \tilde{\mathbf{Q}}, \tag{3.17a}$$

or in components

$$r_{mn} = -\sum_{l} P^{-1}_{ml} Q_{ln}, \tag{3.17b}$$

which describes now the reflection into the m^{th} backward mode due to illumination by the n^{th} forward mode and depends solely on the modal spectra of the two structures.

We are now in a position to link the intermodal reflectance to the impedance. Using Eq. (3.10b), we introduce the relative intermodal impedance

$$Z_{mn} = \frac{1 - \sum_l P^{-1}_{ml} Q_{ln}}{1 + \sum_l P^{-1}_{ml} Q_{ln}}. \tag{3.18}$$

This is a first important result of this Chapter. It is possible to use the rigorous result for intermodal reflection for defining an intermodal impedance.

Equation (3.18) has to be discussed thoroughly. It defines a relative impedance value for two eigenmodes. The quantity Z_{mn} describes the coupling between a forward mode $\left|\psi_m^+\right\rangle$ in the structure of interest and the biorthogonal pair of modes $\left|\phi_n^\pm\right\rangle$ in the reference structure. In order to do so, however, Z_{mn} needs not only information from those three modes but also from *all* backward modes of the reference structure and *all* forward modes of the structure of interest. This is expressed by the summation over the running index l. The total modal reflection coefficient, which takes into account also the excitation, reads as

$$r_m = \sum_n c_n \cdot \frac{Z_{mn} - 1}{Z_{mn} + 1}. \tag{3.19}$$

We arrive at an important conclusion: It is not possible to define a rigorous relative impedance between any two modes independently of all other modes!

This statement seems highly contradictory to the beginning of the Chapter, where we have introduced the free-space impedance in a way we deem to be impossible now. However, this confusion can be resolved by introducing a special case of utmost importance, which is shown later to be either exactly valid (for homogeneous media, RF regime) or at least a reasonable approximation (for photonic crystals, metamaterials, plasmonic waveguides). This leads to rigorous results in a practically relevant fashion.

Fundamental Mode Approximation. If only *one* mode of each kind (for- and backward) would be involved in the interaction, the simplification would be enormous[6]. What seems to be an extremely crude approximation at first glance is in fact often realized in practical situations or at least a practical goal, as we will see later.

The essence of the Fundamental Mode Approximation (FMA) can be summarized in the following assumptions:

[6] »Fundamental Blochmode« does not necessarily mean the mode with the lowest loss but rather the »largest overlap« with the excitation. It should be seen more as a requirement on the field of the mode and its symmetries rather than on the loss of the mode. Strictly speaking, the term »fundamental« has nothing to do with n_{eff} in this context although one will in practical situations prefer a mode with low loss.

- The excitation happens via a single mode, *i. e.*

$$|c_n| = \begin{cases} 1 & \text{for } n = 1 \\ 0 & \text{for } n \geq 1 \end{cases} \tag{3.20}$$

- The overlap integrals $\left\langle \psi_n^+ \middle| \phi_1^\pm \right\rangle$ vanish approximately, except for the case $n = 1$. This ensures that only one reflection and transmission coefficient is non-zero and means that the reference structure excites only one forward mode in the structure of interest and one backward mode in the reference structure.

The validity of the FMA has been shown to be a necessary prerequisite when it comes to the delicate task of assigning effective parameters to metamaterials [32–34]. Only in this case, one can treat the effective index n_{eff} of the fundamental BLOCH mode as »the« index of refraction of the medium. It is thus not surprising that the same mathematical necessity appears again when it comes to impedances.

The quantity $\tilde{\mathbf{P}}^{-1}$ becomes diagonal in this case, and we find for the fundamental mode reflection coefficient

$$r_{11} = -P_{11}^{-1} Q_{11} = -\frac{\left\langle \psi_1^+ \middle| \phi_1^+ \right\rangle}{\left\langle \psi_1^+ \middle| \phi_1^- \right\rangle}. \tag{3.21}$$

This result can be readily inserted into Eq. (3.18), which yields

$$Z_{11} \overset{def}{=} \hat{Z} = \frac{1 - \frac{\left\langle \psi_1^+ \middle| \phi_1^+ \right\rangle}{\left\langle \psi_1^+ \middle| \phi_1^- \right\rangle}}{1 + \frac{\left\langle \psi_1^+ \middle| \phi_1^+ \right\rangle}{\left\langle \psi_1^+ \middle| \phi_1^- \right\rangle}} = \frac{\left\langle \psi_1^+ \middle| \phi_1^- \right\rangle - \left\langle \psi_1^+ \middle| \phi_1^+ \right\rangle}{\left\langle \psi_1^+ \middle| \phi_1^- \right\rangle + \left\langle \psi_1^+ \middle| \phi_1^+ \right\rangle}. \tag{3.22}$$

We will now omit the subscripts for the fundamental mode and rewrite the expression in terms of the electromagnetic fields, using the definition of the inner product based on adjoint reciprocity Eq. (2.56). A new subscript »ref« is introduced to mark fields which belong to the reference structure (*i. e.* $\left|\phi_1^\pm\right\rangle$), whereas we leave the fields belonging to the structure of interest ($\left|\psi_1^+\right\rangle$) without subscript. We arrive at the final formula for the adjoint impedance ratio

$$\frac{Z}{Z_{\text{ref}}} = \frac{\iint \left[\mathbf{E}_{\text{ref}}^-(\mathbf{r},\omega) - \mathbf{E}_{\text{ref}}^+(\mathbf{r},\omega)\right] \times \mathbf{H}^+(\mathbf{r},\omega) - \mathbf{E}^+(\mathbf{r},\omega) \times \left[\mathbf{H}_{\text{ref}}^-(\mathbf{r},\omega) - \mathbf{H}_{\text{ref}}^+(\mathbf{r},\omega)\right] \cdot \mathbf{e}_z \, \mathrm{d}S}{\iint \left[\mathbf{E}_{\text{ref}}^-(\mathbf{r},\omega) + \mathbf{E}_{\text{ref}}^+(\mathbf{r},\omega)\right] \times \mathbf{H}^+(\mathbf{r},\omega) - \mathbf{E}^+(\mathbf{r},\omega) \times \left[\mathbf{H}_{\text{ref}}^-(\mathbf{r},\omega) + \mathbf{H}_{\text{ref}}^+(\mathbf{r},\omega)\right] \cdot \mathbf{e}_z \, \mathrm{d}S}. \tag{3.23}$$

This equation constitutes another main result of this Chapter. It states that an unambiguous rigorous expression for the impedance ratio can be found based on the eigenmodes of the two coupled structures. Only electromagnetic components which are parallel to the interface contribute to the result. The important requirement for the applicability of the method is that the FMA holds. Otherwise, every mutual interaction of modes must be described by a separate impedance, which involves the whole modal spectrum.

It is interesting to investigate Eq. (3.23) with respect to the question whether an *absolute* impedance value can be assigned to a certain structure. Since the formula represents an impedance *ratio* of two structures, it is obvious that this is the case when the RHS of Eq. (3.23) can be written as a ratio of expressions where the nominator involves only $\mathbf{E}^{+}(\mathbf{r},\omega)$ and $\mathbf{H}^{+}(\mathbf{r},\omega)$, whereas the denominator involves just $\mathbf{E}^{\pm}_{\mathrm{ref}}(\mathbf{r},\omega)$ and $\mathbf{H}^{\pm}_{\mathrm{ref}}(\mathbf{r},\omega)$. We will investigate this further in the upcoming section 3.2.

3.2. Application of the adjoint impedance model to different structures

We have derived a generalized impedance ratio definition in the last section that is based on a modal treatment. The result given by Eq. (3.23) showed some unusual consequences that seem to be in contradiction to the common belief and usage of the impedance concept. In this section, we will prove that the derived formula does *not* contradict previous results. We will successively increase the level of complexity and see how the general formula can be specialized. This will give instructive insights how one and the same concept can undergo a generalization and under which circumstances it can be used further with confidence. In this section, we will also skip the explicit dependence of the quantities on ω for readability.

Impedance of z-invariant modal solutions. It is instructive to evaluate MAXWELL's curl equations for the important case of a continuous translational symmetry into one direction. This propagation direction is denoted by z . All modal solutions will have the form $\exp(i\beta z)$ times a mode field function which depends only on x and y. This yields

the two relations

$$\mathbf{H}(x,y) = -i \cdot \frac{1}{Z_0 k_0} \cdot \begin{bmatrix} \frac{\partial E_z(x,y)}{\partial y} - i\beta \cdot E_y(x,y) \\ i\beta \cdot E_x(x,y) - \frac{\partial E_z(x,y)}{\partial x} \\ \frac{\partial E_y(x,y)}{\partial x} - \frac{\partial E_x(x,y)}{\partial y} \end{bmatrix}, \tag{3.24a}$$

$$\mathbf{E}(x,y) = i \cdot \frac{Z_0}{k_0 \varepsilon(x,y)} \cdot \begin{bmatrix} \frac{\partial H_z(x,y)}{\partial y} - i\beta \cdot H_y(x,y) \\ i\beta \cdot H_x(x,y) - \frac{\partial H_z(x,y)}{\partial y} \\ \frac{\partial H_y(x,y)}{\partial x} - \frac{\partial H_x(x,y)}{\partial y} \end{bmatrix}, \tag{3.24b}$$

where we made use of the free space impedance definition. We want to focus on the tangential field components only, since the longitudinal component does not enter Eq. (3.23). We immediately see that no constant ratio exists between any transverse electric and magnetic field component in the general case.

If we, however, include the additional requirement of *transversality*, *i. e.* the solutions split into two systems where either E_z or H_z vanishes, we get

$$\frac{E_x(x,y)}{H_y(x,y)} = -\frac{E_y(x,y)}{H_x(x,y)} = \frac{Z_0}{n_{\text{eff}}} \quad \text{(TE)}, \tag{3.25a}$$

$$\frac{E_x(x,y)}{H_y(x,y)} = -\frac{E_y(x,y)}{H_x(x,y)} = \frac{Z_0 \cdot n_{\text{eff}}}{\varepsilon(x,y)} \quad \text{(TM)}. \tag{3.25b}$$

This has interesting implications. For every transverse TE mode, the ratio of the tangential electromagnetic field components is solely determined by the mode's effective index. In TM polarization, this is just the case when the *geometry* expressed by $\varepsilon(x,y)$ is also *homogeneous*. This is a somehow tragic consequence for plasmonics, since SPPs are inherently TM solutions at an *inhomogeneity* of $\varepsilon(x,y)$ as shown on page 23. Otherwise, the »impedance of a SPP« would simply be given by the term $Z_0 \cdot \left[\frac{\varepsilon_1 \cdot \varepsilon_2}{\varepsilon_1 + \varepsilon_2}\right]^{1/2}$. and one could engineer plasmonic circuits in the same way we do it with coaxial wires. However, this is not so and we have to continue our effort.

We now want to combine these modal properties of z-invariant systems with our impedance framework. The systems continuous translational symmetry allows to use the relations Eqs.(2.57) to calculate the adjoint from the forward modes. This yields a simplification of the general formula Eq. (3.23) which reads

$$\frac{Z}{Z_{\text{ref}}} = \frac{\iint \left[\mathbf{E}^+(x,y) \times \mathbf{H}^+_{\text{ref}}(x,y)\right] \cdot \mathbf{e}_z \, \mathrm{d}S}{\iint \left[\mathbf{E}^+_{\text{ref}}(x,y) \times \mathbf{H}^+(x,y)\right] \cdot \mathbf{e}_z \, \mathrm{d}S}. \tag{3.26}$$

If we insert our findings in Eqs. (3.25), this yields

$$\frac{Z}{Z_{\text{ref}}} = \frac{Z_0 \cdot n_{\text{eff}}^{\text{ref}} \cdot \iint E_y(x,y) \cdot E_y^{\text{ref}}(x,y)\,\mathrm{d}S}{Z_0 \cdot n_{\text{eff}} \cdot \iint E_y^{\text{ref}}(x,y) \cdot E_y(x,y)\,\mathrm{d}S} = \frac{n_{\text{eff}}^{\text{ref}}}{n_{\text{eff}}} \qquad \text{(TE)}, \tag{3.27a}$$

$$\frac{Z}{Z_{\text{ref}}} = \frac{Z_0 \cdot n_{\text{eff}} \cdot \iint \frac{1}{\varepsilon(x,y)} \cdot H_y(x,y) \cdot H_y^{\text{ref}}(x,y)\,\mathrm{d}S}{Z_0 \cdot n_{\text{eff}}^{\text{ref}} \cdot \iint \frac{1}{\varepsilon_{\text{ref}}(x,y)} \cdot H_y^{\text{ref}}(x,y) \cdot H_y(x,y)\,\mathrm{d}S} \qquad \text{(TM)}, \tag{3.27b}$$

and when homogeneity of $\varepsilon(x,y)$ is present

$$\frac{Z}{Z_{\text{ref}}} = \frac{n_{\text{eff}} \cdot \varepsilon_{\text{ref}}}{n_{\text{eff}}^{\text{ref}} \cdot \varepsilon} \qquad \text{(TM)}. \tag{3.27c}$$

The equations show a remarkable consequence. In the derivation of the adjoint modal impedance, we started with the requirement that the quantity should reproduce the correct reflection behavior. We now see that the ratios in Eqs. (3.25), which are mere modal properties, do already represent the *absolute* impedance definition in our sense

$$Z_{\text{abs}} = Z_0 \cdot \frac{1}{n_{\text{eff}}} \qquad \text{(TE)}, \qquad\qquad Z_{\text{abs}} = Z_0 \cdot \frac{n_{\text{eff}}}{\varepsilon} \qquad \text{(TM)}. \tag{3.28}$$

The normalization with Z_0 is just a question of common gauging with respect to vacuum plane waves. The key to this successful derivation was that the ratio of the integrals in Eqs. (3.27) is a constant. The integrals themselves do not even have to converge as is the case for plane waves. The relations must be evaluated using L'HÔSPITAL's rule in that case. It is interesting to note the interplay between *modal* quantities like n_{eff} and *material* properties like the permittivity ε in the TM case.

Homogeneous media. If we apply the findings above to homogeneous media, we have to investigate the interface between two half-spaces, each filled with a material ε and ε_{ref}, respectively. The eigenmodes in each half-space are plane waves with the dispersion relation Eq. (2.27). If we introduce the angle of incidence α and the refraction angle γ, we find that n_{eff} is simply given by the projection of $\mathbf{k}$ on the z-axis divided by k_0, *i. e.*

$$n_{\text{eff}}^{\text{ref}} = \varepsilon_{\text{ref}}^{1/2} \cdot \cos\alpha, \qquad\qquad n_{\text{eff}} = \varepsilon^{1/2} \cdot \cos\gamma. \tag{3.29}$$

By inserting into Eqs. (3.28) we find

$$\begin{aligned} Z_{\mathrm{ref}} &= \frac{Z_0}{\varepsilon_{\mathrm{ref}}^{1/2}} \cdot \frac{1}{\cos\alpha} \\ Z &= \frac{Z_0}{\varepsilon^{1/2}} \cdot \frac{1}{\cos\gamma} \end{aligned} \quad \text{(TE)}, \qquad \begin{aligned} Z_{\mathrm{ref}} &= \frac{Z_0}{\varepsilon_{\mathrm{ref}}^{1/2}} \cdot \cos\alpha \\ Z &= \frac{Z_0}{\varepsilon^{1/2}} \cdot \cos\gamma \end{aligned} \quad \text{(TM)}. \tag{3.30}$$

It is interesting to note the interplay between the *refractive index* $n = \varepsilon^{1/2}$ as a material property and the *effective index* n_{eff} as a purely modal quantity. In *both* polarizations, the factors Z_0/n and Z_0/n_{ref}, respectively, become the essential measure which appear as an absolute impedance at first glance. However, the problem is that an additional degree of freedom occurs in the form of the incidence and refraction angle, which must be included in the impedance definition. In the literature, this is consequently called the »tangential impedance« [186]. Only in the case of normal incidence, where this degree of freedom is absent, the tangential impedance is compatible with an absolute impedance definition. It is instructive, also for the discussion in the following sections, to recall that the specific structure of the mode was the reason that we could resolve the entanglement with the reference components in the general definition Eq. (3.23). The given example, although extremely simple, already shows some of the difficulties associated with defining impedances. This is a first illustration that an impedance definition based on eigenmodes is a good way to tackle the problem rigorously. The tangential impedances derived above will obviously reproduce the classical FRESNEL formulas with the help of Eq. (3.9)

$$r = \frac{n_{\mathrm{ref}}\cos\alpha - n\cos\gamma}{n_{\mathrm{ref}}\cos\alpha + n\cos\gamma} \quad \text{(TE)}, \qquad r = \frac{n_{\mathrm{ref}}\cos\gamma - n\cos\alpha}{n_{\mathrm{ref}}\cos\gamma + n\cos\alpha} \quad \text{(TM)}. \tag{3.31}$$

Waveguides in the RF regime. We shall now show the successful application of the framework to »lumped circuit« structures. The example will be a rectangular hollow-core waveguide. It has a rectangular cross-section of width a, height b and is filled by a non-magnetic dielectric material with a permittivity ε or $\varepsilon_{\mathrm{ref}}$ for the reference waveguide, respectively. The walls are assumed to be perfectly electric conducting, which is a very good approximation for all metals in this frequency range. As a consequence one has DIRICHLET boundary conditions for the fields, which need to vanish at the side walls. The electromagnetic eigenmodes consist of separable functions in x and y and split into two sets of solutions. In the first set, the electric field is purely transverse and has no z-component (TE), whereas this is the case for the magnetic field in the second case (TM) [186].

This property is the key for the applicability of the relations derived above. The modal

fields themselves are highly *in*homogeneous and compactly bound in space, however, they are still *transverse* in the sense of Eq. (3.25) and ε is homogeneous inside the waveguide! This makes the very same formulas Eqs. (3.28) perfectly applicable. In this sense, the lumped RF waveguide does not differ from homogeneous space from the point of view of modal symmetry, except that n_{eff} does *not* play the role of a »refractive index« anymore. It is given by [186]

$$n_{\text{eff}} = \left(\varepsilon - \frac{\pi^2}{k_0^2} \cdot \left[\frac{m^2}{a^2} + \frac{n^2}{b^2} \right] \right)^{1/2}, \tag{3.32}$$

where (m, n) are integers denoting the mode number. If we introduce the cut-off frequency of the mode (m, n)

$$\omega_c = c \cdot \left(\frac{\pi^2}{\varepsilon} \cdot \left[\frac{m^2}{a^2} + \frac{n^2}{b^2} \right] \right)^{1/2}, \tag{3.33}$$

we immediately get from Eqs. (3.28) the impedance of the waveguide

$$Z_{\text{wg}} = \frac{Z_0}{\varepsilon^{1/2}} \cdot \left(1 - \frac{\omega_c^2}{\omega^2} \right)^{-1/2} \quad \text{(TE)}, \qquad Z_{\text{wg}} = \frac{Z_0}{\varepsilon^{1/2}} \cdot \left(1 - \frac{\omega_c^2}{\omega^2} \right)^{1/2} \quad \text{(TM)}. \tag{3.34}$$

These relations are well-known to the electrical engineer. It is interesting to note how the prefactor $Z_0/\varepsilon^{1/2}$ again appears for *both* polarization and is interpreted as the absolute impedance of the waveguide core material. This makes lumped elements and homogeneous space perfectly analogous systems, although the mode-dependent factors differ strongly. In the case of homogeneous media, a continuous degree of freedom exists for the modes in form of the tangential $\mathbf{k}$-vector component while discrete mode indices (m, n) determine the eigensolutions in the RF waveguide case. The key property was z-invariance and transversality of the modal solutions as well as homogeneity of $\varepsilon(x, y)$. We will now drop these requirements and see how the impedance definition is influenced.

Photonic Crystals and Metamaterials – the Bloch Impedance. Let us now consider another important symmetry class, namely a periodicity of $\varepsilon(x, y, z)$ in 1, 2 or 3 dimensions. The structures where these properties typically play a major role are photonic crystals and metamaterials, both being man-made structures intended to influence the flow of electromagnetic radiation at will.

While there exist applications for both of them also in the RF domain, we will explicitly

target for optical frequencies in this section since the nearly perfect electric conducting boundaries would bring no additional insight regarding the question of an impedance framework.

From the previous discussion we have already seen that we need a proper reference structure to define an impedance. Since photonic crystals[7] and metamaterials are typically intended to be used in free-space applications, plane waves as eigenmodes of free space constitute the natural modal reference system. However, the eigenmodes of the structure under consideration are BLOCH modes now and we shall see how this influences the discussion.

At first we have to analyze the implications of the symmetry properties. Translational invariance was replaced by translational periodicity in the z-direction. There exists an ambiguity to define the unit cell, however, not all choices have the same symmetry. We want to concentrate on the important class of structures possessing a mirror symmetry in the z-direction, so that

$$\varepsilon(x,y,-z)=\varepsilon(x,y,z), \qquad \text{and} \qquad \varepsilon(x,y,z+p)=\varepsilon(x,y,z). \tag{3.35}$$

In this case we can apply the symmetry relations Eqs. (2.57) for the relation between eigenmodes and adjoint eigenmodes and make use of Eq. (3.26). The BLOCH modes are, however, no z-invariant solutions but have a form $e^{i\beta_b(\omega)z}\cdot\mathbf{B}_{\beta_b}(\mathbf{r},\omega)$ which was introduced in Eq. (2.42). The derivative of the z-dependent BLOCH function will now give an additional contribution to MAXWELL's curl equations and the impedance cannot be characterized by n_{eff} and ε alone as was the case for z-invariant systems.

We analyze the interface between a half-space of an homogeneous material with ε and a metamaterial/photonic crystal with our adjoint modal impedance framework. The plane waves as reference eigenmodes were treated above and their contribution can be pulled out of the integral. What remains are the contributions of the BLOCH functions which are inhomogeneous across the interface at $z=z_0$

$$\frac{Z}{Z_{\text{ref}}}=\frac{\varepsilon_{\text{ref}}^{1/2}}{Z_0}\cdot\frac{\iint E_{b,y}(x,y,z_0)\,\mathrm{d}S}{\iint H_{b,x}(x,y,z_0)\,\mathrm{d}S} \qquad \text{(TE)}, \tag{3.36a}$$

$$\frac{Z}{Z_{\text{ref}}}=\frac{\varepsilon_{\text{ref}}^{1/2}}{Z_0}\cdot\frac{\iint E_{b,x}(x,y,z_0)\,\mathrm{d}S}{\iint H_{b,y}(x,y,z_0)\,\mathrm{d}S} \qquad \text{(TM)}. \tag{3.36b}$$

[7] Photonic Crystal Waveguides belong logically to the next paragraph within this context.

Since the BLOCH functions are periodic with the lattice, the integration can be restricted to the unit cell. If one divides by the area of the unit cell, the integrals gain the meaning of a surface averaging of the fields across the unit cell and we get

$$Z_B = \frac{\left\langle E_{b,y} \right\rangle_{z=z_0}}{\left\langle H_{b,x} \right\rangle_{z=z_0}} \quad \text{(TE)}, \qquad Z_B = \frac{\left\langle E_{b,x} \right\rangle_{z=z_0}}{\left\langle H_{b,y} \right\rangle_{z=z_0}} \quad \text{(TM)}. \tag{3.37}$$

This result was found before without the use of an adjoint impedance framework [29, 32] and was called the »BLOCH impedance«. It was also shown that in case the FMA is valid, the metamaterial or photonic crystal is homogeneizable and n_{eff} and Z_b are the two effective mode parameters that characterize the behavior of the system completely as if it was truly homogeneous.

The critical question for the success is thus if the structure can be designed to fulfill the requirement for validity of the FMA. This is far from being trivial in practice since the calculation of *all* modal overlaps is required for a definite answer. However, newer works suggest a system of metasurfaces with dielectric spacer layers which prevent modal coupling except for the fundamental BLOCH mode and work towards the design of systems, where the FMA is inherently fulfilled [216].

While metamaterials are more likely to reach this limit, photonic crystals usually show larger dimensions for the period which renders an excitation of higher order BLOCH modes more probable. An FMA-based scalar impedance is thus not of great practical use. Consequently, LAWRENCE and co-workers [36–38, 217] worked with the impedance matrix introduced at the beginning of the Chapter and used a subsequent projection of the BLOCH modes onto a plane wave basis. This approach yields an impedance matrix for every incidence angle, which expresses the mutual impedance of the RAYLEIGH expansion components of the respective BLOCH mode. While this does not require the FMA to be valid, the simplicity of the impedance framework is abandoned significantly. Their work shows a high conceptual clarity of the issue of finding impedance definitions and points at the delicate problems associated with it. As a main problem, they identify the fact that the expressions between the different components are entangled and no proper absolute definition is possible in the multimode excitation case. When we review the derivation using the adjoint impedance framework up to this point, we see that this problem is of fundamental character and eventually an expression of adjoint reciprocity between the eigenmodes of the systems. In the next paragraph, it will be shown that this issue can even occur *although* the FMA is valid.

Plasmonic and hybrid plasmo-dielectric waveguides. The last paragraphs have shown how particular system properties such as absence of dissipation, transversality of the solution or periodicity of the eigenfunctions allow to derive certain absolute impedance definitions. Although the traditional derivations for impedance expressions in the cases of homogeneous media and RF waveguides followed totally different approaches, we were able to show that all of them originate from the general adjoint impedance definition we derived in Eq. (3.23). Thus, we believe it represents the natural generalization of the quantity »impedance« in terms of adjoint eigenmodes.

For the structures that are of main interest in this thesis, *i. e.* nanooptical waveguides and antennas, we are left with the full generality of the formula. The highly localized fields that are typical for plasmonics render the use of a plane wave basis useless for practical means so that no spatially constant factor can be pulled out of the integrals. The high operation frequency and use of noble metals with significant loss in that domain prevent the usage of perfect conducting boundaries and the geometry becomes an open one. This situation concentrates all the methodological problems with defining an impedance when it comes to plasmonic waveguides or waveguides involving plasmonic elements. We will consider here the two structures that are investigated in more detail and with respect to other issues in Chapters IV and V.

The first example considers a standard geometry in plasmonics. It is shown in Fig. 3.2(a). The SPP mode of a thin gold film (denoted $|\phi^+\rangle$; its dispersion relation is found by solving Eq. (2.41)) propagates towards the interface of a periodically structured SPP grating. The fundamental BLOCH mode in the grating is denoted with $|\psi^+\rangle$. This structure can function as a BRAGG mirror for the plasmon, provided that certain conditions are met regarding the proper period and filling factor as we will see later. Our main concern here is not the structure itself, but rather the question if it can be successfully described by the adjoint impedance framework.

The problem possesses the same symmetry properties that allow for the simplified generalized impedance formula Eq. (3.26). The reference mode is the illuminating SPP mode of the gold film. In contrast to plane waves, SPPs as a reference mode system do *not* allow for a further analytical simplification in the sense that the contributions of the structure and the reference modes can be strictly separated. They stay entangled in the integral.

Let us analyze this configuration in detail. Since we deal with a TM solution to the HELMHOLTZ equation, the magnetic field has just a $H_y(x,z)$ component. We want to

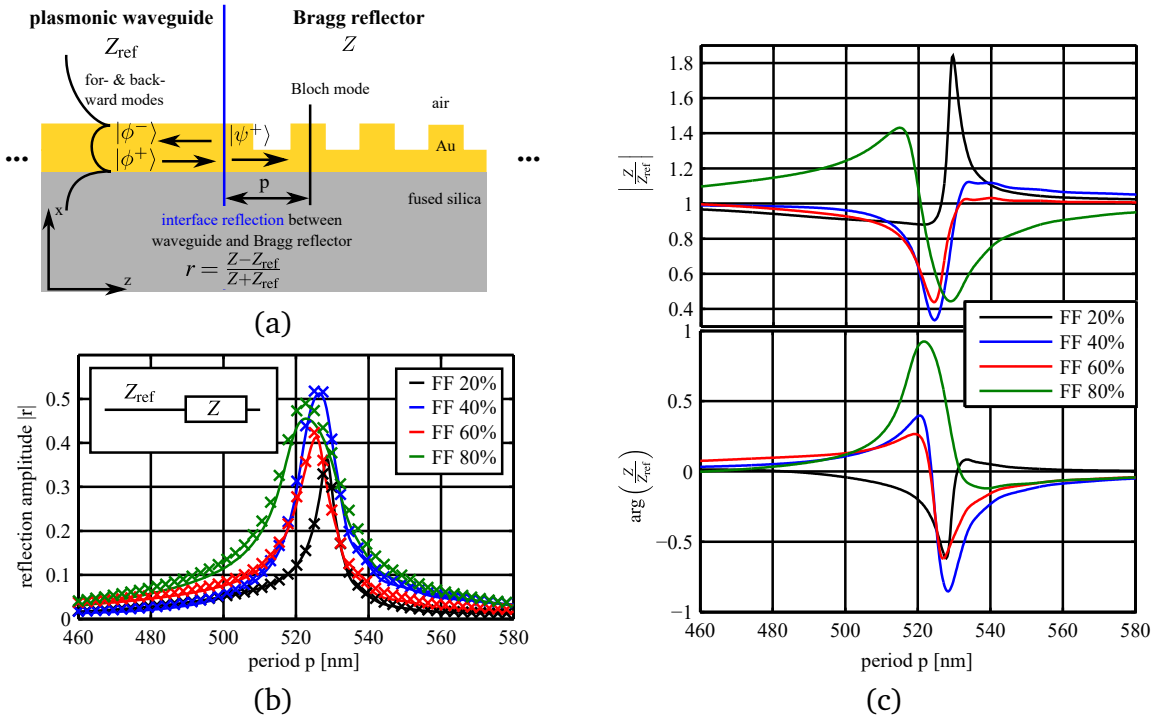

Figure 3.2. (a) Problem geometry: The adjoint modes of a plasmonic waveguide are coupled to the fundamental BLOCH mode of a BRAGG reflector. Note the crucial choice z_0 for the interface and the symmetric choice of the unit cell. FF denotes the filling factor of the grating. (b) Comparison between the rigorous calculation, and the impedance description for an operating wavelength of $\lambda_0 = 1550\,\text{nm}$. (c) Calculated adjoint impedance ratio across the BRAGG resonance position.

identify this component with the functions $\phi(x,z)$ and $\psi(x,z)$ in the two regions by

$$\phi(x) = H_y^{\text{ref}}(x), \qquad \psi(x,z) = H_{b,y}(x,z). \tag{3.38}$$

$\phi(x)$ does not depend on z due to the z-invariance of the reference structure whereas $\psi(x,z)$ does because the mode in the grating is a BLOCH mode. In Appendix A2 we derive the explicit analytical formula for the situation considered here by inserting these functions into Eq. (3.26). This yields

$$\frac{Z}{Z_{\text{ref}}} = \frac{n_{\text{eff}}}{n_{\text{eff}}^{\text{ref}}} \cdot \frac{\left\langle \varepsilon^{-1}(x,z_0)\right\rangle_{\phi\psi}}{\left\langle \varepsilon_{\text{ref}}^{-1}(x)\right\rangle_{\phi\psi}} - \frac{i}{n_{\text{eff}}^{\text{ref}} \cdot k_0} \cdot \frac{\left\langle \varepsilon^{-1}(x,z_0)\right\rangle_{\phi\,\frac{\partial\psi}{\partial z}}}{\left\langle \varepsilon_{\text{ref}}^{-1}(x)\right\rangle_{\phi\psi}}, \tag{3.39}$$

where

$$\left\langle \varepsilon^{-1}(x,z_0)\right\rangle_{fg} = \frac{\int \frac{1}{\varepsilon(x,z_0)} \cdot f(x,z_0) \cdot g(x,z_0)\,\mathrm{d}x}{\int f(x,z_0) \cdot g(x,z_0)\,\mathrm{d}x} \tag{3.40}$$

is an abbreviation for tangential averaging of the impermittivity with the product $f(x,z_0)\cdot g(x,z_0)$ as a (complex valued!) weight function at the interface plane z_0. If we compare with Eqs.(3.28), we see that we find an analogous structure and may define the *absolute* impedance of the SPP waveguide as

$$Z_{\mathrm{ref}} = Z_0 \cdot n_{\mathrm{eff}}^{\mathrm{ref}} \cdot \left\langle \varepsilon_{\mathrm{ref}}^{-1}(x) \right\rangle_{\phi\psi} . \tag{3.41}$$

The absolute impedance of the grating itself,

$$Z = Z_0 \cdot n_{\mathrm{eff}} \left\langle \varepsilon^{-1}(x,z_0) \right\rangle_{\phi\psi} - \frac{i}{k_0} \cdot \left\langle \varepsilon^{-1}(x,z_0) \right\rangle_{\phi \frac{\partial\psi}{\partial z}} , \tag{3.42}$$

however, contains contributions from the reference mode field $\phi(x)$ and is thus not independent of the reference! This reflects the same degree of freedom that the incidence angle brings in for the tangential impedances of the homogeneous media case.

However, although we cannot find the absolute impedance of the SPP grating, we *can* find the impedance of the grating *relative* to the waveguide. What may be the practical use of such an approach? Modern optical systems consist of many functional parts, just like modern microelectronics. One may simply *fix* a specific modal reference system, say the fundamental mode of a single mode optical fiber, a Gaussian laser resonator mode, or the input SPP mode in our case. Then, one may measure the impedance of all functional components relative to this defined reference. In this way, one can use much of the simplicity of the impedance framework for the design of sophisticated nanooptical networks.

The only prerequisite is that the FMA is valid. Fig. 3.2(b) shows a comparison between the rigorous a-FMM calculation with *all* modes and the result using the adjoint impedance framework, which makes use of just the fundamental BLOCH mode. It can be seen that they are in very good agreement inside as well as outside the region of the bandgap, where the BLOCH mode becomes evanescent. Fig. 3.2(c) shows the calculated complex values for the relative adjoint impedance of the SPP grating.

The structure considered in this example is the same that will be used for an enhanced nanoantenna design in Chapter IV. The optimization of the reflection feedback is the key to enhance the performance of the antenna and we have just proven that this design process can be fully handled by the adjoint impedance framework.

Let us repeat this analysis with a structure which will be treated in depth in Chapter V. A dielectric slab waveguide is coupled to a BLOCH periodic structure that supports the

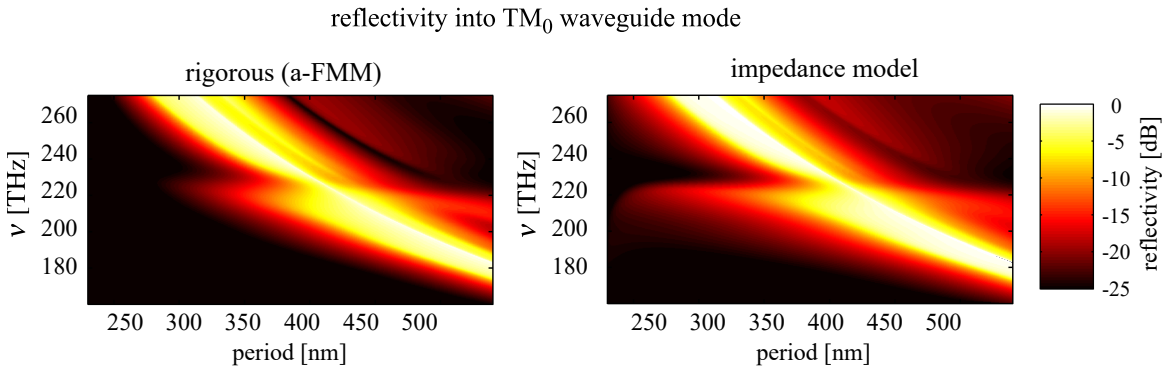

Figure 3.3. Comparison between rigorous calculation and impedance treatment of the structure shown in Fig. 5.3. The hybridization into a Waveguide Plasmon Polariton is well reproduced. The physics of the structure is discussed in Chapter V. $\nu = \omega/2\pi$ is the frequency.

propagation of Waveguide Plasmon Polaritons. The geometry is shown in Fig. 5.3 on page 90. Fig. 3.3 shows the calculated reflectivity into the TM_0 waveguide mode as a function of frequency and period of the BLOCH lattice. We see a bandgap BLOCH mode as well as the localized plasmonic mode of the nanostructures. Although the interaction between them is complicated as will turn out later, it can again be fully described by the adjoint impedance framework. Deviations occur for the plasmonic mode and small periods due to the excitation of higher order modes, which makes the FMA a less good approximation.

If we take a close look at Eq. (3.39) and its derivation in Appendix A2, we see that the critical contribution for determining if $\mathscr{F}_{z_0}$ vanishes or not is $\frac{\partial\psi}{\partial z}\Big|_{z_0}$. If it can be made zero, *e. g.* by an additional symmetry, we get

$$Z_{\text{ref}} = Z_0 \cdot n_{\text{eff}}^{\text{ref}} \cdot \left\langle \varepsilon_{\text{ref}}^{-1}(x) \right\rangle_{\phi\psi} \qquad Z = Z_0 \cdot n_{\text{eff}} \cdot \left\langle \varepsilon^{-1}(x) \right\rangle_{\phi\psi}. \tag{3.43}$$

The modal entanglement is formally reflected by the presence of $\phi(x)$ *and* $\psi(x)$. However, since the FMA needs to be valid, we can put $\phi(x) \approx \psi(x)$ at the interface and achieve a decoupling into *absolute* impedance definitions

$$Z_{\text{ref}} = Z_0 \cdot n_{\text{eff}}^{\text{ref}} \cdot \left\langle \varepsilon_{\text{ref}}^{-1}(x) \right\rangle_{\phi^2} \qquad Z = Z_0 \cdot n_{\text{eff}} \cdot \left\langle \varepsilon^{-1}(x) \right\rangle_{\psi^2}. \tag{3.44}$$

Note that $\phi^2(x)$ and $\psi^2(x)$ are complex valued mode functions in the general case of adjoint reciprocity. If $\varepsilon(x)$ and $\varepsilon_{\text{ref}}(x)$ are real-valued, one can switch to the conjugated reciprocity and the weight functions become $|\phi(x)|^2$ and $|\psi(x)|^2$, *i. e.* the modal intensities. The inhomogeneity of the permittivity is accounted for by introducing the transverse

average of the impermittivity with the proper weight function. For this case, the system behaves entirely analogous to the homogeneous TM case Eq. (3.28) that was introduced earlier in this section and may be described by an *absolute* impedance.

For the case of the simple SPP introduced in Sec. 2.1.2, one can evaluate Eq. (3.44) analytically. This yields

$$Z_{\mathrm{SPP}} = Z_0 \cdot \left[\frac{\varepsilon_1 \cdot \varepsilon_2}{\varepsilon_1 + \varepsilon_2}\right]^{1/2} \cdot \frac{\frac{\varepsilon_1}{\varepsilon_2} + \frac{\varepsilon_2}{\varepsilon_1}}{\varepsilon_1 + \varepsilon_2}. \tag{3.45}$$

This expression represents the adjoint modal impedance of an SPP under Fundamental Mode Approximation in full analogy to the electrical engineering language.

IV. Modally enhanced optical nanoantennas

This chapter investigates the coupling of a localized mode of a nanoantenna to the evanescent mode of a grating, with the goal to enhance the performance of the antenna. This chapter is built on the investigations in Sec. 3.2. While the theoretical description was in the foreground in the last Chapter, we concentrate on how to enhance the practical performance using the adjoint modal framework.

It will be shown that the localized resonance of a plasmonic antenna can be regarded as the resonance of a in- and a outward propagating mode, *i. e.* an adjoint mode pair. This mechanism can be influenced by altering the coupling of the modes to their surrounding. While an antenna usually couples only to the free space modes which characterize the surrounding of the antenna, the tuning of the modal environment will be shown to have a beneficial effect.

4.1. Increase of feedback by modal tuning

A metal nanoparticle can support a localized plasmonic mode. This mode will in general be dependent on its shape, size and material. The electromagnetic properties of this mode (field localization, far-field behavior, resonance frequency, field enhancement) determine whether this particle will make a good antenna [218]. In order to do so, the mode needs to be leaky to the space surrounding the antenna, which is usually associated with a strong dipole contribution in the multipole expansion of the modal field. The surrounding of the antenna is what we want to focus our attention on.

In this section, we want to employ a complete modal picture of the nanoantenna and its surrounding as a Fabry-Pérot-type resonator [125–131]. The nanoantenna itself is theoretically decomposed into a waveguide and two terminations. The geometry and material composition will determine the spectrum of propagating eigenmodes of the waveguide.

The dispersion relation already reveals important properties, such as the level of Ohmic losses (by the imaginary part of the propagation constant) or whether a waveguide mode will leak into one or even both surrounding half-spaces (when its real part lies inside the light cone). The specific excitation conditions determine which modes will actually be present in a specific situation.

The propagating mode(s) will eventually reach a termination where the waveguide ends. The MAXWELL boundary conditions have to be met at this discontinuity and form a modal coupling problem with the surrounding. It can be treated analytically in simple cases, very much as in MIE theory. However, most geometries cannot be solved analytically anymore and require involved numerical techniques as outlined in Sec. 2.2. In the previous Chapter, we have shown under which conditions an impedance treatment of the problem is possible as an engineering-fashion alternative.

The coupling of the adjoint for- and backward propagating modes forms the Fabry-Pérot problem which continuously couples them. A localized resonance forms after a complete round-trip when the phase is matched. This makes the finite nanostructure an antenna.

The aim of this chapter is to demonstrate the enhancement of the antenna functionality by modifying the coupling at the terminations. We will follow the modally resolved picture of that problem, which we pursue throughout this thesis. A logical way to enhance the antenna feedback is to increase the fraction of energy which is coupled back into the structure. This can be done by increasing the modal reflection coefficient at the termination by some kind of modal mirror. We will realize this by modifying the surrounding with a grating structure, such that a bandgap occurs at the frequency of the waveguide mode.

4.1.1. Proof-of-principle: 2D realization

In order to realize this concept, we start with a simple 2D geometry shown in Fig. 4.1. A 30 nm thick gold film is embedded in a dielectric surrounding. We will assume fused silica ($\varepsilon = 2.10$) for the sake of simplicity. The problem is invariant in y-direction. The more realistic but slightly more difficult case of a film on a substrate is treated in the next Section.

The propagating plasmon solutions on the upper and lower side of the film can interact, when it is sufficiently thin [219], which is the case here. As a result, two hybridized bound modes exist. One mode has a symmetric field distribution and a larger propagation

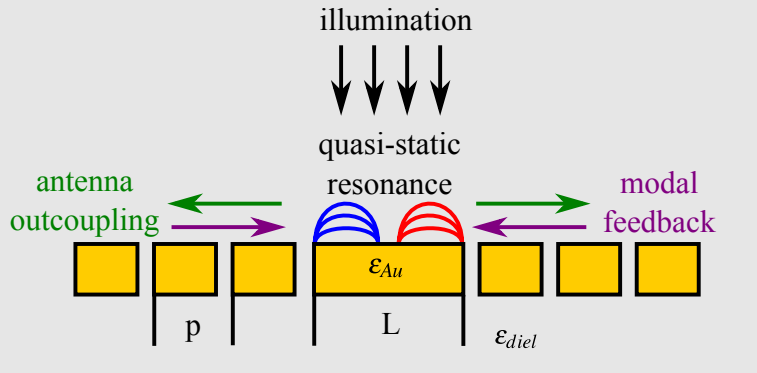

Figure 4.1. A simple 2D structure to test the approach. The antenna is built of a 30 nm thin plasmonic film waveguide. Periodic corrugations to both sides increase the modal feedback which forms the antenna resonance.

constant, while the other has an antisymmetric field and a lower value of β. We take into account the full dispersion of gold [220] and calculate the effective mode index of the symmetric mode at 800 nm operation wavelength by numerically solving Eq. (2.41) as $n_{\text{eff}} = 1.67 + 2.33 \times 10^{-2} i$. This mode is favorably used for operation in the case of an embedding dielectric, since it resembles the overall symmetry of the structure.

We will now have a closer look into the reflection mechanism of the propagating symmetric mode by employing our modal analysis framework. Let it be denoted by $|\phi^+\rangle$ and its complex propagation constant by $\beta = k_0 n_{\text{eff}}$. As the mode propagates along the film, the change in amplitude and phase is given by $\exp[i\beta L]$, until it reaches the termination. L denotes the length of the antenna. Behind the termination, the set of eigenmodes is denoted by $|\psi_n^{\pm}\rangle$. Without any additional structure attached, this will be plane waves. This is the same kind of modal interface problem we treated analytically in chapter III. The mismatch between the sets of eigenmodes reflects the »impedance mismatch« between the waveguide (and eventually the nanoantenna) and free-space. The last chapter has outlined a strategy how this problem can be treated and understood in »RF language«.

We just need to recall Eq. (3.16) in order to solve for the modal reflection coefficient. Many different plane waves $|\psi_n\rangle$ in different directions will in general be excited by the plasmon mode behind the termination due to the strong modal mismatch. We thus use our a-FMM code to solve for the coefficients rigorously.

The modal reflection is determined by the behavior at the termination which constitutes a discontinuity for the eigenmode $|\phi^+\rangle$ and enables back-coupling into the adjoint mode $|\phi^-\rangle$ with a complex reflection coefficient r. A good test system to investigate this is to interrupt the film by a small gap. We numerically calculate r as a function of increasing gap size g. The result is shown in Fig. 4.2. For very small gaps of $g < 20$ nm, the mode can efficiently couple over the gap since it is smaller than the decay length in the surrounding

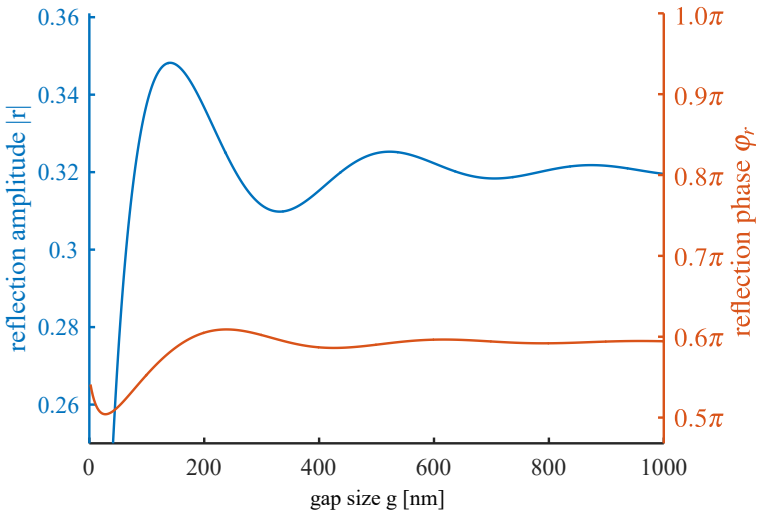

Figure 4.2. Amplitude and phase of the complex reflection coefficient of a SPP mode impinging at a gap in the gold film. The results were calculated using the a-FMM. $|r| = 0.32$ and $\varphi_r = 0.6\pi$ is the converged value for an open termination of the gold film and thus defines the generic feedback for the rod antenna build from a finite sized SPP waveguide.

dielectric, which is the characteristic length scale for that problem. A peak forms at $g \approx 150\,\text{nm}$ and shows a reflection amplitude of $|r| = 0.35$. For higher gap sizes, visible but strongly damped periodic »ripples« occur which can be attributed to a Fabry-Pérot-like problem for the modes $|\psi_n^{\pm}\rangle$ in the gap. The termination acts in a way like an antenna feed point. For large gaps $|r|$ converges to 0.32 and φ_r to $0.6\pi \approx 1.89\,\text{rad}$. This value represents the strength of the feedback for an unmodified surrounding. Interestingly, the phase jump upon reflection is neither exactly 0 nor π, but somewhere in between.

The backward-propagating mode $|\phi^-\rangle$ will eventually reach the termination on the other side, get partially reflected again into $|\phi^+\rangle$ and so on. If we assume both terminations to be equal, r applies to both sides. The total modal amplitude A starts to build up in a Fabry-Pérot-like fashion.

We consider the case that some arbitrary external excitation initially excites the mode of interest with a complex modal amplitude a_0. The finite length L of the structure now leads to a build-up of the total modal amplitude which can be describes as a complex geometric series

$$A = a_0\left[1 + r^2\,e^{2i\beta L} + r^4\,e^{4i\beta L} + \ldots\right] = a_0\sum_{n=0}^{\infty}\left[r^2\,e^{2i\beta L}\right]^n = \frac{a_0}{1 - r^2\,e^{2i\beta L}}\,. \tag{4.1}$$

If we use $r = |r|e^{i\varphi_r}$ and $\beta = k_0 n_{\text{eff}} = 2\pi/\lambda_0 \cdot (n'_{\text{eff}} + i n''_{\text{eff}})$, this becomes

$$A = \frac{a_0}{1 - |r|^2\,e^{-4\pi\, n''_{\text{eff}} L/\lambda_0}\exp\left[2i\,(2\pi\, n'_{\text{eff}} L/\lambda_0 + \varphi_r)\right]}\,. \tag{4.2}$$

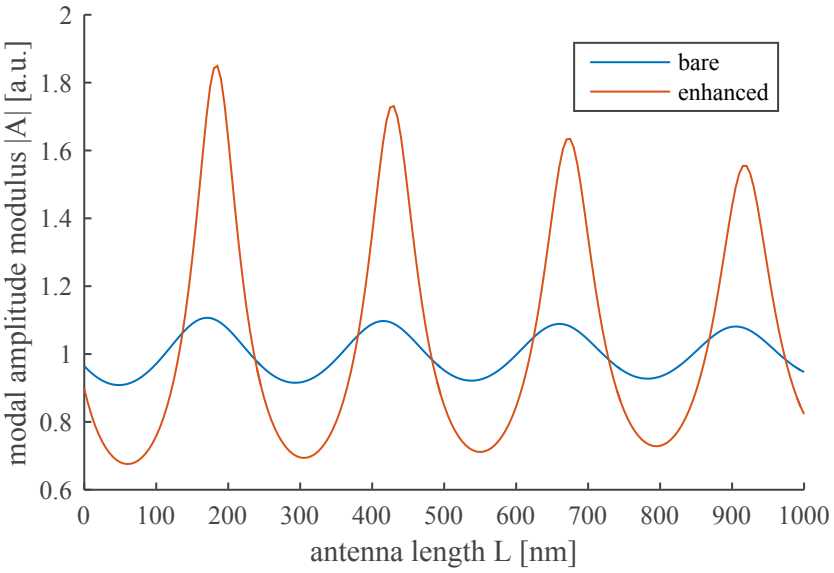

Figure 4.3. Modal amplitude of the antenna SPP mode calculated by Eq. (4.2) for $\lambda_0 = 800\,\text{nm}$. The peaks denote the localized antenna resonances which fulfill Eq. (4.3). By adding the grating structure to the bare antenna, the maximum amplitude is increased by a factor of 1.68.

The phase term leads to an oscillatory nature of the amplitude which becomes resonant when it equals 2π. This translates to a condition for L being

$$2\pi\, n_{\text{eff}}^{'} L/\lambda_0 + \varphi_r \stackrel{!}{=} \nu \cdot \pi, \qquad \nu \in \mathbb{Z}. \tag{4.3}$$

In this condition, we meet again the simple $\lambda_0/2$ dipole antenna, which is realized by having $n'_{\text{eff}} = 1$ and $\varphi_r = 0$. The real part of the transverse mode's effective index $n_{\text{eff}}^{'}$ can be viewed in two ways: it reduces the effective wavelength or it increases the effective length of the antenna. This leads to a reduction in the physical size of the device compared to its RF counterparts. An interesting effect is given by φ_r. If it approaches π, it becomes possible to have the lowest order antenna resonance even for $L \ll \lambda_0$! This case can be viewed as the limit of an antenna that consists »just of terminations«, which was also discussed in [130].

The maximum value for the total modal amplitude is given by

$$A_{\text{max}} = \frac{a_0}{1 - |r|^2\, e^{-4\pi\, n_{\text{eff}}'' L/\lambda_0}}\,, \tag{4.4}$$

and is limited solely by three factors: the excitation efficiency of the mode of interest, the strength of the modal reflection and the round-trip loss of the mode determined by n_{eff}''.

The modulus of the modal amplitude is plotted in Fig. 4.3 as a function of L for two different values of r. The case of the bare antenna corresponds to $r = 0.32\, e^{1.89i}$ as already discussed. Several peaks are visible which constitute the antenna resonances

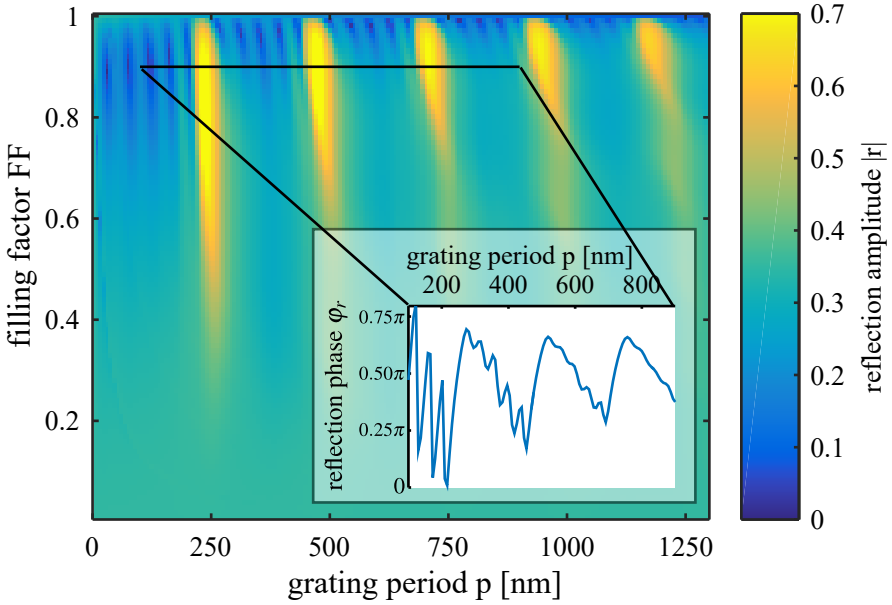

Figure 4.4. Modulus of the SPP mode reflection coefficient calculated by the a-FMM for $\lambda_0 = 800\,\text{nm}$ and a grating with 5 corrugations. The phase is shown as inset for a filling factor of 0.9.

of different orders. They decrease in amplitude for increasing L due to higher round-trip losses. The lowest order antenna mode, which corresponds now to a longitudinal resonance of the symmetric transverse mode in our language, is found at $L = 180\,\text{nm}$. The second plot belongs to the antenna with modified terminations, which is discussed in the next paragraph.

Modified termination. We now consider a periodically corrugated gold film. Instead of a single gap, the reflections from multiple gaps have to be considered. We numerically scan the period p and the filling factor $FF = 1 - g/p$ of a grating made from five corrugations in the metal. We checked that five corrugations were sufficient by simulating the dependence of r on the number of corrugations in another simulation (not shown here, see [TK2014]). The results are shown in Fig. 4.4.

Different peaks evolve for certain values of p. They are attributed to the formation of reflection resonances, where the BRAGG condition

$$\beta = m \cdot \frac{\pi}{p}, \qquad m \in \mathbb{N} \tag{4.5}$$

is met with an arbitrary integer m. This makes the grating a bandgap medium for the fundamental plasmon mode. An optimal filling factor, which works also for higher order resonances, exists at values around 0.9. This corresponds to a gap size with optimal balance between reflection and transmission to the next gap. All resonances wash out for

small filling factors and the reflection amplitude reaches the background value $|r| = 0.32$, which was discussed in the previous paragraph. This effect becomes more pronounced for larger grating periods, since the plasmon mode carries intrinsic loss. At the peak positions, $|r|$ becomes as high as 0.70 and has thus more than doubled, compared to the case without modified termination. The reflection phase is shown as an inset in Fig. 4.4. It shows a rapid change when scanning through the reflection peak, which is characteristic for a Bragg resonance. If we recall the fact that the reflection phase determines also the effective resonant length of the antenna it is clear that the operation bandwidth of the device will become narrower.

Besides the case of the free end termination, Fig. 4.3 shows also the modal amplitude for the enhanced case. As expected, the peak value of the modal amplitude increases. The shift in resonant length comes from a slight change of φ_r compared to the case of a free end.

An increase in the peak modal amplitude by a factor of 1.68 is found for the modified termination. Since the electromagnetic energy density is proportional to the square of the field strength, an enhancement of 2.8 can be expected.

This prediction of the modal model has to be proven by a rigorous numerical treatment, which takes all the modes into account. Such a simulation was performed by Jing Qi in the Institute of Condensed Matter Theory and Optics in Jena using the Finite Difference Time Domain (FDTD) method. The electromagnetic energy density in close vicinity to the terminations of the nanoantenna were compared in the bare and enhanced case. The simulation ran until the parameters of interest had converged, so that we can assume comparability to the steady-state case which was treated here. Details are given in [TK2015]. An increase of 2.9 for the energy density was the result of the FDTD simulation, *i. e.* a very good agreement with the theory. This proves that our modal treatment was able to predict both qualitatively and quantitatively the enhancement mechanism for the nanoantenna.

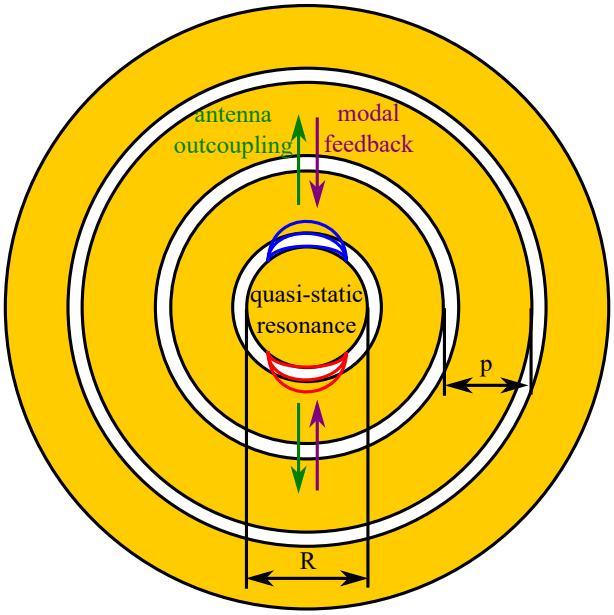

Figure 4.5. Sample layout for the 3D realization. A central circular disc serves as a nanoantenna, which is surrounded by a periodic ring structure that enhances the resonance.

4.2. Experimental demonstration using Scanning Near-Field Optical Microscopy and multiphoton Photoemission Electron Microscopy

In the last section, we have used a simple 2-dimensional nanoantenna geometry to demonstrate the possibilities for enhancing their performance by using modal considerations. These were validated by rigorous numerical simulations. In order to test our theory experimentally, we need a truly 3-dimensional geometry. As a prototype, we use a disc antenna in this section. The symmetry properties of the disc allow us to excite the antenna resonance from normal incident illumination, irrespective of the polarization angle. A sketch of the sample design is shown in Fig. 4.5. A central disc serves as the primary antenna element. In the enhanced case, this disc is surrounded by a number of concentric rings.

The nanophotonic dimensions of the sample exclude the far-field investigation due to the diffraction limit. From the available experimental methods which are not limited by diffraction, we chose to use Scanning Near-Field Optical Microscopy (SNOM) as a quasi-standard and multiphoton Photoemission Electron Microscopy (n-PEEM). Especially the latter is relatively new to the field and becomes increasingly important. The use of ultrafast laser sources to excite the sample and the high achievable spatial resolution open new possibilities for ultrafast nanophotonics. One may also view the antenna in a

different way when using n-PEEM. Since it is the emitted electron yield, which is actually recorded, it becomes possible to see the structure also as an »ultrafast antenna for electrons«. Tailoring the emission of electrons on small space and time scales is an important topic in contemporary physics [221–229]. In this way, nanophotonics helps to create experimental platforms for new fundamental physics.

4.2.1. 3D realization of an enhanced disc antenna

The design of the 3D sample adapts the main concepts of the previous section. As central resonator, we use a circular disc with radius R, which was milled out of a thick gold film using focused ion beam milling (FIB).

The relevant modes in this kind of geometry are so-called HANKEL surface plasmon polaritons (HSPP). The adjoint inward- and outward propagating HSPPs correspond to a field solution which is proportional to the HANKEL functions of first and second kind, respectively. We make use of the same nomenclature as for the single interface problem on page 23. However, the solution is formulated in cylindrical coordinates (r, φ, z), where z is the surface normal and *not* the propagation direction here. The normal component of the electric field is given by [230, 231]

$$E^{\pm}_{\mathrm{hspp},z}(\mathbf{r},\omega) \propto H_l^{(1,2)}\left(\mathbf{k}_{\mathrm{hspp}}\mathbf{r}\right)\cdot\frac{\beta_{\mathrm{hspp}}}{\varepsilon_m}\cdot e^{il\varphi}\cdot e^{ik_m z}, \quad k_{\mathrm{hspp}} = \beta_{\mathrm{hspp}}\mathbf{e}_r = k_0\left[\frac{\varepsilon_1\varepsilon_2}{\varepsilon_1+\varepsilon_2}\right]^{1/2}\mathbf{e}_r. \tag{4.6}$$

The HANKEL functions of first and second kind are denoted by $H_l^{(1,2)}(r)$. Using a mathematical approximation for the HANKEL functions by expanding into orders of $r^{-1/2}$ [232], it is possible to simplify the electric field of the HSPP as follows

$$\mathbf{E}_{\mathrm{hspp}}(\mathbf{r},\omega) \approx \frac{E_0}{\sqrt{\beta_{\mathrm{hspp}} r}}\cdot e^{i\beta_{\mathrm{hspp}} r}\cdot\left(\mathbf{e}_z - \frac{k_m}{\beta_{\mathrm{hspp}}}\mathbf{e}_r\right)\cdot e^{il\varphi}\cdot e^{ik_m z}. \tag{4.7}$$

The next term of the approximation in parenthesis [232] would read

$$\frac{k_m}{\beta^2_{\mathrm{hspp}}}\cdot\left(\frac{1}{2}\mathbf{e}_r + il\mathbf{e}_\varphi\right)\cdot\frac{1}{r} \tag{4.8}$$

and describes the local deviation of the HSPPs polarization properties from plane SPPs (additional E_φ-component). However, it is damped away in the first several oscillations, so that Eq. (4.7) may be called the far-field approximation of the HSPP. Apart from the

stronger $(\beta_{\mathrm{hspp}} r)^{-1/2}$ decay term and the angular φ-dependence, its behavior is locally analogous to the plane SPP. It will become handy in the quantitative analysis of the experimental data in the next section.

In the light of the discussion above, the localized plasmonic resonance of the disc can be regarded as modal Fabry-Pérot-type resonance of the in- and outward propagating HSPPs. The resonance condition reads as

$$\beta'_{\mathrm{hspp}} R + \varphi_r = \nu \cdot \pi, \qquad \nu \in \mathbb{Z} \tag{4.9}$$

in full analogy to the general case Eq. (4.3). The disc radius R plays the role of the generic antenna length, which determines the resonance frequencies together with φ_r, the modal reflection phase of the outward propagating HSPP. In our sample design, the resonant disk radius was 90 nm.

Supporting second order bandgap structure. The goal is to increase the electromagnetic field enhancement by increasing the modal feedback at the disc circumference. As in the previous chapter, we make use of a periodic structure for that purpose. In this case, it will be concentric rings surrounding the central disc, which also will be FIB milled out of the gold layer. The distance between the rings, which form the circular grating period p, play the critical role.

Recalling the results for the one-dimensional case (Fig. 4.4), it is clear that a fulfillment of the BRAGG condition

$$\beta'_{\mathrm{hspp}} = m \cdot \frac{\pi}{p}, \qquad m \in \mathbb{N} \tag{4.10}$$

leads to the desired increase in reflection. Conventional BRAGG grating structures work simply in the first order $m = 1$. Fig. 4.4 suggests, however, that higher orders $m > 1$ yield an equivalently good increase in modal feedback. This opens the possibility to optimize also the coupling of the antenna to the exciting plane wave. The resonant HSPP antenna mode is excited just quasi-statically in the case of the bare disc. No phase-matching is involved in that coupling process. Utilizing a grating, one has the possibility to phase-match the BLOCH mode of the grating to the propagating HSPP mode by conservation of momentum. If we assume a plane wave incident at an angle θ, this »BLOCH-condition«

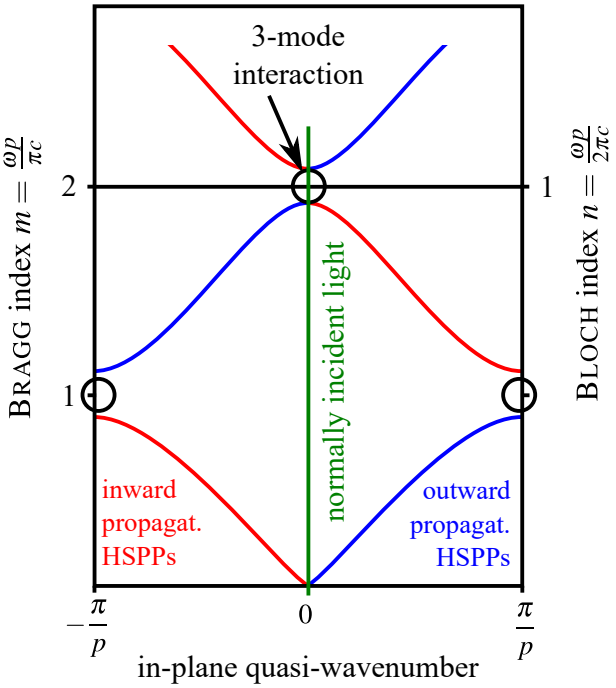

Figure 4.6. Band diagram for the adjoint BLOCH modes in the grating structure, which are given by the inward and outward propagating HSPPs. A second order BRAGG grating allows the interaction of perpendicular incident radiation with both adjoint modes.

reads as

$$\beta'_{\mathrm{hspp}} = k_0 \sin\theta + n \cdot \frac{2\pi}{p}, \qquad n \in \mathbb{Z}. \tag{4.11}$$

Both eqs. (4.10) and (4.11) can have simultaneous solutions for the integers m and n when the condition

$$\sin\theta = \frac{\beta'_{\mathrm{hspp}}}{k_0}\left(1 - 2\frac{n}{m}\right) \tag{4.12}$$

holds. It describes the possible interactions of in- and outward propagating HSPPs with each other, as well as plane wave modes of free space at certain angles θ. The simplest solution is found for the case of normal incidence ($\theta = 0$), with $n = 1$. We would like to call such a grating a »second order« bandgap structure since it works in the second BRAGG order $m = 2$.

The situation becomes clearer when the band diagram for the BLOCH modes of the grating structure in Fig. 4.6 is considered. A bandgap is generated at the band edge in the first order BRAGG resonance $m = 1$. In- and outward propagating HSPP are phase-matched at that point and can couple, which generates the BRAGG mirror effect. However, the second order BRAGG resonance $m = 2$ generates a bandgap at the Γ point in the

band diagram. Besides the BRAGG mirror effect of in- and outward HSPP coupling, a simultaneous phase-matched interaction with normally incident plane waves becomes possible. For $m = 4, n = 2$ for instance and a given $n'_{\text{eff}} = 1.67$ as discussed above, the interaction with plane waves at angles of $\theta = 0°$ or $\pm 54.6°$ would become possible, which are of course the 0 and ± 1 diffraction order. More and more plane waves as eigenmodes of free space can become involved as m grows and the coupling process becomes more and more multimode.

If we take a look back into our generic theory Eq. (4.4), the second order grating should not only increase $|r|$, but also a_0 and so enhance the overall performance even further. The optimization of $|r|$ alone promised a factor of 1.68 in the modal amplitude or 2.8 in the intensity as discussed above. We will now check our assumption by experimental investigations of a fabricated sample.

4.2.2. Experimental investigation

We fabricated two samples according to the considerations in the last paragraph to verify our assumptions experimentally. When it comes to nanooptical structures, the intrinsic sub-wavelength size hinders the use of traditional far-field characterization techniques due to the ABBE diffraction limit [11]. Methods which are sensitive to the optical near-field in direct vicinity of the structures have to be employed.

Among such techniques, scanning near-field optical microscopy (SNOM) is a very widely used one [233–239]. The key principle of SNOM is to bring a deep sub-wavelength probe as tiny perturbation in very close vicinity to the sample which is illuminated by a strong light-source, usually a laser. A small amount of light will be scattered into the far-field and converted to propagating radiation. This is collected either by a fixed, distant detector (scattering-SNOM) or coupled directly to an optical fiber and then analyzed by a detector (collection-mode SNOM). In both cases, the near-field probe is rastered over the sample point-by-point by moving either the sample or the probe to acquire an image. Different homodyne or heterodyne techniques exist using an opical reference to acquire also the local optical phase. Probes are either very sharp tips known from atomic force microscopy (scattering SNOM), or tapered tips which are drawn directly from a dielectric optical fiber which serves as far-field signal collector (collection-mode SNOM).

Although SNOM can be seen as a work horse in experimental nanophotonics, it has a number of drawbacks. The scanning nature of the method prevents high speeds in the image acquisition and makes ultrafast investigations challenging. The requirement of a

probe in close vicinity to the sample under investigation disturbs the optical functionality by adding an additional interaction channel with the modes of free-space (scattering SNOM) or the optical fiber (collection-mode SNOM). The strength of this interaction is hard to judge and depends on the specific sample. Moreover, it must be assumed that it is spatially constant during the scanning process which can be hard to achieve in reality for a sample with resonant nanostructures. For the reasons above, we wish to cross-check and compare the SNOM results also by another method.

Photoemission electron microscopy has achieved an increasing amount of interest in the nanophotonics community in the last years [240–254]. Originating from solid-state physics and surface science as a tool to investigate material properties, the availability of highly reliable ultrafast laser sources with high repetition rates in the last years has fired the imagination to investigate optical excitations such as surface plasmons at the nanoscale with the resolution of an electron microscope. A pump-probe scheme opens the possibility to perform time-resolved experiments with remarkable temporal resolution.

In contrast to SNOM, no probe is required which could disturb the optical functionality. The sample is optically excited from the far-field by a laser. The emitted electrons are accelerated by a static electric field, imaged by electrostatic lenses, amplified by channel-plates and detected by a CCD on a fluorescent screen. No scanning is required although many frames have to be captured in order to collect a sufficient number of electrons.

A third method has to be stated for completeness, although it is not used in this thesis. While SNOM and PEEM rely on optical excitation of the structures under investigation, the required energy can also be provided by other means. An interesting possibility is to use an electron beam and monitor its energy loss when it passes through the structure, exciting plasmons. This techniques is known as Electron Energy Loss Spectroscopy (EELS). It does not require an excitation by light and can consequently also probe modes which would otherwise not be excited due to selection rules. EELS is used to map the eigenmodes of plasmonic structures with high spatial resolution [218, 255–267].

SNOM results. Being a standard method to clarify optical near-field distributions, we use collection-mode SNOM with a gold-coated fiber tip to investigate our 3D nanoantenna sample. This method had been successfully applied to a variety of different samples in our workgroup before [TK2017, 268–273]. The experimental setup is shown on the left side of Fig. 4.7. A laser diode operating at a wavelength of 785 nm was collimated, polarized and used to illuminate the sample from the substrate side. On the top side, the SNOM tip

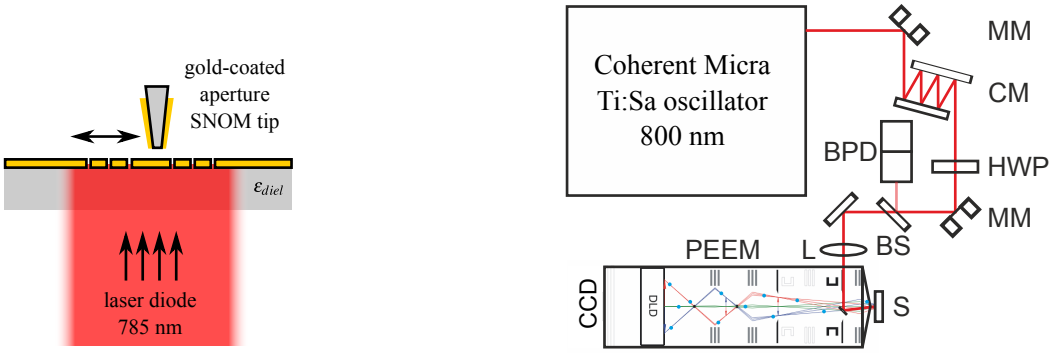

Figure 4.7. Experimental setups used to verify the disc-ring antenna design. (left) A SNOM tip scans over the antenna structure which is illuminated by a laser diode through the substrate. (right) A ultrafast laser source is incident at 4° on the sample. Emitted photoelectrons are imaged by the n-PEEM.

was moved and scanned over the sample by piezoelectric actuators. The collected light was coupled into a single-mode optical fiber and transmitted to the detector.

Due to the experimental circumstances, certain modifications had to be made to the original sample design. The illumination scheme from below required that a trade-off between light coupled through to the antenna and transmitted background light had to be found. We therefore increased the experimental gold film thickness to 50 nm. Moreover, the antenna is now not embedded into a dielectric, but placed on a fused silica substrate ($\varepsilon = 2.10$). In this configuration with broken symmetry, an operation in the antisymmetric hybridized film plasmon mode is more favorable [TK2015]. We used Eq. (2.41) to calculate its effective index numerically as $n_{\text{eff}} = 1.02 + 4.13 \times 10^{-4} i$, which is extremely close to the effective index of the »original« HSPP given by Eq. (4.6) as $1.02 + 1.44 \times 10^{-3} i$ at this wavelength. We adjusted the spatial dimensions of the grating accordingly. The final nanoantenna structure was patterned in a 50 nm gold film using Focused Ion Beam milling (FIB). The central disc had a radius of 90 nm, the rings where 80 nm wide and had a period of 770 nm, which exactly matches the second order bandgap requirement from above. We surrounded the central disc structure with five rings and made a second sample with just the bare disc for comparison.

The results of the measurements are shown in Fig. 4.8. When we investigate just the bare disc, a clear hot-spot of electromagnetic energy is observed at the position of the disc. This indicates that a localized plasmonic resonance is indeed excited on the structure. Apart from that hot-spot, we do not see any further significant features in the field profile.

We find a much different picture for the ring-enhanced structure. Strong side lobes indicate a pronounced interaction with the grating. Taking into account the background

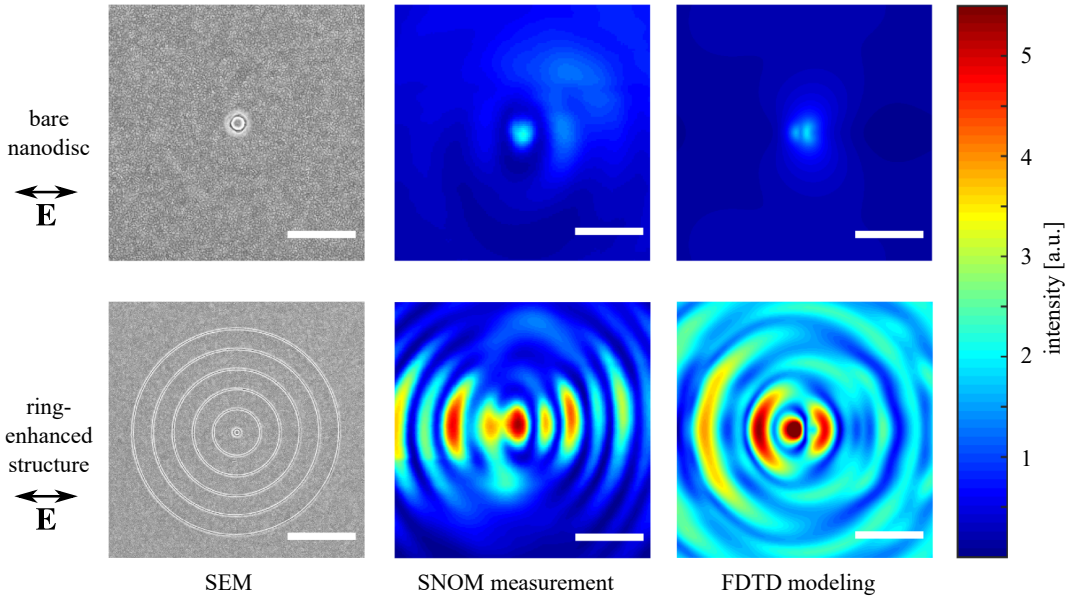

Figure 4.8. SEM image, SNOM measurement results and FDTD modeling of the bare disc antenna as well as the ring-enhanced structure. The scale bar is 2 µm long in each image. The spatial resolution is limited to 180 nm due to the apex size of the aperture SNOM tip.

from the illumination, the intensity in the central area has grown significantly by a factor of ≈ 5. As expected, this is larger than what we have theoretically predicted for a first order BRAGG grating and confirms our design considerations of the nanoantenna.

We also compared the measured field distributions with rigorous FDTD data from simulations. The apex of the gold-coated fiber tip had a diameter of 180 nm and approached the sample at an angle of 30° with respect to the surface normal. This limits the resolution of the image significantly and requires a modification of the raw simulation data to be comparable. We used an extraction distance of 100 nm for the FDTD data and projected the field components to account for the angled SNOM tip [TK2015]. The data results are shown in Fig. 4.8 and are in good agreement with our measurements.

n-PEEM results. We use a near-normal incidence setup and n-PEEM to investigate the 3D nanoantenna sample. This scheme is free from the restrictions regarding the sample design. We deposited a 200 nm thick gold film, where the plasmonic excitations cannot interact with the bottom side of the sample any more, *i. e.* the original design discussed in Sec. 4.2.1. We used an ultrafast laser source at 800 nm central wavelength which corresponds to a photon energy of 1.55 eV. The effective mode index of the HSPP remains almost unaltered to the SNOM experiments, but we accounted for the slightly different

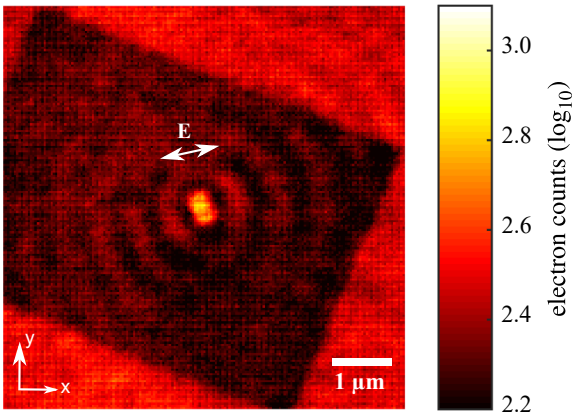

Figure 4.9. Logarithmic plot of the n-PEEM yield for the bare nanodisc in TM polarization. The antenna resonance is clearly visible although the absolute electron count is low (integration time 2 h). A very weak excitation of outward propagating HSPPs is also visible.

wavelength by increasing the period to $p = 780\,\text{nm}$ to meet the second order bandgap requirements. The work function of evaporated gold in our facilities is approximately $W \approx 4.6\,\text{eV}$. Thus, a nonlinear 3-photon process is necessary to emit an electron. This requires a high laser intensity at the sample position.

The experimental setup is shown on the right side of Fig. 4.7. We used a PEEM manufactured by Focus GmbH (Germany) to acquire an image of the photoexcited electrons. For this purpose, emitted electrons where accelerated in a 16 kV static electric field and imaged by an electrostatic lens system. The special design of the PEEM column provides two possibilities for illumination: Grazing incidence under 65° and near-normal incidence at 4°. We used the latter for our experiments. The pulses lateral spatial intensity distribution had a wide Gaussian shape. It was imaged onto the sample by a lens of focal length 250 mm, providing a broad plane-wave-like illumination at the sample position.

We investigated the bare nanodisc first. A small incidence angle of 4° leads to the fact that TE and TM polarization become distinguishable. This is of particular importance, since PEEM is known to be an experimental method which reacts extremely sensitive on the presence of a normal electric field component [240].

The result for TM illumination is shown in Fig. 4.9. The most significant feature is the dark rectangular area, which was found to be identical to the SEM inspection window during sample preparation. A high-energy electron beam scans over the surface and modifies the work function of the last layer of atoms, presumably by enabling bonding of remaining substances in the vacuum chamber onto the surface, such as smallest quantities of carbon. This underlines the extreme surface sensitivity of the PEEM method. Although the purity of the deposited gold suffers from that effect, it might be used in an advantageous way. A drawback of n-PEEM lies in the lack of abilities to acquire topographic images of the sample together with the secondary electron emission picture.

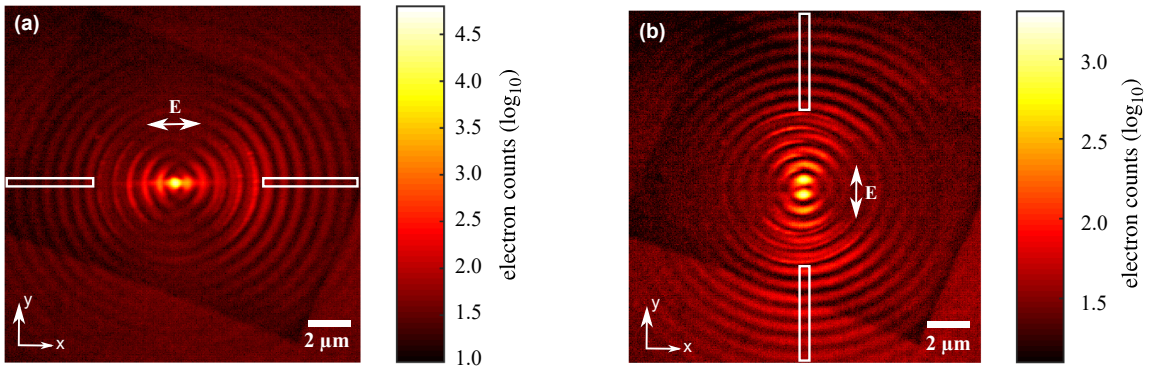

Figure 4.10. Logarithmic plot of the n-PEEM yield for TM (left) and TE (right) polarization of the incident laser for the enhanced antenna. The absolute yield levels are much higher as in the bare nanodisc case (integration time 15 min). The dashed lines denote the areas used for the analytical investigation of the outward propagating HSPPs.

This makes the accurate establishment of a local coordinate system challenging. With the high contrast SEM window, however, there is the possibility to overlay both pictures with high accuracy.

The bare nanodisc acts as an optical antenna and increases electron emission by creating a hot-spot as expected and already seen in the SNOM measurements. The resonance is excited quasi-statically without any involved modal phase-matching process of any kind. This can be seen from the weak excitation of HSPPs on the gold film in the nearby surrounding. Although the enhancement is evident, an exposure time of 2 h had to be used in order to get a picture with good signal contrast. For TE polarization, where the HSPP is the only source of a normal field component as shown in Eq. (4.7), no significant signal contrast could be achieved at all.

A different picture is found, when the ring-enhanced structure is investigated. An exposure time of 15 min already yielded data with high contrast, even in TE polarization. This supports the SNOM results and indicates that the realized structure is not only a good antenna for light, but also for electrons. Fig. 4.10 shows a summary of the measurement results. We find again the SEM window which serves as a marker to determine a coordinate system. The overall enhancement is much more pronounced as in the case of the bare disc. The excitation of HSPPs is clearly visible and follows the theoretical $\cos^2(\varphi)$ dependence when φ measures the angle to the polarization vector in the surface plane. We marked areas where we extracted a one-dimensional cut through the data to analyze the excited HSPP in more detail, which will be discussed later.

In Fig. 4.11, we show a magnified version of the PEEM measurement data with the

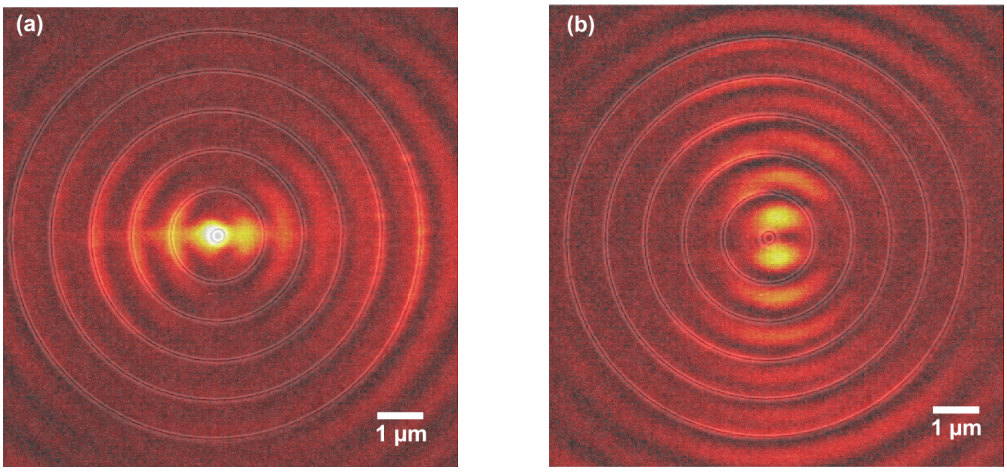

Figure 4.11. n-PEEM images overlaid with the SEM images for TM (left) and TE (right) polarization. The overlay allows a clearer analysis of the resonance behavior.

SEM data as overlay, to clarify the details and spatial origin of the electron yield within the antenna structure.

Although the angle of incidence is very small, a clear difference in the spatial distribution of the n-PEEM yield can be seen for the two different excitation cases. In TM polarization, a very strong excitation of the central disc takes place with minor side lobes. In TE polarization, the excitation is mainly located in two main lobes.

Both cases show increased photoemission from the edges of the rings in the direction of the polarization. This is attributed to an enhanced field emission at sharp sample features.

Physical model for the n-PEEM yield. When one performs n-PEEM measurements, one must not forget that the image data actually reflects a very complex physical process. We do not »see« or measure the actual optical field directly, but the way its presence influences local photoemission. This process, and hence the quantitative explanation of the measurement data (electron counts), would require a deeper look into the light-matter-interaction itself. However, it is still possible to employ a somewhat simpler physical model that is not able to explain all quantitative details, but still manages to »translate« the n-PEEM data into data for the electromagnetic optical field, which we are interested in. These simple models make n-PEEM a promising nanooptical characterization method.

Let us recall the standard three-step model of linear photoemission [274]. A photon of frequency energy $\hbar\omega$ is absorbed by an electron at the FERMI edge of the metal. Due to its increased kinetic energy, the electron can undergo a transport process to the surface

of the metal where it transits into a free electron state in the vacuum. In order to reach the vacuum, the photon energy needs to be larger than the work function of the metal W_m

$$\hbar\omega > W_m. \tag{4.13}$$

The optical field itself only influences the first process while the second and third process is dictated by solid-state physics. We can state that the electron yield will thus be proportional to the photon absorption probability. In our given case, Eq. (4.13) is however violated and a single photon has too less energy to emit an electron. A multiphoton absorption process is therefore needed

$$n \cdot \hbar\omega > W_m \tag{4.14}$$

with $n = 3$ in our case.

The rates for single as well as multiphoton absorption $\Gamma^{(n)}$ are given by FERMI's golden rule and build up for the 1, 2 or 3 photon absorption in the semi-classical case as[1] [275]

$$\Gamma^{(1)} = 2\pi \frac{e}{\hbar^2} \zeta(\omega_{\psi\xi} - \omega) \left| \langle \psi \,|\, \hat{\mathbf{p}} \cdot \mathbf{E} \,|\, \xi \rangle \right|^2, \tag{4.15a}$$

$$\Gamma^{(2)} = 2\pi \frac{e^2}{\hbar^4} \zeta(\omega_{\psi\xi} - 2\omega) \left| \langle \psi \,|\, \hat{\mathbf{p}} \cdot \mathbf{E} \,|\, \alpha \rangle \langle \alpha \,|\, \hat{\mathbf{p}} \cdot \mathbf{E} \,|\, \xi \rangle \right|^2, \tag{4.15b}$$

$$\Gamma^{(3)} = 2\pi \frac{e^3}{\hbar^6} \zeta(\omega_{\psi\xi} - 3\omega) \left| \langle \psi \,|\, \hat{\mathbf{p}} \cdot \mathbf{E} \,|\, \alpha \rangle \langle \alpha \,|\, \hat{\mathbf{p}} \cdot \mathbf{E} \,|\, \beta \rangle \langle \beta \,|\, \hat{\mathbf{p}} \cdot \mathbf{E} \,|\, \xi \rangle \right|^2, \tag{4.15c}$$

where $\zeta(\omega)$ is a normalized lineshape function (*e. g.* Lorentzian), $|\psi\rangle$ and $|\xi\rangle$ denote the initial and resulting quantum-mechanical free electron states, respectively, and $\omega_{\psi\xi}$ is the transition frequency. The quantum mechanical dipole operator is denoted by $\hat{\mathbf{p}} = e\,\hat{\mathbf{r}}$ and $|\alpha\rangle$ and $|\beta\rangle$ denote intermediate electron states in the conduction band.

One sees how the process becomes more and more improbable when the order of the nonlinearity increases, which explains the need for high field strengths for the process in order to happen at all. It builds up from repetitive interactions of an electron with the electric field, which itself is modeled as a *linear* dipole-field interaction. The absolute value squared is a reminiscence of quantum mechanics itself (probability amplitude) and *not* of electrodynamics. We state this here explicitly, because the yield in n-PEEM is

[1] At this single instance in the thesis, we mean quantum mechanical states with the Bra-Ket notation, not the adjoint electromagnetic modes.

often somewhat loosely attributed in literature to powers of the optical *intensity* I^n of the electromagnetic field, which would be given by [276]

$$I^3 = \left\langle \left| \mathbf{S}(\mathbf{r},\omega) \right| \right\rangle^3 = \frac{1}{2} \left| \mathrm{Re}\left[\mathbf{E}(\mathbf{r},\omega) \times \mathbf{H}^*(\mathbf{r},\omega) \right] \right|^3 = \frac{1}{2Z_0} \left[\mathbf{E}(\mathbf{r},\omega) \cdot \mathbf{E}^*(\mathbf{r},\omega) \right]^3. \quad (4.16)$$

This formula has the problem that the different electric field components in plane ($E_\parallel$) and out of plane ($E_\perp$) have equal weights and no cross-terms. This is not compatible with the fact stated above, namely that TM polarization leads to much more yield than TE, and our observation of an interference pattern of the plane wave and the HSPP in the TE case, where the only source of a normal electric field component is the HSPP itself. Our model instead connects the differential n-PEEM yield $Y(\mathbf{r})$ to $\Gamma^{(3)}$ via

$$\mathrm{d}\bar{Y}(\mathbf{r},t) \propto n(\mathbf{r}) \cdot \Gamma^{(3)}(\mathbf{r},t)\,\mathrm{d}t, \quad (4.17)$$

where $n(\mathbf{r})$ is the electron density in gold at the FERMI level. The probability for 3-photon absorption is proportional to the absolute squared triple products of the field in Eq. (4.15c). Technically, $n(\mathbf{r})$ would also vary in time, since the impinging radiation induces plasmonic excitations which are oscillations of the electron density. However, we estimate these variations to be several orders of magnitude smaller than the bulk electron density from the parameters of the laser we used (average power $P_0 = 100\,\mathrm{mW}$, repetition rate $f_{\mathrm{rep}} = 80\,\mathrm{MHz}$, pulse duration $\tau = 30\,\mathrm{fs}$, central wavelength $\lambda_0 = 800\,\mathrm{nm}$). The total yield is obtained by integrating over the measurement time. The model thus is based on triple products of linear combinations of the instantaneous electric field, which is different from using the time-averaged quantity intensity. Cross-terms between $E_\parallel$ and $E_\perp$ show up, which is consistent with our measurement in TE polarization. One learns from Eq. (4.15c) that the coefficients for this linear combination are constructed from the expectation values of the dipole operator in the semi-classical case. They have the potential to explain different yields for different polarizations, since only the paths which lead to a free electron in vacuum can contribute to the n-PEEM yield, in contrast to any bound final electron state (the multiphoton absorption rate itself should not depend on polarization). Calculating these coefficients explicitly – which would perhaps require even a full quantum-electrodynamically treatment including second quantization – is beyond the scope of this thesis. A route for including these effects may be given by the surface corrections of quantum plasmonics within a non-local hydrodynamical model of the electron gas [261, 277–284].

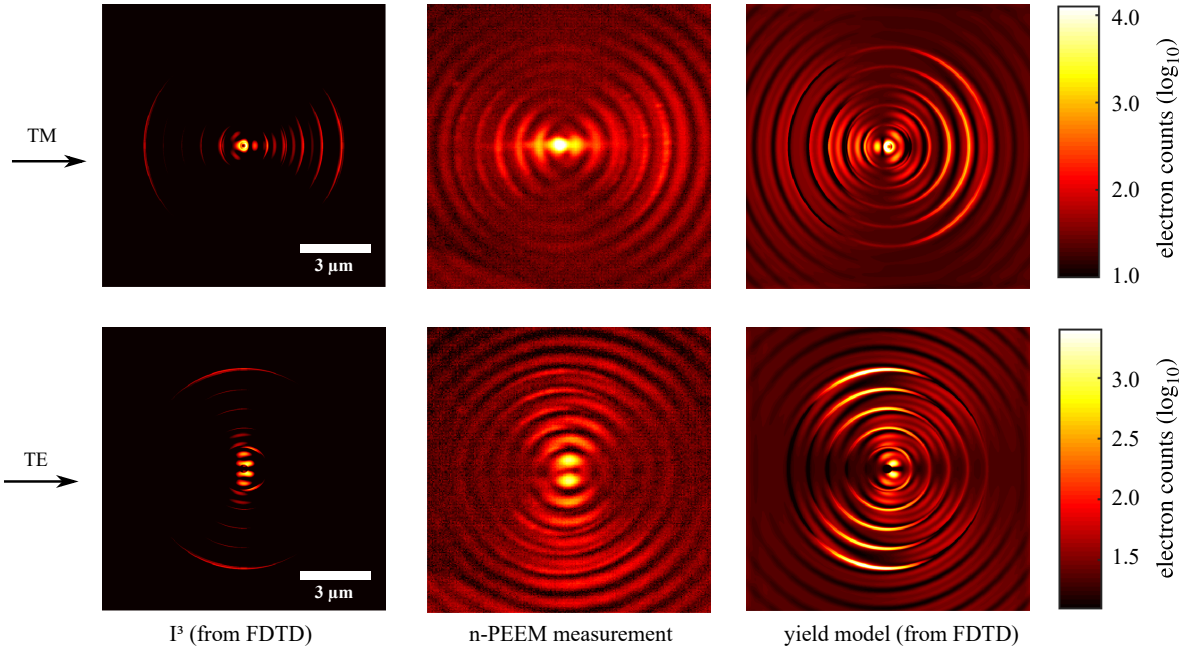

Figure 4.12. Comparison between the n-PEEM measurement data and the »intensity^3« model as well as our temporal yield model. Colorbars apply to all images of the same polarization. Our yield model is very good agreement with the experimental data.

Our essential model assumption will be that the yield is given by

$$Y(\mathbf{r}) \propto \int \left| \left[\bar{E}_{\parallel}(\mathbf{r},t) + a \cdot \bar{E}_{\perp}(\mathbf{r},t) \right]^3 \right|^2 \mathrm{d}t. \tag{4.18}$$

The real parameter a accounts heuristically for the aforementioned lack of knowledge of the quantum-electrodynamical parameters. Furthermore, it accounts for the fact that photoemission is a process which takes place at the very surface, where $E_\perp$ is discontinuous in medium-averaged electrodynamics, see Eqs. (2.14). It even changes its sign in the case of a metal, so that the question arises: Which corrections need to be applied to $E_\perp$ at the very surface? We account for these circumstances by using a as a fit parameter for our model.

Application of the yield model to the experimental data. At first, one has to explain the experimental n-PEEM pictures. Since the transient dynamics of the nanoantenna is impossible to treat analytically, we simulated the ultrashort pulse experiment by FDTD and used our yield model described above on the numerical data. The results are shown in Fig. 4.12. For comparison, we also show the results based on the intensity. Our model

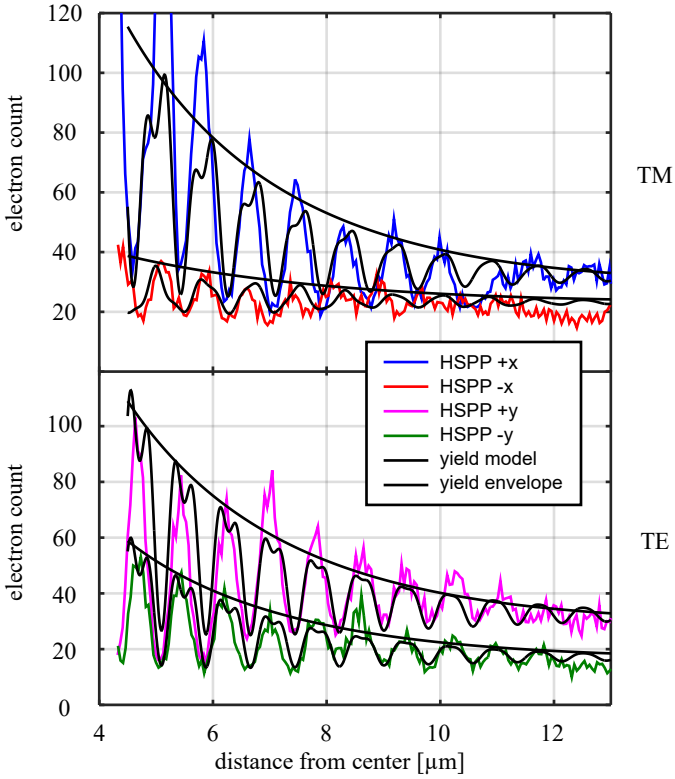

Figure 4.13. Experimental data for the outward propagating HSPPs analyzed in the regions marked in Fig. 4.9 and comparison to the analytical HSPP yield model. A very good agreement is obtained. The spatio-temporal yield envelope is shown as dashed curve.

is obviously much better able to reproduce the experimental results and shows very good agreement. The used fit parameter was $a = 50$.

Besides comparison with rigorous numerical simulations, one desires to have a physical explanation of the experimental data. Although the transient dynamics of the inner antenna is not straight-forward to analyze, the data from the propagating HSPPs can be analyzed analytically. They are observed in the outer region on the gold film. The explicit modal field of the HSPP solution is readily available in Eq. (4.7). The lowest possible HSPP mode for $l = 1$ relates to a dipolar pattern with $\cos^2\varphi$ or $\sin^2\varphi$ dependence of the plasmon energy density, respectively. We recognize these dependencies for the two different excitation polarizations in Fig. 4.10 and also checked the quantitative matching (not shown explicitly).

We analyze the data in further detail by taking a cut through the marked areas in Fig. 4.10. The results are shown in Fig. 4.13. The observed oscillation period of the interference pattern differs for the TE and TM case. The HSPP is propagating perpendicular to the projection of the incident $\mathbf{k}$ vector in the TE case ($\pm y$-direction). Therefore, one measures exactly the plasmon wavelength $\lambda_{\mathrm{hspp}} = 2\pi/\beta_{\mathrm{hspp}}$. In the TM case, however, there is an additional component $\pm k_0 \sin\theta$ to β_{hspp} in the $\pm x$ direction, depending

on if the HSPP is co- or counter-propagating with the in-plane projection of the exciting plane wave pulse. Since $\sin(4°) \approx 0.07$, the deviation from λ_{hspp} is only minimal. We attribute the different background levels for the respective areas to a slight non-uniform illumination strength at the different positions due to the Gaussian beam profile.

Now we have to quantitatively explain the decay rate and interference structure observed in the experiment. According to the yield model in Eq. (4.18), we have to work in the temporal domain. The excitation is modeled as a plane wave with a Gaussian pulse envelop $\bar{\mathbf{E}}_{\mathrm{pw}}(\mathbf{r}, t)$ at an angle of incidence θ

$$\bar{\mathbf{E}}_{\mathrm{pw}}(\mathbf{r}, t) = \mathbf{E}_0 \cos\left[k_0 \sin\theta x - \omega t\right] \cdot \exp\left[-\frac{(t - \sin\theta x/c)^2}{\tau^2}\right], \tag{4.19}$$

where

$$\mathbf{E}_0 = \begin{cases} [0, 1, 0] & \text{(TE)} \\ [\cos\theta, 0, \sin\theta] & \text{(TM)} \end{cases} \tag{4.20}$$

is the polarization vector of the incident radiation and τ is the temporal pulse length. The excited HSPP pulse is modeled in a similar manner as

$$\bar{\mathbf{E}}_{\mathrm{hspp}}(\mathbf{r}, t) = \mathrm{Re}\left[\mathbf{E}_{\mathrm{hspp}}(\mathbf{r}, \omega) \cdot e^{-i\omega t}\right] \cdot \exp\left[-\frac{(t - n_g x/c)^2}{\tau^2}\right], \tag{4.21}$$

where $n_g = c_0[\mathrm{d}\beta'_{\mathrm{hspp}}/\mathrm{d}\omega]$ is the group index of the HSPP at the central wavelength of the laser and $\mathbf{E}_{\mathrm{hspp}}(\mathbf{r}, \omega)$ is given by Eq. (4.7).

The total electric field, which enters the yield model Eq. (4.18), consists of the interference of the two fields at the sample surface

$$\bar{\mathbf{E}}(\mathbf{r}, t) = \bar{\mathbf{E}}_{\mathrm{pw}}(\mathbf{r}, t) + b \cdot \bar{\mathbf{E}}_{\mathrm{hspp}}(\mathbf{r}, t). \tag{4.22}$$

A complex modal factor b accounts for the unknown excitation strength and phase of the HSPPs.

We fit this model parameter to the experimental data and show the result in Fig. 4.13. They are in very good agreement. It is remarkable that this fully analytical ansatz produces not only the correct oscillatory behavior and decay rates, but also correct background levels for the n-PEEM yield far from the excitation point. Slight deviations occur for smaller distances from the center, which we attribute to the deviations of our approximation

Eq. (4.7) from the actual HSPP solution for small values of r.

The observed decay is governed by two contributions. First, there is an intrinsic component which comes from the fact that HSPPs decay with a factor $[\beta'_{\mathrm{hspp}} r]^{-1/2}$ stronger than plane SPPs. Second, the pulse length of just $\tau = 30\,\mathrm{fs}$ leaves only a short temporal »interaction window« in which the interference can take place. The Gaussian temporal envelop therefore translates into a spatial envelop, which represents the width of the HSPP pulse in a co-moving frame along the sample surface with a velocity c_0/n_g. From the dispersion relation Eq. (4.6), we calculate $n_g = 1.08$. The term $\tau c_0/n_g$ is in the order of $9\,\mu\mathrm{m}$, which represents the characteristic spatio-temporal interaction length in the experiment. It is now straight-forward to derive an analytical expression for the yield envelop as

$$Y_{\mathrm{env}}(r) \propto \left\{ [\beta'_{\mathrm{hspp}} r]^{-1/2} \cdot \exp\left[-\left(\frac{n_g r}{\tau c_0} \right)^2 \right] - \mathrm{const.} \right\}^6 , \tag{4.23}$$

which is also plotted in Fig. 4.13 and leads to a remarkable agreement with experimental data. Since all other quantities are known analytically, this expression can in principle even be used inversely to measure the pulse length τ from the n-PEEM image. One may even think of such an ansatz to use n-PEEM to characterize ultrashort pulses.

We emphasize that the envelop model does not even need to consider the Ohmic loss of the metal associated with a term $\exp[-\beta''_{\mathrm{hspp}} r]$. The reason is that the aforementioned contributions are far stronger since $\beta''_{\mathrm{hspp}}/\beta'_{\mathrm{hspp}} \approx 10^{-3}$. It is the limited spatio-temporal extent of the pulse together with the analytical properties of the modal solution which govern the observed experimental data.

V. Hybrid waveguide-nanoparticle systems

This chapter treats planar, dielectric waveguide geometries, which have been hybridized with plasmonic nanoparticles on top. The goal is to incorporate functionalities mediated by the nanostructures (field enhancement, new propagation properties) into the waveguide environment. This opens a perspective for enriching the functionality of traditional integrated optics.

In the focus of the treatment lies the adjoint eigenmode-based description of the coupling between the propagating modes of the waveguide and the localized modes of the nanoparticles. The chapter starts with the basic interaction of a single isolated plasmonic nanoparticle with a dielectric waveguide mode. From there, propagation properties of a waveguide covered with a lattice of nanostructures – a metasurface – are developed. The last section discusses possible application perspectives of the system.

The polarization properties of the waveguide modes will be shown to offer new perspectives for the excitation of nanostructures, which are not possible from free space. Hybridization into a Waveguide-Plasmon-Polariton state in the case of a nanoparticle lattice leads to adjustable dispersion properties (loss, effective index, group velocity and group velocity dispersion).

5.1. Basic configuration: Waveguide to Plasmon mode coupling

Waveguide mode properties. We start by defining the test-configuration we wish to discuss. As a basis, we will use a planar dielectric slab waveguide for simplicity. A high-index dielectric core layer (permittivity ε_2) of thickness d is placed on top of a dielectric lower-index substrate. We will assume fused silica as a substrate material ($\varepsilon_1 = 2.10$) and air as cladding material ($\varepsilon_3 = 1.0$) as a realistic design approach.

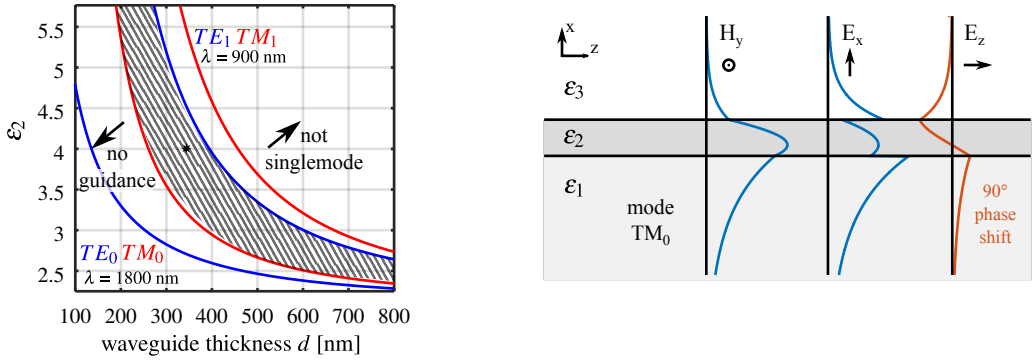

Figure 5.1. (left) Cut-off curves of the fundamental and first-order waveguide modes in a slab-waveguide with fused-silica as substrate and air as cladding. In the shaded region, the waveguide is monomode in the entire wavelength range $\lambda_0 = 900\,\text{nm} - 1800\,\text{nm}$. The operating point is marked with an asterisk. (right) To-scale plot of the electromagnetic field components of the TM_0 waveguide mode. The $E_z(\mathbf{r},\omega)$ component has a high magnitude at the waveguide-cladding interface.

We are targeting for a regime, where the waveguide is single-mode in both polarization directions to allow for a controlled and predictable interaction with the nanostructures in the cladding region. For our investigations, we use a NIR wavelength range $\lambda_0 = 900 \ldots 1\,800\,\text{nm}$. Depending on the core thickness d and permittivity ε_2, there exists a range of possible thicknesses in which both polarizations have only a single mode solution. The cut-off thicknesses can be calculated from Eq. (2.41) for the case $k_1 = 0$, which yields

$$d_{\text{cut-off}}(\lambda_0, \varepsilon_2) = \frac{\lambda_0}{2\pi \cdot [\varepsilon_2 - \varepsilon_1]^{1/2}} \cdot \left\{ \arctan\left[\frac{q_3}{q_2} \cdot \left(\frac{\varepsilon_1 - \varepsilon_3}{\varepsilon_2 - \varepsilon_1} \right)^{1/2} + n \cdot \pi \right] \right\}. \tag{5.1}$$

There is a region of optimal parameters which is shown on the left side of Fig. 5.1. Outside this region, either no guidance at $\lambda_0 = 1800\,\text{nm}$ would be possible due to the fundamental mode cut-off, or the waveguide would not be singlemode at $\lambda_0 = 900\,\text{nm}$.

A second consideration when choosing core material and thickness are the polarization properties of the waveguide modes and possible excitation scenarios for the nanostructures which derive from them. The most simple case is TE polarization. The electric field has just an $E_y(\mathbf{r},\omega)$ component, so the resonant length for quasi-static excitation of the nanoparticle needs to be in the same direction.

The situation is more complicated in TM polarization. From MAXWELL's equation, we see that the $H_y(\mathbf{r},\omega)$ component leads in principle to *two* electric field components in the

cladding $\mathbf{E}_c(\mathbf{r},\omega)$, where the nanostructure is placed

$$\begin{aligned}\mathbf{E}_c(\mathbf{r},\omega) &= -\frac{1}{i\omega\varepsilon_0}\cdot\frac{1}{\varepsilon_1}\cdot\nabla\times\left(H_0\cdot\exp[i\beta z+ik_3x]\,\mathbf{e}_y\right)\\ &= \frac{H_0}{i\omega\varepsilon_0}\cdot\frac{1}{\varepsilon_1}\cdot[i\beta\mathbf{e}_x-ik_3\mathbf{e}_z]\cdot\exp[i\beta z+ik_3x].\end{aligned} \tag{5.2}$$

Both components could in principle be used to excite a plasmonic nanostructure, however, the E_x component would require the fabrication of upright standing structures with a high aspect ratio, which makes the device mechanical fragile.

An interesting possibility is to use the E_z-component, corresponding to a longitudinal excitation scheme which is different from quasi-static excitation. From Eq. (5.2), the magnitude ratio compared to the transverse component is given by

$$\frac{|E_z|}{|E_x|}=\frac{k_3}{\beta}=\left[1-\frac{\varepsilon_3}{n_{\text{eff}}^2}\right]^{1/2}. \tag{5.3}$$

A waveguide in the »weakly-guiding« limit would have $n_{\text{eff}}^2\approx\varepsilon_3$ and the solution becomes plane-wave like, with a negligible longitudinal field component E_z. The effective index of truly guided waveguide modes generally obeys the relation

$$\max\{\varepsilon_1,\varepsilon_3\}<n_{\text{eff}}^2<\varepsilon_2 \tag{5.4}$$

in the case of lossless materials. If we use a high-index core material, the longitudinal electric field component will gain enough strength to excite surface plasmons in propagation direction. This excitation scheme is significantly different from a plane-wave excitation and only possible in such a waveguide environment[1]. We choose Si_3N_4 with $\varepsilon_2=4.0$ for our test system due to its high permittivity and good transparency. From the calculation displayed in Fig. 5.1 the required layer thickness is determined as $d=350\,\text{nm}$. For this test system, the minimum field components ratio in the wavelength range of interest according to Eq. (5.3) is 0.72. The right side of Fig. 5.1 shows a to-scale comparison between the different field components in the TM case, revealing that the E_z-component has indeed a high magnitude at the cladding interface.

[1] The $E_z(\mathbf{r},\omega)$-component could be provided by grazing incidence of a plane wave in TM polarization, but only with wavenumbers *inside* the light cone.

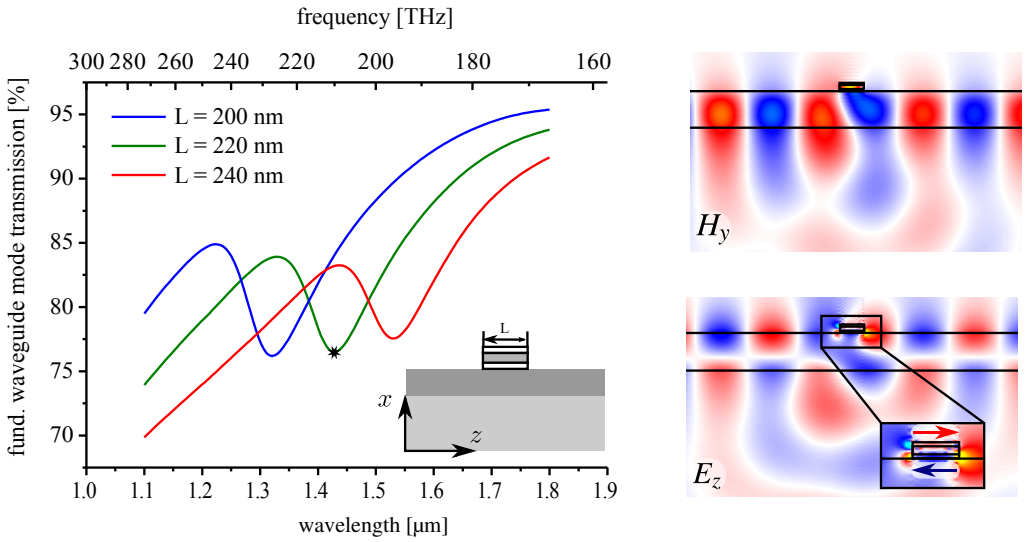

Figure 5.2. A-FMM calculation of the waveguide-nanoparticle interaction. (left) Calculated transmission in the TM_0 waveguide mode for a single double cut-wire on top of the waveguide. The length L shifts the plasmonic particle resonance spectrally. (right) The calculated field components at the resonance position reveal a quadrupolar »dark« mode which shows an effective magnetic response.

Waveguide-Nanoparticle interaction. To test our assumption about the new excitation scheme in TM polarization, we employ the nanoparticle geometry shown in the inset of Fig. 5.2. This two-dimensional structure is known as *cut-wire pair*, a configuration which has been considerably studied in the metamaterial literature [285–288]. Two metal wires are separated by a thin dielectric spacer. A suitable electric polarization along the wires creates a fast-oscillating electric current which gives rise to a plasmon mode in each wire. Depending on the thickness of the spacer, the evanescent fields of the upper and lower plasmon modes overlap, which causes a hybridization into a symmetric (dipolar characteristic) or antisymmetric (quadrupolar characteristic) eigenmode of the entire structure. The latter has the appealing property of creating an unusual response to the incident light. Acting in a coil-like manner, it generates an *effective* magnetic response at optical frequencies [289, 290]. Metamaterials or metasurfaces made of these structures have been investigated in the line of the search for negative refraction [20, 215, 285, 291].

For our purposes, the cut-wire pair geometry is an ideal test structure. We choose the upper and lower wire as 20 nm gold, separated by a 40 nm thick dielectric spacer made of MgO ($\varepsilon = 2.89$).

We want to investigate the possibility to excite the antisymmetric resonance with the longitudinal electric field component E_z and thus generate effective optical magnetism in this waveguide environment. We use the s-FMM to simulate the modal reflection and

transmission. A considerable numerical challenge lies in the very small layer thicknesses, which give rise to a large extent in the spatial frequency domain. Particular care has to be taken in order to assure convergence of the calculation. The x-direction has been sampled using $2^{14} \approx 1.6 \times 10^4$ sampling points, while the size of the computational window was chosen as $5\lambda_0$. One must keep a high number of FOURIER harmonics in the calculation in order to obtain an accurate result. For our case, the truncation order was $N = 125$. In Sec. 3.2 we have already shown that an impedance framework can also be employed to model this type of structures.

Fig. 5.2 shows the result for the transmission in the fundamental TM mode of the waveguide for different lengths of the particle. One finds the general trend that the transmission decreases for decreasing wavelength. This can be explained by the off-resonant scattering of the particle, which is expected to increase with decreasing wavelength [292].

A resonant feature is also visible in the transmission spectrum, which changes its spectral position with changing length of the particle. A nanostructure which is 40 nm longer causes a spectral redshift of ≈ 250 nm. The bandwidth of the feature is ≈ 100 nm. Both properties underline the plasmonic nature of the resonance.

The right side of Fig. 5.2 shows the calculated electromagnetic field at the resonance. One finds exactly the analytically predicted structure of Fig. 5.1 for the E_z-component of the fundamental TM waveguide mode, which possesses its highest magnitude at the interface where the nanoparticle is located. The off-resonant scattering, mainly towards the substrate side, is also visible. The nanoparticle itself shows a strong enhancement of the electromagnetic field in its close vicinity (sub-wavelength localization). The E_z-component in the upper and lower gold layer are anti-parallel. This quadrupolar mode does not enhance the scattering resonantly, since its symmetry limits the overlap to modes propagating in free space. The dip in the spectrum is thus mainly caused by the resonantly increased absorption in the lossy metal. The localized resonance emerges from the repetitive reflection of the anti-parallel mode of the metal-insulator-metal structure at the free termination. Its length as well as its modal dispersion determine the resonance frequencies in full accordance with the description we developed to derive the resonances of nanoantennas in Sec. 4.1.1.

These calculations confirm that it is possible to excite the anti-symmetric (»magnetic«) resonance of a cut-wire pair in a waveguide geometry by exploiting the longitudinal electric field component. This promises interesting features when we switch from a single structure to a regular lattice of structures, *i. e.* we want to investigate what happens if we cover the waveguide by a metasurface made of cut-wire pairs.

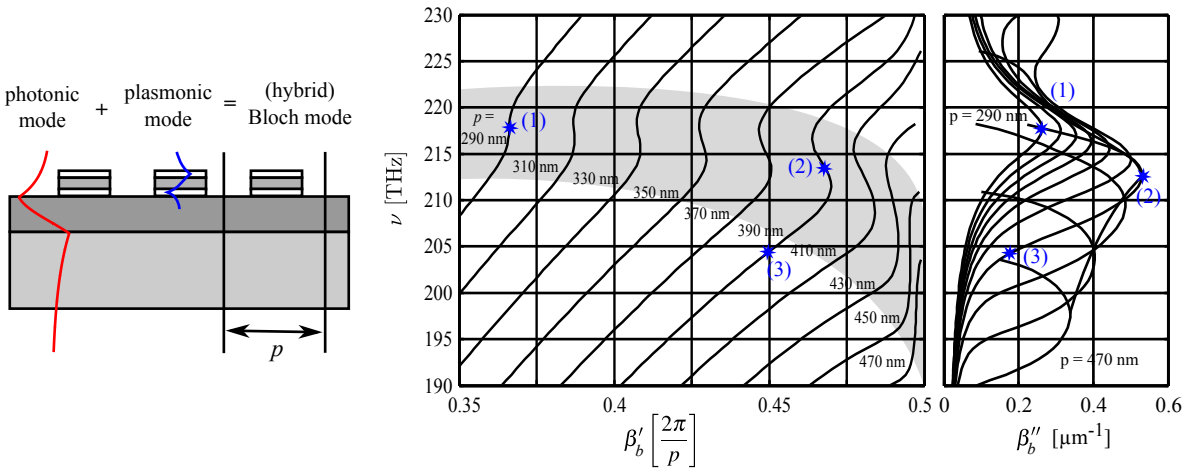

Figure 5.3. (left) Interaction scheme in the lattice configuration. The photonic mode in the waveguide hybridizes with the localized plasmonic modes in the particles to form a Waveguide Plasmon Polariton state. The period p is the critical coupling parameter. (right) Calculated band diagram of the fundamental TM_0 BLOCH mode in the first band. Depending on p, different regimes of hybridization occur which show extreme dispersion properties such as superluminality or negative group velocity. The calculated mode fields of the marked points are shown in Fig. 5.4.

5.2. Lattice configuration: Waveguide-Plasmon-Polariton

We consider the configuration shown on the left side of Fig. 5.3. The dielectric slab waveguide is operated in its fundamental TM mode in the NIR wavelength range as before. The characteristics of the excited localized resonance in the nanoparticle will critically influence the properties of the BLOCH mode in the lattice configuration with period p. For a simple plasmonic wire structure, the excitation of an oscillating dipole mode is most prominent and has been demonstrated experimentally [293–302]. However, a dipolar mode has the disadvantage of high radiative loss in the system due to a continuous out-coupling of energy into far-field radiation. Hybrid modes in such systems will thus generically be of leaky character [303]. This problem is solved by the cut-wire geometry. The last section has proven that it is possible to excite its »dark« resonance from the waveguide's fundamental TM mode. We are now going to investigate the propagation properties of a lattice of these nanostructures on the waveguide.

Waveguide-Plasmon-Polariton. Structures of this kind (nanostructure lattices on top of a waveguiding layer) have been investigated in the literature earlier under the term »metallo-dielectric photonic crystal«. The hybridized state has been given the name »Waveguide-Plasmon-Polariton« (WPP) [304–314]. However, the focus of these inves-

tigations was a regime where the configuration was illuminated by a plane wave from free-space. Consequently, the authors used a second-order BRAGG grating where the period is equal to the wavelength divided by the effective index of the waveguide. When we recall the considerations for the antenna grating in Sec. 4.2.1, we see that this results in a coupling between three modes, since the WPP state is in the light cone and acts with normally incident light at the center of the BRILLOUIN zone. The interaction of localized modes with the continuum of radiation modes has been shown to produce a FANO resonance in the transmission spectrum with an asymmetric line shape [315].

In contrast, we are targeting here for an operation regime of a truly guided, resonant WPP state *outside* the light cone and make use of a *first* order BRAGG grating, where the period is *half* of the wavelength in the medium. While former investigations were conducted from the viewpoint of photonic crystals with metallic resonators, we want to employ the viewpoint of integrated optics with plasmonic nanostructures / metasurfaces here [316, 317].

Dispersion of the fundamental Bloch mode. When switching from a single nanostructure to a lattice with period p, the most important question is if this configuration has a truly guided mode. Due to the periodicity in propagation direction z, modes in the structure are of pseudo-periodic BLOCH type with a pseudo-wavenumber β_b, as has been explained in Sec. 2.1.2. We fix the length of each individual particle to be $L = 220\,\mathrm{nm}$. The minimum of the waveguide transmission for the single particle scattering in Fig. 5.2 for this length is marked with an asterisk. Its frequency is $\omega_{\mathrm{ff}} = 2\pi\cdot 210\,\mathrm{THz}$ ($\lambda_0 = 1430\,\mathrm{nm}$), which can be called the »far-field« resonance frequency.

We now investigated lattice periods p between 290 nm and 470 nm with our a-FMM code. The analysis indeed reveals the existence of a truly guided mode in the first band of the system, where β_b' lies under the substrate light line. The right side of Fig. 5.3 shows its calculated band diagram $\beta_b(\omega)$ for different values of the lattice period p.

In the case of a dense lattice, *i. e.* for small values of the period, the dispersion characteristics follows the photonic mode of the dielectric waveguide, despite the occurrence of a resonant feature at $\omega_{\mathrm{plas}} = 2\pi\cdot 217\,\mathrm{THz}$ ($\lambda_0 = 1382\,\mathrm{nm}$). It is blue-shifted with respect to the far-field resonance $\omega_{\mathrm{plas}} > \omega_{\mathrm{ff}}$, a phenomenon which is well-known for nanoscale scatterers with multipolar resonance characteristics [318]. An investigation of β_b'' reveals a *Lorentzian* instead of a FANO lineshape [319, 320], which was found earlier in plane-wave studies of metallo-dielectric photonic crystals [315]. This underlines that the modal

interference mechanism in the waveguide environment is different from the plane-wave excitation case and depends on the specific eigenmode coupling rather than the mere existence of »bright« and »dark« modes [320]. The frequency of the BRAGG resonance, which determines the spectral position of the band gap $\omega_{\mathrm{bg}} = c/n_{\mathrm{eff}} \cdot \pi/p$, is higher than the resonance frequency of the plasmonic nanoparticles $\omega_{\mathrm{plas}} < \omega_{\mathrm{bg}}$ in this dense lattice case, so that the effects occur in the fundamental band of the BLOCH periodic structure.

The situation changes, when the period of the lattice is increased, so that the plasmonic resonance comes closer to the band edge $\omega_{\mathrm{plas}} \lesssim \omega_{\mathrm{bg}}$. A redshift of the resonant feature indicates a strong interaction regime. The dispersion shows an increasing backbending until $\mathrm{d}\omega/\mathrm{d}\beta_b'$ diverges, *i. e.* a superluminal regime [321]. One has to keep in mind that the group velocity in lossy, periodically structured media $v_g = \mathrm{d}\omega/\mathrm{d}\beta$ becomes a complex quantity since β is complex. CHEN *et al.* [192] have shown, how the group velocity needs to be interpreted in terms of the adjoint modal formalism. It is generalized to a »adjoint field velocity«, which is the ratio of an adjoint flux and an adjoint field density. The latter two quantities are the generalization of the POYNTING flux and energy density for the case of lossy media. When interpreted in this way, the quantity v_g' still yields the velocity of the time-domain peak of a Gaussian pulse, even in the case of superluminality, which has been proven experimentally [322, 323]. A pulse which travels through such a medium undergoes a significant reshaping of the temporal envelop, which is associated to v_g'' [324]. This underlines that the usage of the adjoint modal formalism as generalization for lossy structures is of utmost importance for the interpretation of these complex photonic systems.

In the region where the bandgap and the plasmonic particle resonance overlap spectrally, even a negative group velocity $v_g' < 0$ is reached (»backward wave«). This unusual effect, where the peak of a Gaussian pulse appears at the backside of a structure before the pulse has even entered it, was much debated or even regarded unphysical, until it was experimentally proven [322, 323, 325]. Our systems can be seen in some analogy to previous studies on coupled-resonator optical waveguides, which also predicted the occurrence of a negative group velocity when in the inter-resonator coupling is thoroughly tuned [326]. Periodic structures that include materials with anomalous dispersion have also been shown so exhibit such states with infinite group velocity points or »dispersion bubbles« [327–329].

In our system, the behavior can be understood by the characteristic of the fundamental BLOCH mode. The localized resonances of the individual nanostructures are coupled

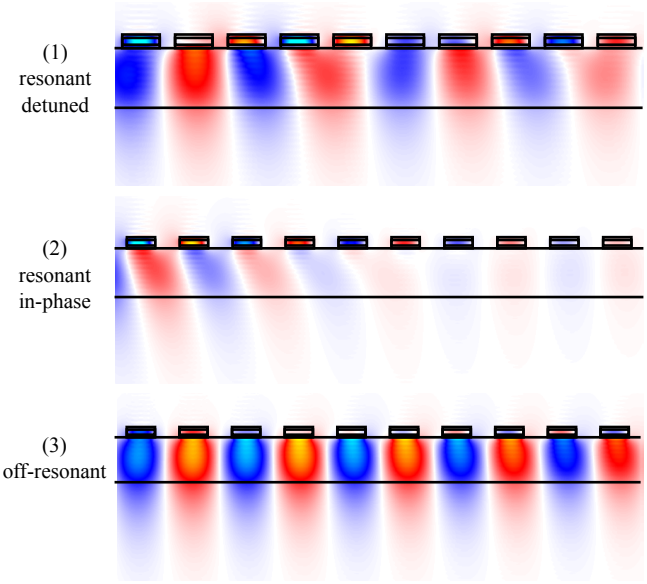

Figure 5.4. H_y field component for the TM_0 BLOCH mode in the lattice configuration calculated by the a-FMM. The three scenarios correspond to the three marked positions in the band diagram Fig. 5.3. (1) Spectral position of the plasmonic resonance in the case of a dense lattice. Although some structures are excited, neighboring structures are detuned in excitation. (2) Phase-matched case at a spectral position of negative group velocity. The magnetic response of all structures is phase-matched. (3) Off-resonant position in the spectrum. The mode behaves as the ordinary slab waveguide mode.

by the photonic mode. This interaction channel is phase dependent and differs fundamentally from the coupling of nanostructures via near-field interaction. The excitation between two neighboring resonators happens with a phase difference $\Delta\varphi = n_{\text{eff}} \cdot k_0 \cdot p$ and can by itself become resonant when it reaches π, *i. e.* close to the band edge. The plasmonic resonances of all nanoparticles will be in-phase here, which leads to a further increase in the resonant field strength. The backbending of the dispersion relation is a sign of the unusual behavior of the BLOCH mode in this regime which can be viewed as a resonant excitation of antisymmetric plasmonic resonances. The POYNTING vector in the near-field does not point into the forward direction everywhere. The Lorentzian shape of β_b'' in the dense lattice case gets altered towards a parabolic shape, which is characteristic for states within the band gap.

Electromagnetic fields of the fundamental Bloch mode. The investigation of the calculated electromagnetic fields of the fundemantal BLOCH mode reveals interesting physical insight into the resonant excitation process. Fig. 5.4(1) shows a time snapshot at the frequency ω_{plas} for the dense lattice case. The field within the Si_3N_4 resembles the field of the unstructured dielectric waveguide. Although the localized plasmon mode is excited in the nanostructures, neighboring particles are phase-mismatched in excitation. This results in a lower overall excitation strength which can consequently not efficiently influence the propagation properties of the hybrid BLOCH mode.

In contrast, Fig. 5.4(2) shows the same fields in the strong coupling regime, where the

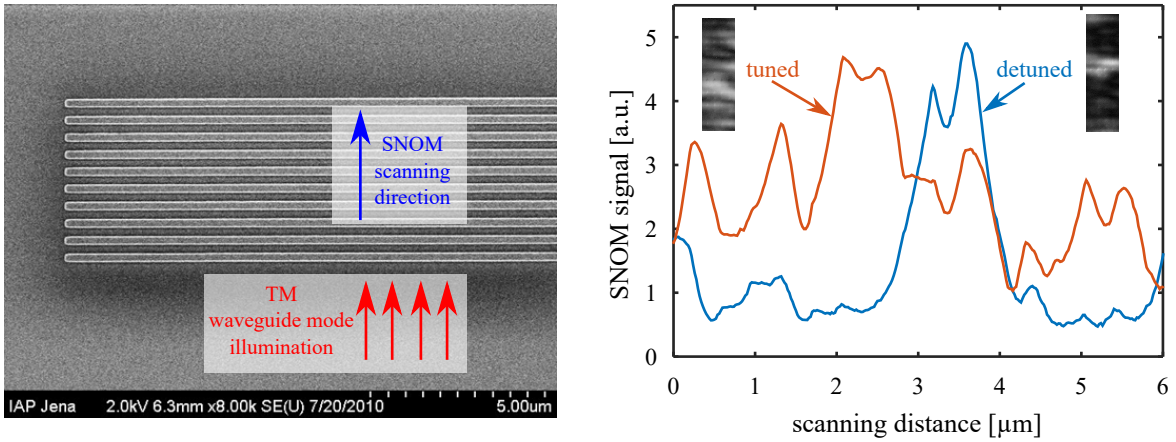

Figure 5.5. (left) SEM image of the fabricated sample for the SNOM experiment. (right) SNOM signal for the »detuned« (1) and the »in-phase« (2) case of Fig. 5.4.

backbending of the dispersion takes place. Neighboring particles are phase-matched in excitation now, leading to a »phase-coupled« resonant excitation of the individual plasmonic resonances. In the off-resonant case (3), however, the waveguide acts much as if the nanoparticles were not there at all.

Effective parameters. Since the analysis revealed just a single guided BLOCH mode, one may regard the lattice of nanostructures as an effective metasurface and the whole structure as a »metawaveguide«. It can be described by the fundamental BLOCH mode's effective index $n_{\text{eff}} = \beta_b/k_0$ and a modal impedance Z_b with respect to the dielectric waveguide as already shown in Chapter III. However, one must keep in mind that the reduction of the optical properties to one predominant mode, the Fundamental BLOCH Mode Approximation, is a necessary prerequisite for this. Other interaction scenarios of similar »nanoparticle-on-waveguide systems« might better be described as antennas coupled to waveguides, since they lack a truly bound state and a continuum of leaky states does not allow for a meaningful simplification to a small number of effective parameters.

Experimental demonstration. We fabricated lattices of cut-wire pairs on top of a Si_3N_4 slab waveguide, as described above. The structure is shown on the left side of Fig. 5.5. A tunable laser source (Santech TSL 1260 nm - 1620 nm) was used to generate an elliptical focus, which was coupled into the fundamental TM waveguide mode. The light propagated to the nanostructured region with low lateral divergence. This resembles the situation we analyzed in theory above. In the nanostructured region, the light is propa-

gating in the fundamental BLOCH mode. We mapped the electromagnetic field from the top using a SNOM in collection-mode with a dielectric tapered fiber tip.

We are interested in the field patterns at resonance for the »detuned« case (1) in Figs. 5.3 and 5.4, as well as the »in-phase« case (2). They are shown on the right side of Fig. 5.5. We excluded the region at the beginning of the nanostructured area for our comparison to eliminate transient effects between the structured and the unstructured region, since we are interested in the BLOCH mode properties.

In the detuned case, we witness a strong increase of the SNOM signal, but only at a specific position in the lattice. The nanostructures show a high excitation strength there, but other nanostructures are not excited, although the laser operates at their individual resonance frequency. This picture changes in the tuned case. The excitation strength reaches the same maximum value, however, many nanostructures everywhere in the lattice are now excited.

This behavior is in agreement with our theory above. In the first case, the phase mismatch between neighboring particles leads to a detuning of the resonant coupling between the nanoparticles in propagation direction. Consequently, only few nanostructures appear excited at the same time. In the second case, the phase mismatch between the particles is eliminated, leading to a resonant interaction as explained in the previous section. All particles appear to be excited at the same time.

Application perspectives. Plasmonic nanostructures are widely used for chemical sensing. The field enhancement at resonance can increase the signal contrast due to a stronger interaction with the analyte [330, 331]. This can boost the sensitivity even down to the single-molecule level. In a waveguide environment, ultra-compact lab-on-a-chip systems become possible. Existing schemes for integrated spectroscopy suffered from the low overlap of the waveguide mode, usually in a high-index semiconductor, and the analyte on top, which is usually in watery solution [332, 333].

At this point, the plasmonic nanostructures we have investigated can help increasing the light overlap with the analyte and at the same time enhance the electromagnetic field. The left side of Fig. 5.6 shows the experimental results, when we scan over an excited particle in the vertical direction. We detect an exponential signal increase with a $1/e$ localization length of 170 nm. With this increased field, particles in very close vicinity of the nanostructure can be spectroscopically detected in the far field by measuring the waveguide fundamental mode transmission.

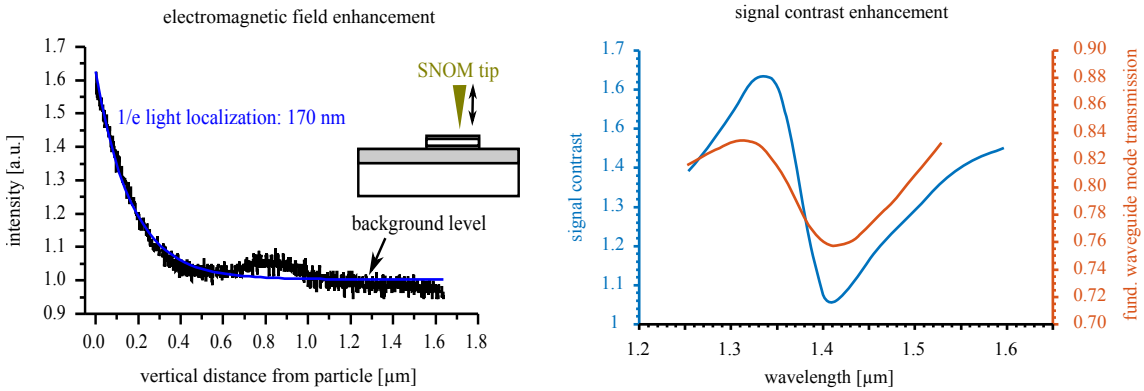

Figure 5.6. (left) The SNOM approach curve to the nanoparticle reveals a sub-wavelength light localization of 170 nm. (right) Signal contrast enhancement by the nanoparticle for integrated absorption spectroscopy. The highest enhancement does spectrally not coincide with the lowest far-field transmission.

We investigate this mechanism further by including an artificial analyte in our a-FMM simulation, which has a Lorentzian absorption peak within the bandwidth of the plasmonic resonance. We compare the far-field waveguide mode transmission without nanostructure and with nanostructure on top on the right side of Fig. 5.6 and plot the waveguide mode transmission *without* analyte for comparison. We see that the presence of the particle increases the signal contrast in the spectral region of the plasmonic resonance. However, the maximum enhancement of ≈ 60 % does spectrally not coincide with the minimum in transmission, but occurs at the spectral position of maximum field strength in the near-field. This can be attributed to the spectral shift between near-and far-field resonance [318] as well as the underlying FANO resonance mechanism [315, 319] in the system [334]. In this manner, ultra-sensitive spectroscopy becomes possible at high transmission levels with this scheme.

A second perspective for applications lies in dispersion engineering. The waveguide environment has been shown to provide a unique coupling scheme for the localized modes of plasmonic nanoparticles which can vice versa create unexpected propagation properties of the hybridized structure.

The system is an interesting class of structures for dispersion engineering in waveguides by modal tuning, although most studies focus on the creation of »slow-light« devices which enhance light-matter-interactions. The combination with plasmonic elements enriches the possibilities of enhancement mechanisms and allows the creation of complex light states [329, 335]. The occurrence of an inflection point in the dispersion relation can have a beneficial effect on the modal coupling properties [336–340].

Phase-coupling via a photonic mode of the waveguide can in principle be much stron-

ger than near-field coupling since it is not intrinsically limited in range. It can make particles interact coherently over a whole lattice while near-field coupling is limited to nearest-neighbor interactions. The system is attractive for exploiting coherent effects like electromagnetically induced transparency in integrated optics [341–344].

By adding plasmonic nanostructures to the cladding of a waveguide, it becomes possible to tailor the relevant dispersion parameters over a large range. Dispersion-engineered integrated optical devices may emerge from such an ansatz which could find use in optical communication or integrated quantum optical technologies. As for many plasmonic applications, the high metal loss is a problem and might be solved by switching to dielectric metasurfaces of the »Huygens-type« [345–347].

However, the platform of waveguides modified by metasurfaces awaits further exploration in the future. The occurring phenomena like negative group velocity, electromagnetically induced transparancy or FANO resonances require an involved theoretical and numerical apparatus to be exploited for applications. We have shown here that using the adjoint modal formalism for computation and theory will play an important role along that way.

VI. Summary and Outlook

At the beginning of the thesis, we started with the question how one can employ a framework for the analysis and design of nanooptical structures that gives maximum insight into the underlying physics. The art of rigorous numerical computing has made a dramatical development throughout the last years and found an established place in nanooptics. Commercial programs are available which perform a »numerical experiment«, irrespective if the operator understands how the program works, which prerequisits it has, or which mathematical assumptions it makes. While this greatly eases the possibilities for optimization of a certain structure design, it leaves almost no insight how a physical model of the structure may look like and what the relevant parameters are. Computers cannot (yet) *understand* a structure and come up with entirely new designs based on *ideas* and *models*. Gravitational waves were not postulated by a computer that solved the non-linear field equations of general relativity rigorously, but by a genius who saw that these equations contain a linearized wave solution as low order expansion term [348].

Modal decomposition of the HELMHOLTZ equation is a natural choice for such a framework and has widely been applied for RF engineering, laser resonator design, or optical fibers in the past. However, the methodology taught by the standard textbooks in the field strictly holds only for *lossless* structures. The reason is simple: Nobody wants loss in optical structures, so one better uses lossless materials. There was no practical need to consider dissipation beyond a level which can be treated perturbatively. In plasmonics, where noble metals are used at optical frequencies, this is not possible anymore. Material loss is an inevitable companion when designing functional plasmonic structures.

To tackle this problem, we went back to a basic relation contained in MAXWELL's equations: reciprocity. While »the« reciprocity theorem is usually formulated using the time-averaged POYNTING flux density $\langle \mathbf{S}(\mathbf{r}) \rangle$ and energy density $\langle U(\mathbf{r}) \rangle$, it is not well-reflected in the literature that this just works when the system is entirely free of dissipation. Only for this case the HELMHOLTZ operator is Hermitian with the consequence that its eigen-

functions form a complete orthonormal basis. These properties are destroyed by the presence of loss.

However, we could restore them by switching to an alternative formulation of reciprocity which is complex valued in general and not related to energy considerations. The »adjoint formulation« makes use of the biorthogonality relation which exists between the eigenfunctions of the non-selfadjoint operator $\hat{H}$ and $\hat{H}^\dagger$. They are linked to the forward and backward modes of the system. The span of all modes in one direction, which was a orthonormal complete set in the lossless case, is now only biorthogonal complete with its adjoint counterpart. However, the mathematical framework stays fully intact, albeit with unusual consequences (modes are orthogonal on themselves). The POYNTING flux density $\mathbf{S}(\mathbf{r})$ is replaced by the »adjoint density« $\mathbf{F}(\mathbf{r})$, which is preserved during propagation also in the dissipative case.

The calculation of the modes themselves is a task where numerical computational support is indispensable. From the several numerical methods at hand we chose to implement the aperiodic Fourier Modal Method (a-FMM) because it allowed the calculation of the modes relevant for this thesis on the one hand, but provided also a means to compare our models to rigorously calculated reflection and transmission data. Since we investigated exclusively waveguiding structures in the thesis, the usage of anisotropic Perfectly Matched Layers was necessary. The use of FOURIER series for these kind of structures requires to keep a high number or FOURIER harmonics in the calculation in order to be accurate. For future works, one may thus think of a numerical method which uses a different technique to calculate the modes, *e. g.* by the Finite Element Method, and keeps the scattering matrix approach of the FMM based on the adjoint mode fields, *i. e.* a »Finite Element Adjoint Modal Method«. This would significantly improve the workflow of the adjoint modal analysis.

In the thesis, we have entirely concentrated on the formulation of the HELMHOLTZ problem with a complex eigenvalue $\beta^2(\omega)$ and ω as a real parameter. Future works should also explore the implications of the formulation with a complex ω^2, which is well suited to model the temporal behavior of localized resonators. One could combine these with the spatial multipole expansion to better understand the ultrafast resonance behavior of these structures.

The central goal of making a physical model for complicated structures is to describe them by simple parameters, preferably in the same way as one describes homogeneous media. Much of the homogenization debate for metamaterials was about how to obtain

and interpret the »negative refractive index«. The solution was that the effective index of a particular BLOCH mode plays that role when only this one is predominantly excited. This was called the Fundamental Mode Approximation (FMA) and led to the concept of »BLOCH lattices« with »BLOCH material parameters«. Among them is also the impedance which describes the coupling of a structure with its surrounding. We investigated how an impedance definition may look like based on the adjoint mode formalism. Our central requirement was that the impedance would reproduce the complex reflection coefficient from an interface of discontinuity between two structures. It turned out that the introduction of a *scalar* impedance is directly linked to the validity of the FMA. We derived a master equation for the adjoint impedance ratio of a structure under consideration and a reference structure. The modal contributions are entangled in the integral and not separable in the general case. When there are additional modal symmetries present or when a modal reference frame with high symmetry is used, however, the expression allows for a significant simplification. In this way *absolute* impedance definitions become possible. We were able to show that our master equation in that way reproduces the expressions for genuinely homogeneous media, waveguides in the radio frequency range (such as coaxial wires) and the BLOCH impedance of homogenizeable metamaterials. It thus represents a natural generalization of the impedance which is valid all the way from electronics to plasmonics. Especially *transversality* in conjunction with invariance in propagation direction was shown to be a key feature which allowed to derive a generalization of the classical tangential impedances. Remarkably, the difference just occurs in TM polarization in the form of the adjoint-mode-averaged impermittivity $\left\langle \varepsilon^{-1} \right\rangle$. This explains many of the difficulties which occurred especially in plasmonics, since the whole field is based on TM polarized modal solutions. However one must always keep in mind that also an *absolute* value for the impedance of a certain structure is just valid with respect to the reference frame. The impedance of a nanoantenna with respect to free space will hardly have the same value as the impedance of the same nanoantenna with respect to an optical feed waveguide.

From our investigations we can now give a full systematic of the generalization of model paramters based on the adjoint modal framework. It is shown in Tab. A.1 in appendix A3.

There are a couple of structures which are at the heart of nanooptics: nanoantennas for light, plasmonic waveguides, grating structures and lattices of plasmonic elements, so called »metasurfaces«. Therefore, we demonstrated our impedance formalism successfully

for two examples: a grating reflector for a Surface Plasmon Polariton (SPP) waveguide and a dielectric waveguide covered by a metasurface of double cut-wire pairs, which also played a role in Chapters IV and V.

Further investigations should attempt to investigate more symmetry groups of structures, especially in 3D. Examples can include chiral structures or structures with an effective anisotropy. Since our general formula for the adjoint impedance ratio is valid irrespective of the modal symmetry, it is a good starting point from which one can explore the possibilities of finding impedance expression for these cases.

In Chapter IV, we investigate how the impedance mismatch of a finite sized waveguide leads to a localized antenna resonance when the coupling between the adjoint mode pair is phase matched. This led to a Fabry-Pérot-type round-trip model based on adjoint modal parameters and allowed the identification of a tuning strategy. The evanescent BLOCH mode of an SPP grating was used to increase the feedback from the antenna termination. We used the second BRAGG resonance in order to allow also an increased coupling to normally incident radiation, the »disc-ring antenna«. While we performed our theoretical investigations on plane SPP gratings, we experimentally realized a concentric version. Conceptually it differs only in the detail that the radial mode function is not a plane wave any more but a slightly more complicated HANKEL function which has deviating near-field terms close to the origin. The dispersion relation, however, remains unaltered. The adjoint mode pair is given by the inward and outward-propagating HANKEL Surface Plasmon Polaritons (HSPP). We experimentally investigated the theoretical predictions by Scanning Near-field Optical Microscopy (SNOM) and multiphoton Photoemission Electron Microscopy (n-PEEM). Especially for the latter we had to develop a model for the spatial distribution of the nonlinear electron yield, which we think is *not* attributed to the »intensity^n-model«, but rather a time-domain formula which accounts for the repetitive *linear* dipole-field interactions based on FERMI's golden rule. This was necessary because we used a ultrafast 30 fs laser source which required substantial spatio-temporal modeling of the process. The results of the experiments are in very good agreement with the analytical modal considerations.

Future works can use much more sophisticated approaches to realize a modal tuning of antenna geometries. In the field of n-PEEM, more experiments are necessary to clarify the specific details of the yield model.

In Chapter V, we investigated the coupling between a dielectric waveguide and plasmonic nanostructures placed on top of it. We used the double cut-wire geometry to explore

the possibility of exciting a »dark« mode with quadrupolar character. The specific polarization properties of the fundamental TM waveguide mode made it possible to excite the structure with the longitudinal component of the electric field. The system which is composed of the dielectric waveguide and a periodic lattice of these structures (metasurface) on top shows interesting dispersion properties. Close to the band edge, the adjoint mode pair of waveguide modes gets coupled and hybridizes with the localized plasmonic resonance into a Waveguide Plasmon Polariton state. The group velocity, *i. e.* $\mathrm{d}\omega/\mathrm{d}\beta'$, gets superluminal and even negative in the spectral region of the hybridization (backward wave). This needs to be understood in terms of the adjoint field velocity that was introduced based on the adjoint modal formalism earlier. The system thus represents an interesting platform to realize extreme light properties in an relatively easy to fabricate waveguide environment.

Another application lies in integrated absorption spectroscopy, when an analyte with a spectral absorption peak is placed on top of a waveguide and the transmission in the fundamental waveguide mode is measured. If one compares the signal contrast per unit length for the case with and without nanostructures on top, we have shown that a $\approx 60\,\%$ increase is possible at the spectral position of the highest near-field enhancement. The possibilities for a practical use of the system for dispersion engineering or spectroscopy are still largely unexplored and can be subject of further studies.

If we summarize the content of the whole thesis, we must first note that the adjoint modal formalism should become a textbook knowledge for any physicist dealing with lossy plasmonic structures since it resolves many uncertainties and mysteries about effects such as negative refraction, perfect lensing, superluminality or backward waves. The generalization of model quantities such as the refractive index or the impedance allows to treat sophisticated dissipative structures in the fashion of engineer's formulas. This way leads to a much clearer understanding of the analysis and design process of future functional nanooptical structures.

A. Appendix

A1. Derivation of the modified Gauss' theorem for electromagnetic modes.

We start with a vector function $\mathbf{A}$ and define a finite volume V in which $\mathbf{A}$ is well-behaved (integrable). GAUSS' theorem relates the volume integral over the divergence of $\mathbf{A}$ to a closed surface integral of second kind [232]

$$\iiint_V \nabla \cdot \mathbf{A}\,\mathrm{d}V = \oiint_{\partial V} \mathbf{A}\,\mathrm{d}\mathbf{S}. \tag{A-1}$$

As integration volume we specify a cylinder with radius R and the cylinder axis parallel to the z-direction (between z_1 and z_2). We split the surface integral into contribution from the three different surfaces and their outward pointing surface normals, which yields using cylindrical coordinates [232]

$$\oiint_{\partial V} \mathbf{A}\,\mathrm{d}\mathbf{S} = \int_0^{2\pi}\int_0^{R} \mathbf{A}(r,\varphi,z_2)\cdot\mathbf{e}_z\, r\,\mathrm{d}r\,\mathrm{d}\varphi - \int_0^{2\pi}\int_0^{R} \mathbf{A}(r,\varphi,z_1)\cdot\mathbf{e}_z\, r\,\mathrm{d}r\,\mathrm{d}\varphi + \int_{z_1}^{z_2}\int_0^{2\pi} \mathbf{A}(R,\varphi,z)\cdot\mathbf{e}_r\, R\,\mathrm{d}\varphi\,\mathrm{d}z. \tag{A-2}$$

We will now make a transition $z_2 \to z_1, R \to \infty$, while V stays constant. The important part is the behavior of the last term. In the light of LORENTZ' reciprocity theorem, $\mathbf{A}$ has the meaning of a bilinear form on the electromagnetic modes. For bound modes, the last term in Eq. (A-2) vanishes since the electromagnetic fields must be square-integrable. $\mathbf{A}$ will consequently vanish at infinity. More delicate are radiative and leaky modes, since they formally carry an infinite amount of energy and $\mathbf{A}$ does not vanish on the outer boundary. However, one has to reconsider the finiteness of the volume while reaching the limit. As long as A stays integrable within any *finite* volume, the cladding term will vanish in the limiting case of a vanishing boundary at infinity, even if $\mathbf{A}$ does *not* vanish

on this boundary itself. Integrability over a finite volume applies to any electromagnetic radiation (square integrable within a finite volume). With this argumentation we can state with confidence that the last term in Eq. (A-2) will vanish for *any* electromagnetic mode, may it be bound, evanescent, radiative or leaky.

The next step is to understand the volume integral in Eq. (A-2) as the variation of a (now *non*-closed!) surface integral along the z-direction

$$\left[\iint\limits_{(x,y)\in\mathbb{R}^2} \nabla\cdot\mathbf{A}\,\mathrm{d}S \right] \delta z = \delta \left[\iint\limits_{(x,y)\in\mathbb{R}^2} \mathbf{A}\cdot\mathbf{e}_z\,\mathrm{d}S \right]. \tag{A-3}$$

We can therefore deduce the final result

$$\iint\limits_{(x,y)\in\mathbb{R}^2} \nabla\cdot\mathbf{A}\,\mathrm{d}S = \frac{\partial}{\partial z} \left[\iint\limits_{(x,y)\in\mathbb{R}^2} \mathbf{A}\cdot\mathbf{e}_z\,\mathrm{d}S \right]. \tag{A-4}$$

A2. Adjoint impedance ratio of a SPP-grating interface

Here, we want to find the explicit expression for the relative impedance of a SPP-to-grating interface to illustrate our findings in Sec. 3.2.

An SPP mode has a simple field dependence. In the coordinate system used throughout this thesis, only the H_y-component is non-zero, compare Sec. 2.1.2. The general expression for the relative impedance Eq. (3.23) simplifies to

$$\frac{Z}{Z_{\mathrm{ref}}} = \frac{\int E_x(x,z_0)\cdot H_y^{\mathrm{ref}}(x,z_0)\,\mathrm{d}x}{\int E_x^{\mathrm{ref}}(x,z_0)\cdot H_y(x,z_0)\,\mathrm{d}x}. \tag{A-5}$$

We can express $E_x(x)$ by $H_y(x)$ in homogeneous and source-free regions of the geometry using MAXWELL's equations. This yields

$$E_x(x,z_0) = -i\,\frac{Z_0}{k_0\varepsilon(x)}\cdot\left.\frac{\partial H_y(x,z)}{\partial z}\right|_{z_0}. \tag{A-6}$$

The interesting feature is the different mathematical structure of the modal solutions on both half-spaces. The reference mode (simple SPP) is a z-invariant solution and yet of

the form

$$H_y^{\text{ref}}(x,z) = (\text{some mode function of x}) \cdot \exp(i\beta_{\text{ref}} z) \tag{A-7}$$

$$= \phi(x) \cdot \exp(i\beta_{\text{ref}} z). \tag{A-8}$$

The mode in the grating region is a BLOCH mode. It has the form

$$H_y(x,z) = \begin{pmatrix} \text{some BLOCH mode function of } (x,z); \\ \text{periodic in } z;\ \text{usually not separable} \end{pmatrix} \cdot \exp(i\beta z) \tag{A-9}$$

$$= \psi(x,z) \cdot \exp(i\beta z). \tag{A-10}$$

This effects directly the derivative with respect to z and generates an additional term for the BLOCH mode. We find

$$E_x^{\text{ref}}(x,z_0) = \frac{\beta_{\text{ref}} Z_0}{k_0 \varepsilon_{\text{ref}}(x)} \cdot H_y^{\text{ref}}(x,z_0) = n_{\text{eff}}^{\text{ref}} \frac{Z_0}{\varepsilon_{\text{ref}}(x)} \cdot \phi(x) \cdot \exp(i\beta_{\text{ref}} z) \tag{A-11}$$

$$= \frac{Z_0}{\varepsilon(x)} \left[n_{\text{eff}} \psi(x,z_0) - \frac{i}{k_0} \left. \frac{\partial \psi(x,z)}{\partial z} \right|_{z_0} \right] \exp(i\beta z_0). \tag{A-12}$$

Note that a dependence on the cutting-plane position z_0 of the BLOCH mode enters the equation – a problem well known in Photonic Crystal literature, since their description is entirely based on the discussion of BLOCH modes.

If we insert our findings into Eq. (A-5), we find

$$\frac{Z}{Z_{\text{ref}}} = \frac{n_{\text{eff}}}{n_{\text{eff}}^{\text{ref}}} \cdot \frac{\int \frac{1}{\varepsilon(x,z_0)} \cdot \phi(x) \cdot \psi(x,z_0)\,\mathrm{d}x}{\int \frac{1}{\varepsilon_{\text{ref}}(x)} \cdot \phi(x) \cdot \psi(x,z_0)\,\mathrm{d}x} - \frac{i}{n_{\text{eff}}^{\text{ref}} \cdot k_0} \cdot \frac{\int \frac{1}{\varepsilon(x,z_0)} \cdot \phi(x) \cdot \left. \frac{\partial \psi(x,z)}{\partial z} \right|_{z_0} \mathrm{d}x}{\int \frac{1}{\varepsilon_{\text{ref}}(x)} \cdot \phi(x) \cdot \psi(x,z_0)\ \mathrm{d}x} \tag{A-13}$$

$$= \frac{n_{\text{eff}}}{n_{\text{eff}}^{\text{ref}}} \cdot \frac{\left\langle \varepsilon^{-1}(x,z_0) \right\rangle_{\phi\psi}}{\left\langle \varepsilon_{\text{ref}}^{-1}(x) \right\rangle_{\phi\psi}} - \frac{i}{n_{\text{eff}}^{\text{ref}} \cdot k_0} \cdot \frac{\left\langle \varepsilon^{-1}(x,z_0) \right\rangle_{\phi \frac{\partial\psi}{\partial z}}}{\left\langle \varepsilon_{\text{ref}}^{-1}(x) \right\rangle_{\phi\psi}} \tag{A-14}$$

$$= \frac{n_{\text{eff}}}{n_{\text{eff}}^{\text{ref}}} \cdot \left[1 - \frac{i}{n_{\text{eff}} \cdot k_0} \cdot \mathscr{F}_{z_0}\left(\phi, \psi, \frac{\partial \psi}{\partial z} \right) \right]. \tag{A-15}$$

The term $\left\langle \varepsilon^{-1} \right\rangle_{fg}$ is an abbreviation for tangential averaging of the impermittivity with the product $f \cdot g$ as (complex valued!) weight function. The last step was only possible

because $\varepsilon_{\text{ref}}(x)$ and $\varepsilon(x, z_0)$ are identical at the interface for this special geometry. $\mathscr{F}_{z_0}$ is a functional which contains the mode field functions and their derivative and characterizes the coupling as a measure of entanglement between the two modal systems. This outlines the importance of the choice of the cutting plane z_0, which is in the middle between two corrugations. The interface scattering parameters – most importantly the reflection in our case – need to be evaluated with respect to that plane. A discussion of the implications of this formula is given at the end of Sec. 3.2 where this geometry is investigated.

A3. Summary of adjoint modal generalizations of important quantities

The following table summarizes the adjoint modal generalizations of the most important photonic quantities under the Fundamental Mode Approximation (FMA), as they are used in this thesis. The role of the effective index $n_{\text{eff}}(\omega)$ as a refractive index, especially in the case of a homogenizable metamaterial, is comprehensively discussed in [29, 31–34, 181]. The adjoint modal generalization of the impedance was introduced in [TK2013] and is the main result of Chapter III. The special case of a plane wave reference frame and a violation of the FMA, as it is common for photonic crystals, leads to the matrix impedances introduced by LAWRENCE and co-workers [36–38]. The adjoint field velocity is especially discussed in [192, 329].

lossless homogeneous quantity	adjoint modal generalization	notes
time-averaged POYNTING flux density $\langle \mathbf{S}(\mathbf{r}) \rangle_T = \frac{1}{4} \cdot [\mathbf{E} \times \mathbf{H}^* + \mathbf{E}^* \times \mathbf{H}]$	adjoint flux density $\mathbf{F}(\mathbf{r}) = \frac{1}{4} \cdot \left[\mathbf{E} \times \mathbf{H}^\dagger - \mathbf{E}^\dagger \times \mathbf{H}\right]$	adjoint flux is preserved during propagation also for dissipative systems
energy density $U(\mathbf{r}) = \frac{1}{4} \cdot \left[\frac{\mathrm{d}(\varepsilon\omega)}{\omega} \lvert\mathbf{E}\rvert^2 + \lvert\mathbf{H}\rvert^2\right]$	adjoint field density $N(\mathbf{r}) = \frac{1}{4} \cdot \left[\frac{\mathrm{d}(\varepsilon\omega)}{\omega} \mathbf{E}\mathbf{E}^\dagger - \mathbf{H}\mathbf{H}^\dagger\right]$	$N(\mathbf{r})$ as well as $\mathbf{F}(\mathbf{r})$ loose connection to energy considerations
refractive index $n(\omega) = \varepsilon^{1/2}(\omega)$	effective index $n_{\mathrm{eff}}(\omega) = \frac{\beta(\omega)}{k_0}$	$n'_{\mathrm{eff}}(\omega) < 0 \Rightarrow$ negative refraction
impedance $Z(\omega) = \frac{Z_0}{\varepsilon^{1/2}(\omega)}$	adjoint impedance ratio $\frac{Z(\omega)}{Z_{\mathrm{ref}}(\omega)} = \frac{\iint \left(\mathbf{E}^\dagger_{\mathrm{ref}} - \mathbf{E}_{\mathrm{ref}}\right) \times \mathbf{H} - \mathbf{E} \times \left(\mathbf{H}^\dagger_{\mathrm{ref}} - \mathbf{H}_{\mathrm{ref}}\right) \cdot \mathbf{e}_z \, \mathrm{d}S}{\iint \left(\mathbf{E}^\dagger_{\mathrm{ref}} + \mathbf{E}_{\mathrm{ref}}\right) \times \mathbf{H} - \mathbf{E} \times \left(\mathbf{H}^\dagger_{\mathrm{ref}} + \mathbf{H}_{\mathrm{ref}}\right) \cdot \mathbf{e}_z \, \mathrm{d}S}$	master equation, contributions entangled, no absolute definition possible
tangential impedance $Z_\perp(\omega) = \frac{Z_0}{n_{\mathrm{eff}}(\omega)}$ (TE) $Z_\perp(\omega) = \frac{Z_0}{\varepsilon(\omega)} \cdot n_{\mathrm{eff}}(\omega)$ (TM)	transverse adjoint modal impedance $Z_\perp(\omega) = \frac{Z_0}{n_{\mathrm{eff}}(\omega)}$ (TE) $Z_\perp(\omega) = Z_0 \cdot n_{\mathrm{eff}}(\omega) \cdot \left\langle \varepsilon^{-1}(\omega) \right\rangle_{\phi\psi}$ (TM)	z-invariance and transversality required, $\langle\cdot\rangle_{\phi\psi}$ means tangential averaging with a weight function $(H_x H_x^{\mathrm{ref}} + H_y H_y^{\mathrm{ref}})$
	BLOCH impedance (metamaterials[a]) $Z_B(\omega) = \frac{\langle E_x \rangle_{\mathrm{uc}}}{\langle H_y \rangle_{\mathrm{uc}}}$ (TE) $Z_B(\omega) = \frac{\langle E_y \rangle_{\mathrm{uc}}}{\langle H_x \rangle_{\mathrm{uc}}}$ (TM)	periodicity and plane waves as reference required $\langle\cdot\rangle_{\mathrm{uc}}$ means tangential averaging over the unit cell
phase velocity $v_p(\omega) = \frac{c}{n(\omega)}$	$v'_p(\omega) = \frac{\omega}{\beta'(\omega)} = \frac{c}{n'_{\mathrm{eff}}(\omega)}$	phase and group velocity can both be negative or antiparallel in the case of negative refraction
group velocity $v_g(\omega) = \frac{\mathrm{d}\omega}{\mathrm{d}\beta(\omega)}$ energy velocity $v_e(\omega) = \frac{\langle \mathbf{S}(\mathbf{r}) \cdot \mathbf{e}_z \rangle_{\mathrm{uc}}}{\langle U(\mathbf{r}) \rangle_{\mathrm{uc}}} = v_g$	adjoint field velocity $v_a(\omega) = \frac{\mathrm{d}\omega}{\mathrm{d}\beta(\omega)} = p \cdot \frac{\langle \mathbf{F}(\mathbf{r}) \cdot \mathbf{e}_z \rangle_{\mathrm{uc}}}{\langle N(\mathbf{r}) \rangle_{\mathrm{uc}}}$	$v'_a(\omega)$ describes the propagation velocity of Gaussian pulse peak, also when $v'_a(\omega) > c$

Table A.1. Adjoint field quantities which characterize nanophotonic structures in the Fundamental mode approximation case. Materials are assumed non-magnetic ($\mu = 1$). Every quantity which is not explicitly specified depends on $\mathbf{r}$ and ω.

[a] The FMA does often not hold for Photonic Crystals. A matrix version of the BLOCH impedance must be used [36–38].

Cited References

[1] M. Planck,
»Zur Theorie des Gesetzes der Energieverteilung im Normalspectrum«,
Verhandlungen der Deutschen Physikalischen Gesellschaft **2**, 245, (1900).

[2] A. A. Michelson and E. W. Moreley,
»On the relative motion of the Earth and the Luminiferous Ether«,
American Journal of Science **34**, 333, (1887).

[3] A. Einstein, »Zur Elektrodynamik bewegter Körper«,
Annalen der Physik **322**, 891, (1905).

[4] H. Hertz, »Ueber sehr schnelle electrische Schwingungen«,
Annalen der Physik **267**, 421, (1887).

[5] H. Hertz, »Ueber die Ausbreitungsgeschwindigkeit der
electrodynamischen Wirkungen«, *Annalen der Physik* **270**, 551, (1888).

[6] J. C. Maxwell, »A Dynamical Theory of the Electromagnetic Field«,
Royal Society Transactions **155**, 459, (1865).

[7] R. Courant and D. Hilbert, *Mathemathical Methods of Physics*, 2nd ed.,
Wiley, 1953.

[8] A. Siegman,
»Orthogonality properties of optical resonator eigenmodes«,
Optics Communications **31**, 369, (1979).

[9] A. E. Siegman, »Excess spontaneous emission in non-Hermitian optical
systems. I. Laser amplifiers«, *Physical Review A* **39**, 1253, (1989).

[10] A. E. Siegman, »Eigenmodes in nonnormal optical systems«,
in: *Proceedings of the SPIE*, ed. by F. Wyrowski, vol. 4436, 650, 2001, 1.

[11] E. Abbe, »Beiträge zur Theorie des Mikroskops und der mikroskopischen
Wahrnehmung«, *Archiv für Mikroskopische Anatomie* **9**, 440, (1873).

[12] C. M. Bender and S. Boettcher,
»Real Spectra in Non-Hermitian Hamiltonians Having PT Symmetry«,
Physical Review Letters **80**, 5243, (1998).

[13] C. M. Bender, »Making sense of non-Hermitian Hamiltonians«,
Reports on Progress in Physics **70**, 947, (2007).

[14] S. Ha, A. a. Sukhorukov, K. B. Dossou, L. C. Botten, C. M. de Sterke, and Y. S. Kivshar,
»Bloch-mode extraction from near-field data in periodic waveguides«,
Optics Letters **34**, 3776, (2009).

[15] B. C. P. Sturmberg, K. B. Dossou, L. C. Botten, A. A. Asatryan, C. G. Poulton, C. M. de Sterke, and R. C. McPhedran,
»Modal analysis of enhanced absorption in silicon nanowire arrays«,
Optics Express **19**, A1067, (2011).

[16] F. J. Lawrence, L. C. Botten, K. B. Dossou, R. C. McPhedran, and C. Martijn de Sterke,
»A flexible Bloch mode method for computing complex band structures and impedances of two-dimensional photonic crystals«,
Journal of Applied Physics **111**, 013105, (2012).

[17] K. B. Dossou, L. C. Botten, A. A. Asatryan, B. C. P. Sturmberg, M. A. Byrne, C. G. Poulton, R. C. McPhedran, and C. M. de Sterke,
»Modal formulation for diffraction by absorbing photonic crystal slabs«,
Journal of the Optical Society of America A **29**, 817, (2012).

[18] J. L. Donnelly, B. C. P. Sturmberg, K. B. Dossou, L. C. Botten, A. A. Asatryan, C. G. Poulton, R. C. McPhedran, and C. Martijn de Sterke, »Mode-based analysis of silicon nanohole arrays for photovoltaic applications«, *Optics Express* **22**, A1343, (2014).

[19] J. D. Joannopoulos, S. G. Johnson, J. N. Winn, and R. D. Meade,
Photonic Crystals: Molding the Flow of Light, 2nd ed.,
Princeton University Press, 2008.

[20] W. Cai and V. Shalaev,
Optical Metamaterials: Fundamentals and Applications, Springer, 2009.

[21] O. Heaviside, »Protection of Buildings from Lightning«, *Science* **ns-12**, 17, (1888).

[22] S. Schelkunoff, »The Impedance Concept and Its Application to Problems of Reflection, Refraction, Shielding and Power Absorption«, *Bell System Technical Journal* **17**, 17, (1938).

[23] R. M. Walker, »Waveguide Impedance – too many definitions«, *Electronic Communication* **1**, 13, (1966).

[24] S. Boscolo, C. Conti, M. Midrio, and C. Someda, »Numerical analysis of propagation and impedance matching in 2D photonic crystal waveguides with finite length«, *Journal of Lightwave Technology* **20**, 304, (2002).

[25] R. Biswas, Z. Y. Li, and K. M. Ho, »Impedance of photonic crystals and photonic crystal waveguides«, *Applied Physics Letters* **84**, 1254, (2004).

[26] B. Momeni, A. A. Eftekhar, and A. Adibi, »Effective impedance model for analysis of reflection at the interfaces of photonic crystals«, *Optics Letters* **32**, 778, (2007).

[27] Z. Lu and D. W. Prather, »Calculation of effective permittivity, permeability, and surface impedance of negative-refraction photonic crystals«, *Optics Express* **15**, 8340, (2007).

[28] W. Śmigaj and B. Gralak, »Validity of the effective-medium approximation of photonic crystals«, *Physical Review B* **77**, 235445, (2008).

[29] C. R. Simovski, »Bloch material parameters of magneto-dielectric metamaterials and the concept of Bloch lattices«, *Metamaterials* **1**, 62, (2007).

[30] C. R. Simovski and S. A. Tretyakov, »Local constitutive parameters of metamaterials from an effective-medium perspective«, *Physical Review B* **75**, 195111, (2007).

[31] C. R. Simovski, »On electromagnetic characterization and homogenization of nanostructured metamaterials«, *Journal of Optics* **13**, 013001, (2011).

[32] T. Paul, C. Menzel, W. Śmigaj, C. Rockstuhl, P. Lalanne, and F. Lederer, »Reflection and transmission of light at periodic layered metamaterial films«, *Physical Review B* **84**, 115142, (2011).

[33] C. Menzel, »Characterisation of Optical Metamaterials - Effective Parameters and Beyond«, doctoral thesis, Friedrich-Schiller-Universität Jena, 2011.

[34] T. Paul, »Light Propagation in Optical Metamaterials – A Bloch Modal Approach«, doctoral thesis, Friedrich-Schiller-Universität Jena, 2012.

[35] R. W. Wood, »On a remarkable case of uneven distribution of light in a diffraction grating spectrum«, *Philos. Mag.* **4**, 396, (1902).

[36] F. J. Lawrence, L. C. Botten, K. B. Dossou, and C. M. de Sterke, »Antireflection coatings for two-dimensional photonic crystals using a rigorous impedance definition«, *Applied Physics Letters* **93**, 121114, (2008).

[37] F. Lawrence, L. Botten, K. Dossou, C. M. de Sterke, and R. McPhedran, »Impedance of square and triangular lattice photonic crystals«, *Physical Review A* **80**, 023826, (2009).

[38] F. J. Lawrence, C. M. de Sterke, L. C. Botten, R. C. McPhedran, and K. B. Dossou, »Modeling photonic crystal interfaces and stacks: impedance-based approaches«, *Advances in Optics and Photonics* **5**, 385, (2013).

[39] N. Engheta, A. Salandrino, and A. Alù, »Circuit Elements at Optical Frequencies: Nanoinductors, Nanocapacitors, and Nanoresistors«, *Physical Review Letters* **95**, 095504, (2005).

[40] N. Engheta, »Circuits with light at nanoscales: optical nanocircuits inspired by metamaterials«, *Science* **317**, 1698, (2007).

[41] A. Alù and N. Engheta, »Input Impedance, Nanocircuit Loading, and Radiation Tuning of Optical Nanoantennas«, *Physical Review Letters* **101**, 043901, (2008).

[42] A. Alù and N. Engheta, »Tuning the scattering response of optical nanoantennas with nanocircuit loads«, *Nature Photonics* **2**, 307, (2008).

[43] G. Veronis and S. Fan, »Bends and splitters in metal-dielectric-metal subwavelength plasmonic waveguides«, *Applied Physics Letters* **87**, 131102, (2005).

[44] W. Cai, W. Shin, S. Fan, and M. L. Brongersma, »Elements for plasmonic nanocircuits with three-dimensional slot waveguides.«, *Advanced Materials* **22**, 5120, (2010).

[45] H. Nejati and A. Beirami, »Theoretical Analysis of the Characteristic Impedance in Metal-Insulator-Metal Plasmonic Transmission Lines«, *Optics Letters* **37**, 1050, (2012).

[46] J.-J. Greffet, M. Laroche, and F. Marquier, »Impedance of a Nanoantenna and a Single Quantum Emitter«, *Physical Review Letters* **105**, 117701, (2010).

[47] G. Marconi, *Wireless telegraphic communication*, 1909.

[48] L. Novotny, »The history of near-field optics«, *Progress in Optics* **50**, 137, (2007).

[49] R. P. Feynman, »There's plenty of room at the bottom«, *Engineering and science* **23**, 22, (1960).

[50] O. Keller, »Near-field optics: The nightmare of the photon«, *The Journal of Chemical Physics* **112**, 7856, (2000).

[51] P. Biagioni, J.-S. Huang, and B. Hecht, »Nanoantennas for visible and infrared radiation«, *Reports on Progress in Physics* **75**, 024402, (2012).

[52] J. Wessel, »Surface-enhanced optical microscopy«, *Journal of the Optical Society of America B* **2**, 1538, (1985).

[53] U. C. Fischer and D. W. Pohl, »Observation of Single-Particle Plasmons by Near-Field Optical Microscopy«, *Physical Review Letters* **62**, 458, (1989).

[54] D. W. Pohl, »Near field optics seen as an antenna problem«, *Near-field Optics, Principles and Applications*, 9, (2000).

[55] R. D. Grober, R. J. Schoelkopf, and D. E. Prober, »Optical antenna: Towards a unity efficiency near-field optical probe«, *Applied Physics Letters* **70**, 1354, (1997).

[56] E. Oesterschulze, G. Georgiev, M. Muller-Wiegand, A. Vollkopf, and O. Rudow, »Transmission line probe based on a bow-tie antenna«, *Journal of Microscopy* **202**, 39, (2001).

[57] T. Kalkbrenner, U. Håkanson, A. Schädle, S. Burger, C. Henkel, and V. Sandoghdar, »Optical Microscopy via Spectral Modifications of a Nanoantenna«, *Physical Review Letters* **95**, 200801, (2005).

[58] A. Cvitkovic, N. Ocelic, J. Aizpurua, R. Guckenberger, and R. Hillenbrand, »Infrared Imaging of Single Nanoparticles via Strong Field Enhancement in a Scanning Nanogap«, *Physical Review Letters* **97**, 060801, (2006).

[59] J. N. Farahani, H.-J. Eisler, D. W. Pohl, M. Pavius, P. Flückiger, P. Gasser, and B. Hecht, »Bow-tie optical antenna probes for single-emitter scanning near-field optical microscopy«, *Nanotechnology* **18**, 125506, (2007).

[60] T. H. Taminiau, R. J. Moerland, F. B. Segerink, L. Kuipers, and N. F. van Hulst, »$\lambda/4$ Resonance of an Optical Monopole Antenna Probed by Single Molecule Fluorescence«, *Nano Letters* **7**, 28, (2007).

[61] B. Deutsch, R. Hillenbrand, and L. Novotny, »Near-field amplitude and phase recovery using phase-shifting interferometry«, *Optics Express* **16**, 494, (2008).

[62] C. Höppener and L. Novotny, »Imaging of membrane proteins using antenna-based optical microscopy«, *Nanotechnology* **19**, 384012, (2008).

[63] C. Höppener and L. Novotny, »Antenna-Based Optical Imaging of Single Ca 2+ Transmembrane Proteins in Liquids«, *Nano Letters* **8**, 642, (2008).

[64] R. Vogelgesang, J. Dorfmüller, R. Esteban, R. T. Weitz, A. Dmitriev, and K. Kern, »Plasmonic nanostructures in aperture-less scanning near-field optical microscopy (aSNOM)«, *Physica Status Solidi (B)* **245**, 2255, (2008).

[65] B. Lounis and M. Orrit, »Single-photon sources«, *Reports on Progress in Physics* **68**, 1129, (2005).

[66] S. Kühn, U. Håkanson, L. Rogobete, and V. Sandoghdar, »Enhancement of Single-Molecule Fluorescence Using a Gold Nanoparticle as an Optical Nanoantenna«, *Physical Review Letters* **97**, 017402, (2006).

[67] P. Anger, P. Bharadwaj, and L. Novotny, »Enhancement and Quenching of Single-Molecule Fluorescence«, *Physical Review Letters* **96**, 113002, (2006).

[68] O. L. Muskens, V. Giannini, J. A. Sánchez-Gil, and J. Gómez Rivas, »Strong Enhancement of the Radiative Decay Rate of Emitters by Single Plasmonic Nanoantennas«, *Nano Letters* **7**, 2871, (2007).

[69] J. N. Farahani, D. W. Pohl, H.-J. Eisler, and B. Hecht, »Single Quantum Dot Coupled to a Scanning Optical Antenna: A Tunable Superemitter«, *Physical Review Letters* **95**, 017402, (2005).

[70] A. Kinkhabwala, Z. Yu, S. Fan, Y. Avlasevich, K. Müllen, and W. E. Moerner, »Large single-molecule fluorescence enhancements produced by a bowtie nanoantenna«, *Nature Photonics* **3**, 654, (2009).

[71] T. H. Taminiau, F. D. Stefani, and N. F. van Hulst, »Enhanced directional excitation and emission of single emitters by a nano-optical Yagi-Uda antenna«, *Optics Express* **16**, 10858, (2008).

[72] A. G. Curto, G. Volpe, T. H. Taminiau, M. P. Kreuzer, R. Quidant, and N. F. van Hulst, »Unidirectional Emission of a Quantum Dot Coupled to a Nanoantenna«, *Science* **329**, 930, (2010).

[73] M. Ren, M. Chen, W. Wu, L. Zhang, J. Liu, B. Pi, X. Zhang, Q. Li, S. Fan, and J. Xu, »Linearly Polarized Light Emission from Quantum Dots with Plasmonic Nanoantenna Arrays«, *Nano Letters* **15**, 2951, (2015).

[74] K. Kneipp, Y. Wang, H. Kneipp, L. T. Perelman, I. Itzkan, R. R. Dasari, and M. S. Feld, »Single Molecule Detection Using Surface-Enhanced Raman Scattering (SERS)«, *Physical Review Letters* **78**, 1667, (1997).

[75] S. Nie, »Probing Single Molecules and Single Nanoparticles by Surface-Enhanced Raman Scattering«, *Science* **275**, 1102, (1997).

[76] R. M. Stöckle, Y. D. Suh, V. Deckert, and R. Zenobi, »Nanoscale chemical analysis by tip-enhanced Raman spectroscopy«, *Chemical Physics Letters* **318**, 131, (2000).

[77] A. Hartschuh, E. J. Sánchez, X. S. Xie, and L. Novotny, »High-Resolution Near-Field Raman Microscopy of Single-Walled Carbon Nanotubes«, *Physical Review Letters* **90**, 095503, (2003).

[78] M. Moskovits, »Surface-enhanced Raman spectroscopy: a brief retrospective«, *Journal of Raman Spectroscopy* **36**, 485, (2005).

[79] A. Rasmussen and V. Deckert, »Surface- and tip-enhanced Raman scattering of DNA components«, *Journal of Raman Spectroscopy* **37**, 311, (2006).

[80] D. P. Fromm, A. Sundaramurthy, A. Kinkhabwala, P. J. Schuck, G. S. Kino, and W. E. Moerner, »Exploring the chemical enhancement for surface-enhanced Raman scattering with Au bowtie nanoantennas«, *The Journal of Chemical Physics* **124**, 061101, (2006).

[81] E. Bailo and V. Deckert, »Tip-enhanced Raman scattering«, *Chemical Society Reviews* **37**, 921, (2008).

[82] E. J. Smythe, M. D. Dickey, J. Bao, G. M. Whitesides, and F. Capasso, »Optical Antenna Arrays on a Fiber Facet for in Situ Surface-Enhanced Raman Scattering Detection«, *Nano Letters* **9**, 1132, (2009).

[83] R. Esteban, M. Laroche, and J.-J. Greffet, »Influence of metallic nanoparticles on upconversion processes«, *Journal of Applied Physics* **105**, 033107, (2009).

[84] D. Wang, W. Zhu, Y. Chu, and K. B. Crozier, »High Directivity Optical Antenna Substrates for Surface Enhanced Raman Scattering«, *Advanced Materials* **24**, 4376, (2012).

[85] J.-S. Huang, T. Feichtner, P. Biagioni, and B. Hecht, »Impedance Matching and Emission Properties of Nanoantennas in an Optical Nanocircuit«, *Nano Letters* **9**, 1897, (2009).

[86] J. Wen, S. Romanov, and U. Peschel, »Excitation of plasmonic gap waveguides by nanoantennas«, *Optics Express* **17**, 5925, (2009).

[87] A. Alù and N. Engheta, »Wireless at the Nanoscale: Optical Interconnects using Matched Nanoantennas«, *Physical Review Letters* **104**, 213902, (2010).

[88] J. Wen, P. Banzer, A. Kriesch, D. Ploss, B. Schmauss, and U. Peschel, »Experimental cross-polarization detection of coupling far-field light to highly confined plasmonic gap modes via nanoantennas«, *Applied Physics Letters* **98**, 101109, (2011).

[89] Z. Fang, L. Fan, C. Lin, D. Zhang, A. J. Meixner, and X. Zhu, »Plasmonic Coupling of Bow Tie Antennas with Ag Nanowire«, *Nano Letters* **11**, 1676, (2011).

[90] A. Andryieuski, R. Malureanu, G. Biagi, T. Holmgaard, and A. Lavrinenko, »Compact dipole nanoantenna coupler to plasmonic slot waveguide«, *Optics Letters* **37**, 1124, (2012).

[91] J. Berthelot, A. Bouhelier, C. Huang, J. Margueritat, G. Colas-des-Francs, E. Finot, J.-C. Weeber, A. Dereux, S. Kostcheev, H. I. E. Ahrach, A.-L. Baudrion, J. Plain, R. Bachelot, P. Royer, and G. P. Wiederrecht, »Tuning of an Optical Dimer Nanoantenna by Electrically Controlling Its Load Impedance«, *Nano Letters* **9**, 3914, (2009).

[92] F. Huang and J. J. Baumberg, »Actively Tuned Plasmons on Elastomerically Driven Au Nanoparticle Dimers«, *Nano Letters* **10**, 1787, (2010).

[93] N. Large, M. Abb, J. Aizpurua, and O. L. Muskens, »Photoconductively Loaded Plasmonic Nanoantenna as Building Block for Ultracompact Optical Switches«, *Nano Letters* **10**, 1741, (2010).

[94] C. De Angelis, A. Locatelli, D. Modotto, S. Boscolo, M. Midrio, and A.-D. Capobianco, »Frequency addressing of nano-objects by electrical tuning of optical antennas«, *Journal of the Optical Society of America B* **27**, 997, (2010).

[95] M. Abb, P. Albella, J. Aizpurua, and O. L. Muskens, »All-Optical Control of a Single Plasmonic Nanoantenna–ITO Hybrid«, *Nano Letters* **11**, 2457, (2011).

[96] A. L. Falk, F. H. L. Koppens, C. L. Yu, K. Kang, N. de Leon Snapp, A. V. Akimov, M.-H. Jo, M. D. Lukin, and H. Park, »Near-field electrical detection of optical plasmons and single-plasmon sources«, *Nature Physics* **5**, 475, (2009).

[97] P. Neutens, P. Van Dorpe, I. De Vlaminck, L. Lagae, and G. Borghs, »Electrical detection of confined gap plasmons in metal–insulator–metal waveguides«, *Nature Photonics* **3**, 283, (2009).

[98] R. J. Walters, R. V. A. van Loon, I. Brunets, J. Schmitz, and A. Polman, »A silicon-based electrical source for surface plasmon polaritons«, in: *2009 6th IEEE International Conference on Group IV Photonics*, vol. 9, 1, IEEE, 2009, 74.

[99] A. I. Denisyuk, G. Adamo, K. F. MacDonald, J. Edgar, M. D. Arnold, V. Myroshnychenko, M. J. Ford, F. J. García de Abajo, and N. I. Zheludev, »Transmitting Hertzian Optical Nanoantenna with Free-Electron Feed«, *Nano Letters* **10**, 3250, (2010).

[100] P. Bharadwaj, A. Bouhelier, and L. Novotny, »Electrical Excitation of Surface Plasmons«, *Physical Review Letters* **106**, 226802, (2011).

[101] F. Bigourdan, J.-P. Hugonin, F. Marquier, C. Sauvan, and J.-J. Greffet, »Nanoantenna for Electrical Generation of Surface Plasmon Polaritons«, *Physical Review Letters* **116**, 106803, (2016).

[102] M. I. Stockman, »Femtosecond Optical Responses of Disordered Clusters, Composites, and Rough Surfaces: “The Ninth Wave” Effect«, *Physical Review Letters* **84**, 1011, (2000).

[103] M. I. Stockman, S. V. Faleev, and D. J. Bergman, »Coherent Control of Femtosecond Energy Localization in Nanosystems«, *Physical Review Letters* **88**, 067402, (2002).

[104] J. S. Huang, D. V. Voronine, P. Tuchscherer, T. Brixner, and B. Hecht, »Deterministic spatiotemporal control of optical fields in nanoantennas and plasmonic circuits«, *Physical Review B* **79**, 195441, (2009).

[105] M. Aeschlimann, M. Bauer, D. Bayer, T. Brixner, S. Cunovic, F. Dimler, A. Fischer, W. Pfeiffer, M. Rohmer, C. Schneider, F. Steeb, C. Struber, and D. V. Voronine, »Spatiotemporal control of nanooptical excitations«, *Proceedings of the National Academy of Sciences* **107**, 5329, (2010).

[106] T. Utikal, M. I. Stockman, A. P. Heberle, M. Lippitz, and H. Giessen, »All-Optical Control of the Ultrafast Dynamics of a Hybrid Plasmonic System«, *Physical Review Letters* **104**, 113903, (2010).

[107] S. Choi, M. F. Ciappina, J. A. Pérez-Hernández, A. S. Landsman, Y.-J. Kim, S. C. Kim, and D. Kim, »Active tailoring of nanoantenna plasmonic fields using few-cycle laser pulses«, *Physical Review A* **93**, 021405, (2016).

[108] D. J. Bergman and M. I. Stockman, »Surface Plasmon Amplification by Stimulated Emission of Radiation: Quantum Generation of Coherent Surface Plasmons in Nanosystems«, *Physical Review Letters* **90**, 027402, (2003).

[109] M. Ambati, S. H. Nam, E. Ulin-Avila, D. A. Genov, G. Bartal, and X. Zhang, »Observation of Stimulated Emission of Surface Plasmon Polaritons«, *Nano Letters* **8**, 3998, (2008).

[110] M. A. Noginov, G. Zhu, M. Mayy, B. A. Ritzo, N. Noginova, and V. A. Podolskiy, »Stimulated Emission of Surface Plasmon Polaritons«, *Physical Review Letters* **101**, 226806, (2008).

[111] M. A. Noginov, G. Zhu, A. M. Belgrave, R. Bakker, V. M. Shalaev, E. E. Narimanov, S. Stout, E. Herz, T. Suteewong, and U. Wiesner, »Demonstration of a spaser-based nanolaser«, *Nature* **460**, 1110, (2009).

[112] R. F. Oulton, V. J. Sorger, T. Zentgraf, R.-M. Ma, C. Gladden, L. Dai, G. Bartal, and X. Zhang, »Plasmon lasers at deep subwavelength scale«, *Nature* **461**, 629, (2009).

[113] M. T. Hill, »Status and prospects for metallic and plasmonic nano-lasers [Invited]«, *Journal of the Optical Society of America B* **27**, B36, (2010).

[114] R.-M. Ma, R. F. Oulton, V. J. Sorger, G. Bartal, and X. Zhang, »Room-temperature sub-diffraction-limited plasmon laser by total internal reflection«, *Nature Materials* **10**, 110, (2011).

[115] S.-W. Chang, C.-Y. A. Ni, and S.-L. Chuang, »Theory for bowtie plasmonic nanolasers«, *Optics Express* **16**, 10580, (2008).

[116] F. Aieta, P. Genevet, N. Yu, M. A. Kats, Z. Gaburro, and F. Capasso, »Out-of-Plane Reflection and Refraction of Light by Anisotropic Optical Antenna Metasurfaces with Phase Discontinuities«, *Nano Letters* **12**, 1702, (2012).

[117] N. Yu and F. Capasso, »Flat optics: Controlling wavefronts with optical antenna metasurfaces«, in: *2013 IEEE Antennas and Propagation Society International Symposium (APSURSI)*, vol. 19, 3, IEEE, 2013, 2341.

[118] R. Guo, E. Rusak, I. Staude, J. Dominguez, M. Decker, C. Rockstuhl, I. Brener, D. N. Neshev, and Y. S. Kivshar, »Multipolar Coupling in Hybrid Metal–Dielectric Metasurfaces«, *ACS Photonics* **3**, 349, (2016).

[119] P. Bharadwaj, B. Deutsch, and L. Novotny, »Optical Antennas«, *Advances in Optics and Photonics* **1**, 438, (2009).

[120] L. Novotny and N. van Hulst, »Antennas for light«, *Nature Photonics* **5**, 83, (2011).

[121] G. Mie, »Beiträge zur Optik trüber Medien, speziell kolloidaler Metallösungen«, *Annalen der Physik* **330**, 377, (1908).

[122] A. Mohammadi, V. Sandoghdar, and M. Agio, »Gold nanorods and nanospheroids for enhancing spontaneous emission«, *New Journal of Physics* **10**, 105015, (2008).

[123] L. Novotny and C. Hafner, »Light propagation in a cylindrical waveguide with a complex, metallic, dielectric function«, *Physical Review E* **50**, 4094, (1994).

[124] J. Dorfmüller, R. Vogelgesang, W. Khunsin, C. Rockstuhl, C. Etrich, and K. Kern, »Plasmonic Nanowire Antennas: Experiment, Simulation, and Theory«, *Nano Letters* **10**, 3596, (2010).

[125] H. Ditlbacher, A. Hohenau, D. Wagner, U. Kreibig, M. Rogers, F. Hofer, F. R. Aussenegg, and J. R. Krenn, »Silver Nanowires as Surface Plasmon Resonators«, *Physical Review Letters* **95**, 257403, (2005).

[126] S. A. Maier, »Effective Mode Volume of Nanoscale Plasmon Cavities«, *Optical and Quantum Electronics* **38**, 257, (2006).

[127] L. Novotny, »Effective Wavelength Scaling for Optical Antennas«, *Physical Review Letters* **98**, 266802, (2007).

[128] E. Feigenbaum and M. Orenstein, »Ultrasmall Volume Plasmons, yet with Complete Retardation Effects«, *Physical Review Letters* **101**, 163902, (2008).

[129] J. Dorfmüller, R. Vogelgesang, R. T. Weitz, C. Rockstuhl, C. Etrich, T. Pertsch, F. Lederer, and K. Kern, »Fabry-Pérot Resonances in One-Dimensional Plasmonic Nanostructures«, *Nano Letters* **9**, 2372, (2009).

[130] S. B. Hasan, R. Filter, A. Ahmed, R. Vogelgesang, R. Gordon, C. Rockstuhl, and F. Lederer, »Relating localized nanoparticle resonances to an associated antenna problem«, *Physical Review B* **84**, 195405, (2011).

[131] T. H. Taminiau, F. D. Stefani, and N. F. van Hulst, »Optical Nanorod Antennas Modeled as Cavities for Dipolar Emitters: Evolution of Sub- and Super-Radiant Modes«, *Nano Letters* **11**, 1020, (2011).

[132] O. Merchiers, F. Moreno, F. González, and J. M. Saiz, »Light scattering by an ensemble of interacting dipolar particles with both electric and magnetic polarizabilities«, *Physical Review A* **76**, 043834, (2007).

[133] A. B. Evlyukhin, C. Reinhardt, A. Seidel, B. S. Luk'yanchuk, and B. N. Chichkov, »Optical response features of Si-nanoparticle arrays«, *Physical Review B* **82**, 045404, (2010).

[134] A. I. Kuznetsov, A. E. Miroshnichenko, Y. H. Fu, J. Zhang, and B. Luk'yanchuk, »Magnetic light«, *Scientific Reports* **2**, 1, (2012).

[135] A. E. Krasnok, A. E. Miroshnichenko, P. A. Belov, and Y. S. Kivshar, »Huygens optical elements and Yagi—Uda nanoantennas based on dielectric nanoparticles«, *JETP Letters* **94**, 593, (2011).

[136] D. S. Filonov, A. E. Krasnok, A. P. Slobozhanyuk, P. V. Kapitanova, E. A. Nenasheva, Y. S. Kivshar, and P. A. Belov, »Experimental verification of the concept of all-dielectric nanoantennas«, *Applied Physics Letters* **100**, 201113, (2012).

[137] A. E. Krasnok, A. E. Miroshnichenko, P. A. Belov, and Y. S. Kivshar, »All-dielectric optical nanoantennas«, *Optics Express* **20**, 20599, (2012).

[138] A. E. Krasnok, D. S. Filonov, C. R. Simovski, Y. S. Kivshar, and P. A. Belov, »Experimental demonstration of superdirective dielectric antenna«, *Applied Physics Letters* **104**, 133502, (2014).

[139] A. E. Krasnok, C. R. Simovski, P. A. Belov, and Y. S. Kivshar, »Superdirective dielectric nanoantennas«, *Nanoscale* **6**, 7354, (2014).

[140] S. V. Li, D. G. Baranov, A. E. Krasnok, and P. A. Belov, »All-dielectric nanoantennas for unidirectional excitation of electromagnetic guided modes«, *Applied Physics Letters* **107**, 171101, (2015).

[141] R. S. Savelev, S. V. Makarov, A. E. Krasnok, and P. A. Belov, »From optical magnetic resonance to dielectric nanophotonics (A review)«, *Optics and Spectroscopy* **119**, 551, (2015).

[142] M. Peter, A. Hildebrandt, C. Schlickriede, K. Gharib, T. Zentgraf, J. Förstner, and S. Linden, »Directional Emission from Dielectric Leaky-Wave Nanoantennas«, *Nano Letters* **17**, 4178, (2017).

[143] P. Mühlschlegel, »Resonant Optical Antennas«, *Science* **308**, 1607, (2005).

[144] P. Pramod and K. G. Thomas, »Plasmon Coupling in Dimers of Au Nanorods«, *Advanced Materials* **20**, 4300, (2008).

[145] P. Ghenuche, S. Cherukulappurath, T. H. Taminiau, N. F. van Hulst, and R. Quidant, »Spectroscopic Mode Mapping of Resonant Plasmon Nanoantennas«, *Physical Review Letters* **101**, 116805, (2008).

[146] W. Rechberger, A. Hohenau, A. Leitner, J. Krenn, B. Lamprecht, and F. Aussenegg, »Optical properties of two interacting gold nanoparticles«, *Optics Communications* **220**, 137, (2003).

[147] E. Prodan, C. Radloff, N. J. Halas, and P. Nordlander, »A Hybridization Model for the Plasmon Response of Complex Nanostructures«, *Science* **302**, 419, (2003).

[148] J. Petschulat, »The Multipole Description of Complex Plasmonic Nanostructures«, doctoral thesis, Friedrich-Schiller-Universität Jena, 2011.

[149] L. Rogobete, F. Kaminski, M. Agio, and V. Sandoghdar, »Design of plasmonic nanoantennae for enhancing spontaneous emission«, *Optics Letters* **32**, 1623, (2007).

[150] A. Alù and N. Engheta, »Hertzian plasmonic nanodimer as an efficient optical nanoantenna«, *Physical Review B* **78**, 195111, (2008).

[151] D. P. Fromm, A. Sundaramurthy, P. J. Schuck, G. Kino, and W. E. Moerner, »Gap-Dependent Optical Coupling of Single “Bowtie” Nanoantennas Resonant in the Visible«, *Nano Letters* **4**, 957, (2004).

[152] P. J. Schuck, D. P. Fromm, A. Sundaramurthy, G. S. Kino, and W. E. Moerner, »Improving the Mismatch between Light and Nanoscale Objects with Gold Bowtie Nanoantennas«, *Physical Review Letters* **94**, 017402, (2005).

[153] N. Yu, E. Cubukcu, L. Diehl, D. Bour, S. Corzine, J. Zhu, G. Höfler, K. B. Crozier, and F. Capasso, »Bowtie plasmonic quantum cascade laser antenna«, *Optics Express* **15**, 13272, (2007).

[154] B. J. Roxworthy, K. D. Ko, A. Kumar, K. H. Fung, E. K. C. Chow, G. L. Liu, N. X. Fang, and K. C. Toussaint, »Application of Plasmonic Bowtie Nanoantenna Arrays for Optical Trapping, Stacking, and Sorting«, *Nano Letters* **12**, 796, (2012).

[155] J. Li, A. Salandrino, and N. Engheta, »Shaping light beams in the nanometer scale: A Yagi-Uda nanoantenna in the optical domain«, *Physical Review B* **76**, 245403, (2007).

[156] T. Kosako, Y. Kadoya, and H. F. Hofmann, »Directional control of light by a nano-optical Yagi–Uda antenna«, *Nature Photonics* **4**, 312, (2010).

[157] J. Dorfmüller, D. Dregely, M. Esslinger, W. Khunsin, R. Vogelgesang, K. Kern, and H. Giessen, »Near-Field Dynamics of Optical Yagi-Uda Nanoantennas«, *Nano Letters* **11**, 2819, (2011).

[158] P. Biagioni, J. S. Huang, L. Duò, M. Finazzi, and B. Hecht, »Cross Resonant Optical Antenna«, *Physical Review Letters* **102**, 256801, (2009).

[159] P. Biagioni, M. Savoini, J.-S. Huang, L. Duò, M. Finazzi, and B. Hecht, »Near-field polarization shaping by a near-resonant plasmonic cross antenna«, *Physical Review B* **80**, 153409, (2009).

[160] T. Zentgraf, T. P. Meyrath, A. Seidel, S. Kaiser, H. Giessen, C. Rockstuhl, and F. Lederer, »Babinet's principle for optical frequency metamaterials and nanoantennas«, *Physical Review B* **76**, 033407, (2007).

[161] Y. Alaverdyan, B. Sepúlveda, L. Eurenius, E. Olsson, and M. Käll, »Optical antennas based on coupled nanoholes in thin metal films«, *Nature Physics* **3**, 884, (2007).

[162] Z. J. Zhang, R. W. Peng, Z. Wang, F. Gao, X. R. Huang, W. H. Sun, Q. J. Wang, and M. Wang, »Plasmonic antenna array at optical frequency made by nanoapertures«, *Applied Physics Letters* **93**, 171110, (2008).

[163] X. Shi, L. Hesselink, and R. L. Thornton, »Ultrahigh light transmission through a C-shaped nanoaperture«, *Optics Letters* **28**, 1320, (2003).

[164] L. Wang and X. Xu, »High transmission nanoscale bowtie-shaped aperture probe for near-field optical imaging«, *Applied Physics Letters* **90**, 261105, (2007).

[165] H. Guo, T. P. Meyrath, T. Zentgraf, N. Liu, L. Fu, H. Schweizer, and H. Giessen, »Optical resonances of bowtie slot antennas and their geometry and material dependence«, *Optics Express* **16**, 7756, (2008).

[166] T. W. Ebbesen, H. J. Lezec, H. F. Ghaemi, T. Thio, and P. A. Wolff, »Extraordinary optical transmission through sub-wavelength holearrays«, *Nature* **391**, 667, (1998).

[167] P. Lalanne and E. Silberstein, »Fourier-modal methods applied to waveguide computational problems.«, *Optics Letters* **25**, 1092, (2000).

[168] E. Silberstein, P. Lalanne, J.-P. Hugonin, and Q. Cao, »Use of grating theories in integrated optics«, *Journal of the Optical Society of America A* **18**, 2865, (2001).

[169] Q. Cao, P. Lalanne, and J.-p. Hugonin, »Stable and efficient Bloch-mode computational method for one-dimensional grating waveguides«, *Journal of the Optical Society of America A* **19**, 335, (2002).

[170] J. P. Hugonin, P. Lalanne, I. D. Villar, and I. R. Matias, »Fourier modal methods for modeling optical dielectric waveguides«, *Optical and Quantum Electronics* **37**, 107, (2005).

[171] J. Hugonin and P. Lalanne, »Perfectly matched layers as nonlinear coordinate transforms: a generalized formalization«, *Journal of the Optical Society of America A* **22**, 1844, (2005).

[172] G. Lecamp, J. P. Hugonin, and P. Lalanne, »Theoretical and computational concepts for periodic optical waveguides.«, *Optics Express* **15**, 11042, (2007).

[173] E. Noponen and J. Turunen, »Eigenmode method for electromagnetic synthesis of diffractive elements with three-dimensional profiles«, *Journal of the Optical Society of America A* **11**, 2494, (1994).

[174] J. D. Jackson, *Classical Electrodynamics*, 3rd ed., New York: Wiley, 1998.

[175] L. D. Landau and E. M. Lifshitz, *Course of Theoretical Physics Vol. 8: Electrodynamics of Continuous Media*, Pergamon Press, 1960.

[176] A. Zangwill, *Modern Electrodynamics*, Cambridge University Press, 2013.

[177] B. Saleh and M. Teich, *Fundamentals of Photonics*, 2nd ed., New York: John Wiley & Sons, 2007.

[178] N. W. Ashcroft and N. D. Mermin, *Solid State Physics*, Saunders College Publishing, 1976.

[179] K. Busch, G. von Freymann, S. Linden, S. Mingaleev, L. Tkeshelashvili, and M. Wegener, »Periodic nanostructures for photonics«, *Physics Reports* **444**, 101, (2007).

[180] G. Dolling, C. Enkrich, M. Wegener, C. Soukoulis, and S. Linden, »Simultaneous Negative Phase and Group Velocity of Light in a Metamaterial«, *Science* **312**, 892, (2006).

[181] C. Menzel, T. Paul, C. Rockstuhl, T. Pertsch, S. Tretyakov, and F. Lederer, »Validity of effective material parameters for optical fishnet metamaterials«, *Physical Review B* **81**, 035320, (2010).

[182] W. Karthe and R. Mülller, *Inegrierte Optik*, Akademische Verlagsgesellschaft Geest und Portig, 1991.

[183] G. Floquet,
»Sur les équations différentielles linéaires à coefficients périodiques«,
Annales scientifiques de l'École Normale Supérieure **12**, 47, (1883).

[184] F. Bloch, »Über die Quantenmechanik der Elektronen in Kristallgittern«,
Zeitschrift für Physik **52**, 555, (1929).

[185] A. W. Snyder and J. D. Love, *Optical Waveguide Theory*,
Chapman and Hall, 1983.

[186] R. E. Collin, *Foundations for Microwave Engineering*, 2nd ed.,
McGraw-Hill, 1992.

[187] D. Michaelis, U. Peschel, C. Wächter, and A. Bräuer, »Reciprocity
theorem and perturbation theory for photonic crystal waveguides.«,
Physical Review E **68**, 065601, (2003).

[188] I. F. Balashov and V. A. Berenberg,
»Nonstationary modes of an open resonator«,
Soviet Journal of Quantum Electronics **5**, 159, (1975).

[189] E. Wright and W. Firth,
»Orthogonality properties of general optical resonator eigenmodes«,
Optics Communications **40**, 410, (1982).

[190] E. P. Wigner, »The Unreasonable Effectiveness of Mathematics in the
Natural Sciences«,
Communications on Pure and Applied Mathematics **13**, 1, (1960).

[191] I. Botten, M. Craig, R. McPhedran, J. Adams, and J. Andrewartha,
»The Finitely Conducting Lamellar Diffraction Grating«,
Optica Acta **28**, 1087, (1981).

[192] P. Y. Chen, R. C. McPhedran, C. M. de Sterke, C. G. Poulton,
A. A. Asatryan, L. C. Botten, and M. J. Steel,
»Group velocity in lossy periodic structured media«,
Physical Review A **82**, 053825, (2010).

[193] A. A. Sukhorukov, A. S. Solntsev, S. S. Kruk, D. N. Neshev, and
Y. S. Kivshar, »Nonlinear coupled-mode theory for periodic waveguides
and metamaterials with loss and gain«, *Optics Letters* **39**, 462, (2014).

[194] S. Saravi, S. Diziain, M. Zilk, F. Setzpfandt, and T. Pertsch, »Phase-matched second-harmonic generation in slow-light photonic crystal waveguides«, *Physical Review A* **92**, 063821, (2015).

[195] P. M. Morse and H. Feshbach, *Methods of Theoretical Physics, Vol. 1*, New York: McGraw-Hill, 1953.

[196] E. A. Coddington and N. Levinson, *Theory of Ordinary Differential Equations*, New York: McGraw-Hill, 1955.

[197] P. T. Leung, S. Y. Liu, and K. Young, »Completeness and time-independent perturbation of the quasinormal modes of an absorptive and leaky cavity«, *Physical Review A* **49**, 3982, (1994).

[198] J. E. Sipe, »Vector kp approach for photonic band structures«, *Physical Review E* **62**, 5672, (2000).

[199] J. Petschulat, C. Menzel, A. Chipouline, C. Rockstuhl, A. Tünnermann, F. Lederer, and T. Pertsch, »Multipole approach to metamaterials«, *Physical Review A* **78**, 043811, (2008).

[200] J. Petschulat, A. Chipouline, A. Tünnermann, T. Pertsch, C. Menzel, C. Rockstuhl, T. Paul, and F. Lederer, »Simple and versatile analytical approach for planar metamaterials«, *Physical Review B* **82**, 1, (2010).

[201] M. G. Moharam, E. B. Grann, D. A. Pommet, and T. K. Gaylord, »Formulation for stable and efficient implementation of the rigorous coupled-wave analysis of binary gratings«, *Journal of the Optical Society of America A* **12**, 1068, (1995).

[202] G. Granet and B. Guizal, »Efficient implementation of the coupled-wave method for metallic lamellar gratings in TM polarization«, *Journal of the Optical Society of America A* **13**, 1019, (1996).

[203] P. Lalanne and G. M. Morris, »Highly improved convergence of the coupled-wave method for TM polarization«, *Journal of the Optical Society of America A* **13**, 779, (1996).

[204] L. Li, »New formulation of the Fourier modal method for crossed surface-relief gratings«, *Journal of the Optical Society of America A* **14**, 2758, (1997).

[205] W. Press, S. Teukolsky, W. Vetterling, and B. Flannery, *Numerical Recipes in C++*, Cambridge University Press, 2007.

[206] L. Li and G. Granet, »Field singularities at lossless metal-dielectric right-angle edges and their ramifications to the numerical modeling of gratings«, *Journal of the Optical Society of America A* **28**, 738, (2011).

[207] L. Li, »Use of Fourier series in the analysis of discontinuous periodic structures«, *Journal of the Optical Society of America A* **13**, 1870, (1996).

[208] L. Li, »Formulation and comparison of two recursive matrix algorithms for modeling layered diffraction gratings«, *Journal of the Optical Society of America A* **13**, 1024, (1996).

[209] L. Botten, N. Nicorovici, R. McPhedran, C. M. de Sterke, and A. Asatryan, »Photonic band structure calculations using scattering matrices«, *Physical Review E* **64**, 046603, (2001).

[210] B. Gralak, S. Enoch, and G. Tayeb, »From scattering or impedance matrices to Bloch modes of photonic crystals«, *Journal of the Optical Society of America A* **19**, 1547, (2002).

[211] J.-P. Bérenger, »A perfectly matched layer for the absorption of electromagnetic waves«, *Journal of Computational Physics* **114**, 185, (1994).

[212] A. Taflove, *Computational Electrodynamics: The Finite- Difference Time-Domain Method*, Boston: Artech House, 1995.

[213] L. Li, »Fourier modal method for crossed anisotropic gratings with arbitrary permittivity and permeability tensors«, *Journal of Optics A: Pure and Applied Optics* **5**, 345, (2003).

[214] M. L. Boas, *Mathematical methods in the physical sciences*, 3rd ed., Wiley, 2006.

[215] V. M. Shalaev, »Optical negative-index metamaterials«, *Nature Photonics* **1**, 41, (2007).

[216] C. Menzel, J. Sperrhake, and T. Pertsch, »Efficient treatment of stacked metasurfaces for optimizing and enhancing the range of accessible optical functionalities«, *Physical Review A* **93**, 063832, (2016).

[217] F. J. Lawrence, »Photonic crystal antireflection coatings , surface modes, and impedances«, PhD thesis, University of Sydney, 2012.

[218] L. Peng and N. A. Mortensen, »Plasmonic-cavity model for radiating nano-rod antennas«, *Scientific Reports* **4**, 3825, (2015).

[219] S. A. Maier, *Plasmonics: Fundamentals and Applications*, Springer, 2007.

[220] P. Johnson and R. Christy, »Optical constants of the noble metals«, *Physical Review B* **6**, 4370, (1972).

[221] A. L. Cavalieri et al., »Attosecond spectroscopy in condensed matter«, *Nature* **449**, 1029, (2007).

[222] F. Krausz and M. Ivanov, »Attosecond physics«, *Reviews of Modern Physics* **81**, 163, (2009).

[223] S. Zherebtsov et al., »Controlled near-field enhanced electron acceleration from dielectric nanospheres with intense few-cycle laser fields«, *Nature Physics* **7**, 656, (2011).

[224] P. Rácz, S. E. Irvine, M. Lenner, A. Mitrofanov, A. Baltuška, A. Y. Elezzabi, and P. Dombi, »Strong-field plasmonic electron acceleration with few-cycle, phase-stabilized laser pulses«, *Applied Physics Letters* **98**, 111116, (2011).

[225] M. Schultze, E. M. Bothschafter, A. Sommer, S. Holzner, W. Schweinberger, M. Fiess, M. Hofstetter, R. Kienberger, V. Apalkov, V. S. Yakovlev, M. I. Stockman, and F. Krausz, »Controlling dielectrics with the electric field of light«, *Nature* **493**, 75, (2012).

[226] P. Dombi, A. Hörl, P. Rácz, I. Márton, A. Trügler, J. R. Krenn, and U. Hohenester, »Ultrafast Strong-Field Photoemission from Plasmonic Nanoparticles«, *Nano Letters* **13**, 674, (2013).

[227] A. Feist, K. E. Echternkamp, J. Schauss, S. V. Yalunin, S. Schäfer, and C. Ropers, »Quantum coherent optical phase modulation in an ultrafast transmission electron microscope«, *Nature* **521**, 200, (2015).

[228] K. Iwaszczuk, M. Zalkovskij, A. C. Strikwerda, and P. U. Jepsen, »Nitrogen plasma formation through terahertz-induced ultrafast electron field emission«, *Optica* **2**, 116, (2015).

[229] K. E. Echternkamp, G. Herink, S. V. Yalunin, K. Rademann, S. Schäfer, and C. Ropers, »Strong-field photoemission in nanotip near-fields: from quiver to sub-cycle electron dynamics«, *Applied Physics B* **122**, 80, (2016).

[230] S. Nerkararyan, K. Nerkararyan, N. Janunts, and T. Pertsch, »Generation of Hankel-type surface plasmon polaritons in the vicinity of a metallic nanohole«, *Physical Review B* **82**, 245405, (2010).

[231] R. Filter, J. Qi, C. Rockstuhl, and F. Lederer, »Circular optical nanoantennas: an analytical theory«, *Physical Review B* **85**, 125429, (2012).

[232] M. Abramowitz and I. A. Stegun, *Handbook of mathematical functions: with formulas, graphs, and mathematical tables*, Dover, 1964.

[233] U. Dürig, D. W. Pohl, and F. Rohner, »Near-field optical-scanning microscopy«, *Journal of Applied Physics* **59**, 3318, (1986).

[234] M. L. M. Balistreri, J. P. Korterik, L. Kuipers, and N. F. van Hulst, »Local Observations of Phase Singularities in Optical Fields in Waveguide Structures«, *Physical Review Letters* **85**, 294, (2000).

[235] B. Hecht, B. Sick, U. P. Wild, V. Deckert, R. Zenobi, O. J. F. Martin, and D. W. Pohl, »Scanning near-field optical microscopy with aperture probes: Fundamentals and applications«, *The Journal of Chemical Physics* **112**, 7761, (2000).

[236] S. I. Bozhevolnyi and L. Kuipers,
»Near-field characterization of photonic crystal waveguides«,
Semiconductor Science and Technology **21**, R1, (2006).

[237] N. Rotenberg and L. Kuipers, »Mapping nanoscale light fields«,
Nature Photonics **8**, 919, (2014).

[238] A. E. Klein, »Scanning near-field optical microscopy: from single-tip to dual-tip operation«,
PhD thesis, Friedrich-Schiller-Universität Jena, 2014.

[239] S. Schmidt, A. E. Klein, T. Paul, H. Gross, S. Diziain, M. Steinert, A. C. Assafrao, T. Pertsch, H. P. Urbach, and C. Rockstuhl,
»Image formation properties and inverse imaging problem in aperture based scanning near field optical microscopy«,
Optics Express **24**, 4128, (2016).

[240] G. H. Fecher, O. Schmidt, Y. Hwu, and G. Schönhense, »Multiphoton photoemission electron microscopy using femtosecond laser radiation«,
Journal of Electron Spectroscopy and Related Phenomena **126**, 77, (2002).

[241] O. Schmidt, M. Bauer, C. Wiemann, R. Porath, M. Scharte, O. Andreyev, G. Schönhense, and M. Aeschlimann,
»Time-resolved two photon photoemission electron microscopy«,
Applied Physics B **74**, 223, (2002).

[242] M. Cinchetti, A. Gloskovskii, S. a. Nepjiko, G. Schönhense, H. Rochholz, and M. Kreiter, »Photoemission Electron Microscopy as a Tool for the Investigation of Optical Near Fields«,
Physical Review Letters **95**, 047601, (2005).

[243] F.-J. Meyer zu Heringdorf, L. I. Chelaru, S. Möllenbeck, D. Thien, and M. Horn-von Hoegen, »Femtosecond photoemission microscopy«,
Surface Science **601**, 4700, (2007).

[244] A. Kubo, N. Pontius, and H. Petek,
»Femtosecond Microscopy of Surface Plasmon Polariton Wave Packet Evolution at the Silver/Vacuum Interface«, *Nano Letters* **7**, 470, (2007).

[245] L. I. Chelaru and F.-J. Meyer zu Heringdorf, »In situ monitoring of surface plasmons in single-crystalline Ag-nanowires«, *Surface Science* **601**, 4541, (2007).

[246] M. I. Stockman, M. F. Kling, U. Kleineberg, and F. Krausz, »Attosecond nanoplasmonic-field microscope«, *Nature Photonics* **1**, 539, (2007).

[247] M. Aeschlimann, M. Bauer, D. Bayer, T. Brixner, F. J. García de Abajo, W. Pfeiffer, M. Rohmer, C. Spindler, and F. Steeb, »Adaptive subwavelength control of nano-optical fields«, *Nature* **446**, 301, (2007).

[248] L. Zhang, A. Kubo, L. Wang, H. Petek, and T. Seideman, »Imaging of surface plasmon polariton fields excited at a nanometer-scale slit«, *Physical Review B* **84**, 245442, (2011).

[249] S. H. Chew, F. Süßmann, C. Späth, A. Wirth, J. Schmidt, S. Zherebtsov, A. Guggenmos, A. Oelsner, N. Weber, J. Kapaldo, A. Gliserin, M. I. Stockman, M. F. Kling, and U. Kleineberg, »Time-of-flight-photoelectron emission microscopy on plasmonic structures using attosecond extreme ultraviolet pulses«, *Applied Physics Letters* **100**, 051904, (2012).

[250] N. Buckanie, P. Kirschbaum, S. Sindermann, and F.-J. M. zu Heringdorf, »Interaction of light and surface plasmon polaritons in Ag Islands studied by nonlinear photoemission microscopy«, *Ultramicroscopy* **130**, 49, (2013).

[251] C. Lemke, C. Schneider, T. Leißner, D. Bayer, J. W. Radke, A. Fischer, P. Melchior, A. B. Evlyukhin, B. N. Chichkov, C. Reinhardt, M. Bauer, and M. Aeschlimann, »Spatiotemporal Characterization of SPP Pulse Propagation in Two-Dimensional Plasmonic Focusing Devices«, *Nano Letters* **13**, 1053, (2013).

[252] C. Lemke, T. Leißner, A. Evlyukhin, J. W. Radke, A. Klick, J. Fiutowski, J. Kjelstrup-Hansen, H. G. Rubahn, B. N. Chichkov, C. Reinhardt, and M. Bauer, »The interplay between localized and propagating plasmonic excitations tracked in space and time«, *Nano Letters* **14**, 2431, (2014).

[253] P. Melchior, D. Kilbane, E. J. Vesseur, A. Polman, and M. Aeschlimann, »Photoelectron imaging of modal interference in plasmonic whispering gallery cavities«, *Optics Express* **23**, 31619, (2015).

[254] Y. Gong, A. G. Joly, D. Hu, P. Z. El-Khoury, and W. P. Hess, »Ultrafast Imaging of Surface Plasmons Propagating on a Gold Surface«, *Nano Letters* **15**, 3472, (2015).

[255] B. Schaffer, U. Hohenester, A. Trügler, and F. Hofer, »High-resolution surface plasmon imaging of gold nanoparticles by energy-filtered transmission electron microscopy«, *Physical Review B* **79**, 041401, (2009).

[256] J. J. Cha, Z. Yu, E. Smith, M. Couillard, S. Fan, and D. A. Muller, »Mapping local optical densities of states in silicon photonic structures with nanoscale electron spectroscopy«, *Physical Review B* **81**, 113102, (2010).

[257] G. Boudarham, N. Feth, V. Myroshnychenko, S. Linden, J. García de Abajo, M. Wegener, and M. Kociak, »Spectral Imaging of Individual Split-Ring Resonators«, *Physical Review Letters* **105**, 255501, (2010).

[258] O. Nicoletti, M. Wubs, N. A. Mortensen, W. Sigle, P. A. van Aken, and P. A. Midgley, »Surface plasmon modes of a single silver nanorod: an electron energy loss study«, *Optics Express* **19**, 15371, (2011).

[259] S. Raza, N. Stenger, S. Kadkhodazadeh, S. V. Fischer, N. Kostesha, A.-P. Jauho, A. Burrows, M. Wubs, and N. A. Mortensen, »Blueshift of the surface plasmon resonance in silver nanoparticles studied with EELS«, *Nanophotonics* **2**, 131, (2013).

[260] M. Husnik, F. von Cube, S. Irsen, S. Linden, J. Niegemann, K. Busch, and M. Wegener, »Comparison of electron energy-loss and quantitative optical spectroscopy on individual optical gold antennas«, *Nanophotonics* **2**, 241, (2013).

[261] T. Christensen, W. Yan, S. Raza, A.-P. Jauho, N. A. Mortensen, and M. Wubs, »Nonlocal Response of Metallic Nanospheres Probed by Light, Electrons, and Atoms«, *ACS Nano* **8**, 1745, (2014).

[262] S. Raza, N. Stenger, A. Pors, T. Holmgaard, S. Kadkhodazadeh, J. B. Wagner, K. Pedersen, M. Wubs, S. I. Bozhevolnyi, and N. A. Mortensen, »Extremely confined gap surface-plasmon modes excited by electrons«, *Nature Communications* **5**, 1, (2014).

[263] F. von Cube, J. Niegemann, S. Irsen, D. C. Bell, and S. Linden, »Angular-resolved electron energy loss spectroscopy on a split-ring resonator«, *Physical Review B* **89**, 115434, (2014).

[264] B. Schröder, T. Weber, S. V. Yalunin, T. Kiel, C. Matyssek, M. Sivis, S. Schäfer, F. von Cube, S. Irsen, K. Busch, C. Ropers, and S. Linden, »Real-space imaging of nanotip plasmons using electron energy loss spectroscopy«, *Physical Review B* **92**, 085411, (2015).

[265] S. Raza, S. Kadkhodazadeh, T. Christensen, M. Di Vece, M. Wubs, N. A. Mortensen, and N. Stenger, »Multipole plasmons and their disappearance in few-nanometre silver nanoparticles«, *Nature Communications* **6**, 8788, (2015).

[266] S. Raza, M. Esfandyarpour, A. L. Koh, N. A. Mortensen, M. L. Brongersma, and S. I. Bozhevolnyi, »Electron energy-loss spectroscopy of branched gap plasmon resonators«, *Nature Communications* **7**, 13790, (2016).

[267] H. Shen, L. Chen, L. Ferrari, M.-H. Lin, N. A. Mortensen, S. Gwo, and Z. Liu, »Optical Observation of Plasmonic Nonlocal Effects in a 2D Superlattice of Ultrasmall Gold Nanoparticles«, *Nano Letters* **17**, 2234, (2017).

[268] A. E. Klein, A. Minovich, M. Steinert, N. Janunts, A. Tünnermann, D. N. Neshev, Y. S. Kivshar, and T. Pertsch, »Controlling plasmonic hot spots by interfering Airy beams«, *Optics Letters* **37**, 3402, (2012).

[269] C. Schmidt, M. Liebsch, A. Klein, N. Janunts, A. Chipouline, T. Käsebier, C. Etrich, F. Lederer, E.-B. Kley, A. Tünnermann, and T. Pertsch, »Near-field mapping of optical eigenstates in coupled disk microresonators«, *Physical Review A* **85**, 033827, (2012).

[270] A. E. Klein, C. Schmidt, M. Liebsch, N. Janunts, M. Dobynde, A. Tünnermann, and T. Pertsch, »Highly sensitive mode mapping of whispering-gallery modes by scanning thermocouple-probe microscopy«, *Optics Letters* **39**, 1157, (2014).

[271] A. E. Klein, N. Janunts, M. Steinert, A. Tünnermann, and T. Pertsch, »Polarization-Resolved Near-Field Mapping of Plasmonic Aperture Emission by a Dual-SNOM System«, *Nano Letters* **14**, 5010, (2014).

[272] A. E. Klein, N. Janunts, M. Steinert, A. Tünnermann, and T. Pertsch, »Polarization-Resolved Near-Field Mapping of Plasmonic Aperture Emission by a Dual-SNOM System«, *Nano Letters* **14**, 5010, (2014).

[273] A. E. Minovich, A. E. Klein, D. N. Neshev, T. Pertsch, Y. S. Kivshar, and D. N. Christodoulides, »Airy plasmons: non-diffracting optical surface waves«, *Laser & Photonics Reviews* **8**, 221, (2014).

[274] K. H. Herrmann, *Der Photoeffekt: Grundlagen der Strahlungsmessung*, Braunschweig: Vieweg, 1994.

[275] Boyd, *Nonlinear Optics*, 3rd ed., Elsevier / Academic Press, 2008.

[276] M. Born and E. Wolf, *Principles of Optics*, 6th ed., Pergamon Press, 1991.

[277] N. A. Mortensen, »Nonlocal formalism for nanoplasmonics: Phenomenological and semi-classical considerations«, *Photonics and Nanostructures - Fundamentals and Applications* **11**, 303, (2013).

[278] G. Toscano, S. Raza, W. Yan, C. Jeppesen, S. Xiao, M. Wubs, A.-P. Jauho, S. I. Bozhevolnyi, and N. A. Mortensen, »Nonlocal response in plasmonic waveguiding with extreme light confinement«, *Nanophotonics* **2**, 161, (2013).

[279] N. A. Mortensen, S. Raza, M. Wubs, T. Søndergaard, and S. I. Bozhevolnyi, »A generalized non-local optical response theory for plasmonic nanostructures«, *Nature Communications* **5** (2014).

[280] G. Toscano, J. Straubel, A. Kwiatkowski, C. Rockstuhl, F. Evers, H. Xu, N. Asger Mortensen, and M. Wubs, »Resonance shifts and spill-out effects in self-consistent hydrodynamic nanoplasmonics«, *Nature Communications* **6**, 7132, (2015).

[281] W. Yan, M. Wubs, and N. Asger Mortensen, »Projected Dipole Model for Quantum Plasmonics«, *Physical Review Letters* **115**, 137403, (2015).

[282] C. Tserkezis, J. R. Maack, Z. Liu, M. Wubs, and N. Asger Mortensen, »Robustness of the far-field response of nonlocal plasmonic ensembles«, *Scientific Reports* **6**, 1, (2016).

[283] S. I. Bozhevolnyi and N. A. Mortensen, »Plasmonics for emerging quantum technologies«, *Nanophotonics* **6**, 1185, (2017).

[284] T. Christensen, W. Yan, A.-P. Jauho, M. Soljačić, and N. A. Mortensen, »Quantum Corrections in Nanoplasmonics: Shape, Scale, and Material«, *Physical Review Letters* **118**, 157402, (2017).

[285] G. Dolling, C. Enkrich, M. Wegener, J. F. Zhou, C. M. Soukoulis, and S. Linden, »Cut-wire pairs and plate pairs as magnetic atoms for optical metamaterials.«, *Optics Letters* **30**, 3198, (2005).

[286] N. Liu, H. Guo, L. Fu, S. Kaiser, H. Schweizer, and H. Giessen, »Plasmon Hybridization in Stacked Cut-Wire Metamaterials«, *Advanced Materials* **19**, 3628, (2007).

[287] S. N. Burokur, A. Sellier, B. Kanté, and A. de Lustrac, »Symmetry breaking in metallic cut wire pairs metamaterials for negative refractive index«, *Applied Physics Letters* **94**, 201111, (2009).

[288] N. J. Halas, S. Lal, W.-S. Chang, S. Link, and P. Nordlander, »Plasmons in Strongly Coupled Metallic Nanostructures«, *Chemical Reviews* **111**, 3913, (2011).

[289] S. Linden, C. Enkrich, M. Wegener, J. Zhou, T. Koschny, and C. Soukoulis, »Magnetic Response of Metamaterials at 100 Terahertz«, *Science* **306**, 1351, (2004).

[290] C. Enkrich, M. Wegener, S. Linden, S. Burger, L. Zschiedrich, F. Schmidt, J. F. Zhou, T. Koschny, and C. M. Soukoulis, »Magnetic Metamaterials at Telecommunication and Visible Frequencies«, *Physical Review Letters* **95**, 203901, (2005).

[291] E. Pshenay-Severin, »Design , realization , and characterization of optical negative index metamaterials«, doctoral thesis, Friedrich-Schiller-Universität Jena, 2011.

[292] C. F. Bohren and D. R. Huffman, *Absorption and Scattering of Light by Small Particles*, Weinheim: Wiley-VCH, 2004.

[293] F. Bernal Arango, A. Kwadrin, and a. F. Koenderink, »Plasmonic antennas hybridized with dielectric waveguides.«, *ACS nano* **6**, 10156, (2012).

[294] M. Février, P. Gogol, A. Aassime, R. Mégy, C. Delacour, A. Chelnokov, A. Apuzzo, S. Blaize, J.-M. Lourtioz, and B. Dagens, »Giant Coupling Effect between Metal Nanoparticle Chain and Optical Waveguide«, *Nano Letters* **12**, 1032, (2012).

[295] M. Fevrier, P. Gogol, A. Aassime, D. Bouville, R. Megy, and B. Dagens, »Integrated localized surface plasmon waveguides«, *Applied Physics A* **109**, 967, (2012).

[296] M. Fevrier, P. Gogol, A. Aassime, R. Megy, D. Bouville, J. M. Lourtioz, and B. Dagens, »Localized surface plasmon Bragg grating on SOI waveguide at telecom wavelengths«, *Applied Physics A* **109**, 935, (2012).

[297] M. Février, P. Gogol, G. Barbillon, A. Aassime, R. Mégy, B. Bartenlian, J.-M. Lourtioz, and B. Dagens, »Integration of short gold nanoparticles chain on SOI waveguide toward compact integrated bio-sensors«, *Optics Express* **20**, 17403, (2012).

[298] A. Apuzzo, M. Février, R. Salas-Montiel, A. Bruyant, A. Chelnokov, G. Lérondel, B. Dagens, and S. Blaize, »Observation of Near-Field Dipolar Interactions Involved in a Metal Nanoparticle Chain Waveguide«, *Nano Letters* **13**, 1000, (2013).

[299] M. Février, P. Gogol, J.-M. Lourtioz, and B. Dagens, »Metallic nanoparticle chains on dielectric waveguides: coupled and uncoupled situations compared«, *Optics Express* **21**, 24504, (2013).

[300] R. Tellez-Limon, M. Fevrier, A. Apuzzo, R. Salas-Montiel, and S. Blaize, »Theoretical analysis of Bloch mode propagation in an integrated chain of gold nanowires«, *Photonics Research* **2**, 24, (2014).

[301] B. Dagens, M. Février, P. Gogol, S. Blaize, A. Apuzzo, G. Magno, R. Mégy, and G. Lerondel, »Direct Observation of Optical Field Phase Carving in the Vicinity of Plasmonic Metasurfaces«, *Nano Letters* **16**, 4014, (2016).

[302] G. Magno, M. Fevrier, P. Gogol, A. Aassime, A. Bondi, R. Mégy, and B. Dagens, »Strong coupling and vortexes assisted slow light in plasmonic chain-SOI waveguide systems«, *Scientific Reports* **7**, 7228, (2017).

[303] J. Hu and C. R. Menyuk, »Understanding leaky modes: slab waveguide revisited«, *Advances in Optics and Photonics* **1**, 58, (2009).

[304] S. Linden, J. Kuhl, and H. Giessen, »Controlling the Interaction between Light and Gold Nanoparticles: Selective Suppression of Extinction«, *Physical Review Letters* **86**, 4688, (2001).

[305] S. Linden, A. Christ, J. Kuhl, and H. Giessen, »Selective suppression of extinction within the plasmon resonance of gold nanoparticles«, *Applied Physics B: Lasers and Optics* **73**, 311, (2001).

[306] A. Christ, S. Tikhodeev, N. Gippius, J. Kuhl, and H. Giessen, »Waveguide-Plasmon Polaritons: Strong Coupling of Photonic and Electronic Resonances in a Metallic Photonic Crystal Slab«, *Physical Review Letters* **91**, 183901, (2003).

[307] A. Christ, T. Zentgraf, J. Kuhl, S. Tikhodeev, N. Gippius, and H. Giessen, »Optical properties of planar metallic photonic crystal structures: Experiment and theory«, *Physical Review B* **70**, 125113, (2004).

[308] T. Zentgraf, A. Christ, J. Kuhl, and H. Giessen, »Tailoring the Ultrafast Dephasing of Quasiparticles in Metallic Photonic Crystals«, *Physical Review Letters* **93**, 243901, (2004).

[309] V. Yannopapas and N. Stefanou, »Optical excitation of coupled waveguide-particle plasmon modes: A theoretical analysis«, *Physical Review B* **69**, 12408, (2004).

[310] S. Linden, N. Rau, U. Neuberth, A. Naber, M. Wegener, S. Pereira, K. Busch, A. Christ, and J. Kuhl, »Near-field optical microscopy and spectroscopy of one-dimensional metallic photonic crystal slabs«, *Physical Review B* **71**, 245119, (2005).

[311] S. Linden, M. Decker, and M. Wegener, »Model System for a One-Dimensional Magnetic Photonic Crystal«, *Physical Review Letters* **97**, 083902, (2006).

[312] T. Utikal, T. Zentgraf, S. Tikhodeev, M. Lippitz, and H. Giessen, »Tailoring the photonic band splitting in metallodielectric photonic crystal superlattices«, *Physical Review B* **84**, 075101, (2011).

[313] S. Rodriguez, S. Murai, M. Verschuuren, and J. Rivas, »Light-Emitting Waveguide-Plasmon Polaritons«, *Physical Review Letters* **109**, 166803, (2012).

[314] A. Ishikawa, R. F. Oulton, T. Zentgraf, and X. Zhang, »Slow-light dispersion by transparent waveguide plasmon polaritons«, *Physical Review B* **85**, 155108, (2012).

[315] B. Luk'yanchuk, N. I. Zheludev, S. A. Maier, N. J. Halas, P. Nordlander, H. Giessen, and C. T. Chong, »The Fano resonance in plasmonic nanostructures and metamaterials«, *Nature Materials* **9**, 707, (2010).

[316] Z. Li, M. H. Kim, C. Wang, Z. Han, S. Shrestha, A. C. Overvig, M. Lu, A. Stein, A. M. Agarwal, M. Lončar, and N. Yu, »Controlling propagation and coupling of waveguide modes using phase-gradient metasurfaces«, *Nature Nanotechnology* **12**, 675, (2017).

[317] C. Wang, X. Xiong, N. Andrade, V. Venkataraman, X.-F. Ren, G.-C. Guo, and M. Lončar, »Second harmonic generation in nano-structured thin-film lithium niobate waveguides«, *Optics Express* **25**, 6963, (2017).

[318] C. Menzel, E. Hebestreit, S. Mühlig, C. Rockstuhl, S. Burger, F. Lederer, and T. Pertsch, »The spectral shift between near- and far-field resonances of optical nano-antennas«, *Optics Express* **22**, 9971, (2014).

[319] A. Miroshnichenko, S. Flach, and Y. Kivshar, »Fano resonances in nanoscale structures«, *Reviews of Modern Physics* **82**, 2257, (2010).

[320] B. Hopkins, A. N. Poddubny, A. E. Miroshnichenko, and Y. S. Kivshar, »Revisiting the physics of Fano resonances for nanoparticle oligomers«, *Physical Review A* **88**, 053819, (2013).

[321] C. G. B. Garrett and D. E. McCumber, »Propagation of a Gaussian Light Pulse through an Anomalous Dispersion Medium«, *Physical Review A* **1**, 305, (1970).

[322] S. Chu and S. Wong, »Linear Pulse Propagation in an Absorbing Medium«, *Physical Review Letters* **48**, 738, (1982).

[323] L. J. Wang, A. Kuzmich, and A. Dogariu, »Gain-assisted superluminal light propagation«, *Nature* **406**, 277, (2000).

[324] J. Peatross, S. A. Glasgow, and M. Ware, »Average Energy Flow of Optical Pulses in Dispersive Media«, *Physical Review Letters* **84**, 2370, (2000).

[325] G. Dolling, C. Enkrich, M. Wegener, C. M. Soukoulis, and S. Linden, »Simultaneous negative phase and group velocity of light in a metamaterial.«, *Science* **312**, 892, (2006).

[326] J. Poon, J. Scheuer, S. Mookherjea, G. T. Paloczi, Y. Huang, and A. Yariv, »Matrix analysis of microring coupled-resonator optical waveguides«, *Optics Express* **12**, 90, (2004).

[327] D. Hermann, M. Diem, S. F. Mingaleev, A. García-Martín, P. Wölfle, and K. Busch, »Photonic crystals with anomalous dispersion: Unconventional propagating modes in the photonic band gap«, *Physical Review B* **77**, 035112, (2008).

[328] P. Y. Chen, C. G. Poulton, A. A. Asatryan, M. J. Steel, L. C. Botten, C. Martijn de Sterke, and R. C. McPhedran, »Folded bands in metamaterial photonic crystals«, *New Journal of Physics* **13**, 053007, (2011).

[329] C. Wolff, K. Busch, and N. A. Mortensen, »Modal expansions in periodic photonic systems with material loss and dispersion«, *arXiv preprint*, 1801.01791, (2018).

[330] J. Kundu, F. Le, P. Nordlander, and N. J. Halas, »Surface enhanced infrared absorption (SEIRA) spectroscopy on nanoshell aggregate substrates«, *Chemical Physics Letters* **452**, 115, (2008).

[331] C. Huck, F. Neubrech, J. Vogt, A. Toma, D. Gerbert, J. Katzmann, T. Härtling, and A. Pucci, »Surface-enhanced infrared spectroscopy using nanometer-sized gaps«, *ACS Nano* **8**, 4908, (2014).

[332] X. Wang, S.-S. Kim, R. Rossbach, M. Jetter, P. Michler, and B. Mizaikoff, »Ultra-sensitive mid-infrared evanescent field sensors combining thin-film strip waveguides with quantum cascade lasers«, *The Analyst* **137**, 2322, (2012).

[333] M. Sieger, F. Balluff, X. Wang, S.-S. Kim, L. Leidner, G. Gauglitz, and B. Mizaikoff, »On-Chip Integrated Mid-Infrared GaAs/AlGaAs Mach-Zehnder Interferometer«, *Analytical Chemistry* **85**, 3050, (2013).

[334] X. Wang, »Theoretical Analysis of Plasmonic Particle Resonance and its Application for Integrated Absorption Spectroscopy«, Master Thesis, Friedrich-Schiller-Universität Jena, 2015.

[335] M. G. Reuter, »A unified perspective of complex band structure: interpretations, formulations, and applications«, *Journal of Physics: Condensed Matter* **29**, 053001, (2017).

[336] C. M. de Sterke, J. Walker, K. B. Dossou, and L. C. Botten, »Efficient slow light coupling into photonic crystals«, *Optics Express* **15**, 10984, (2007).

[337] C. Martijn de Sterke, K. B. Dossou, T. P. White, L. C. Botten, and R. C. McPhedran, »Efficient coupling into slow light photonic crystal waveguide without transition region: role of evanescent modes«, *Optics Express* **17**, 17338, (2009).

[338] C. Monat, M. de Sterke, and B. J. Eggleton, »Slow light enhanced nonlinear optics in periodic structures«, *Journal of Optics* **12**, 104003, (2010).

[339] N. Gutman, C. Martijn de Sterke, A. A. Sukhorukov, and L. C. Botten, »Slow and frozen light in optical waveguides with multiple gratings: Degenerate band edges and stationary inflection points«, *Physical Review A* **85**, 033804, (2012).

[340] N. Gutman, W. H. Dupree, Y. Sun, A. a. Sukhorukov, and C. M. de Sterke, »Frozen and broadband slow light in coupled periodic nanowire waveguides«, *Optics Express* **20**, 3519, (2012).

[341] M. Fleischhauer, A. Imamoglu, and J. Marangos, »Electromagnetically induced transparency: Optics in coherent media«, *Reviews of Modern Physics* **77**, 633, (2005).

[342] R. Kekatpure, E. Barnard, W. Cai, and M. Brongersma, »Phase-Coupled Plasmon-Induced Transparency«, *Physical Review Letters* **104**, 243902, (2010).

[343] J. Zhang, S. Xiao, C. Jeppesen, A. Kristensen, and N. A. Mortensen, »Electromagnetically induced transparency in metamaterials at near-infrared frequency«, *Optics Express* **18**, 17187, (2010).

[344] B. Tang, L. Dai, and C. Jiang, »Electromagnetically induced transparency in hybrid plasmonic-dielectric system«, *Optics Express* **19**, 628, (2011).

[345] I. Staude, A. E. Miroshnichenko, M. Decker, N. T. Fofang, S. Liu, E. Gonzales, J. Dominguez, T. S. Luk, D. N. Neshev, I. Brener, and Y. Kivshar, »Tailoring Directional Scattering through Magnetic and

Electric Resonances in Subwavelength Silicon Nanodisks«, *ACS Nano* **7**, 7824, (2013).

[346] M. Decker, I. Staude, M. Falkner, J. Dominguez, D. N. Neshev, I. Brener, T. Pertsch, and Y. S. Kivshar, »High-Efficiency Dielectric Huygens' Surfaces«, *Advanced Optical Materials* **3**, 813, (2015).

[347] K. E. Chong, I. Staude, A. James, J. Dominguez, S. Liu, S. Campione, G. S. Subramania, T. S. Luk, M. Decker, D. N. Neshev, I. Brener, and Y. S. Kivshar, »Polarization-Independent Silicon Metadevices for Efficient Optical Wavefront Control«, *Nano Letters* **15**, 5369, (2015).

[348] A. Einstein, »Über Gravitationswellen«, *Sitzungsberichte der Königlich-Preußischen Akademie der Wissenschaften*, 154, (1918).

Publications

Peer-reviewed journal articles

[TK2009] T. Kaiser, D. Flamm, S. Schröter, and M. Duparré, »Complete modal decomposition for optical fibers using CGH-based correlation filters«, *Optics Express* **17**, 9347, (2009).

[TK2010] D. Flamm, O. A. Schmidt, C. Schulze, J. Borchardt, T. Kaiser, S. Schröter, and M. Duparré,
»Measuring the spatial polarization distribution of multimode beams emerging from passive step-index large-mode-area fibers«,
Optics Letters **35**, 3429, (2010).

[TK2011] O. A. Schmidt, C. Schulze, D. Flamm, R. Brüning, T. Kaiser, S. Schröter, and M. Duparré, »Real-time determination of laser beam quality by modal decomposition.«, *Optics Express* **19**, 6741, (2011).

[TK2012] D. Flamm, C. Schulze, R. Brüning, O. A. Schmidt, T. Kaiser, S. Schröter, and M. Duparré,
»Fast M^2 measurement for fiber beams based on modal analysis«,
Applied Optics **51**, 987, (2012).

[TK2013] T. Kaiser, S. B. Hasan, T. Paul, T. Pertsch, and C. Rockstuhl,
»Impedance generalization for plasmonic waveguides beyond the lumped circuit model«, *Physical Review B* **88**, 035117, (2013).

[TK2014] J. Qi, T. Kaiser, R. Peuker, T. Pertsch, F. Lederer, and C. Rockstuhl,
»Highly resonant and directional optical nanoantennas«,
J. Opt. Soc. Am. A **31**, 388, (2014).

[TK2015] J. Qi, T. Kaiser, A. E. Klein, M. Steinert, T. Pertsch, F. Lederer, and C. Rockstuhl,
»Enhancing resonances of optical nanoantennas by circular gratings«,
Optics Express **23**, 14583, (2015).

[TK2016] T. Kaiser, M. Falkner, J. Qi, A. Klein, M. Steinert, C. Menzel, C. Rockstuhl, and T. Pertsch, »Characterization of a circular optical nanoantenna by nonlinear photoemission electron microscopy«,
Applied Physics B **122**, 53, (2016).

[TK2017] A. E. Klein, N. Janunts, S. Schmidt, S. Bin Hasan, C. Etrich, S. Fasold, T. Kaiser, C. Rockstuhl, and T. Pertsch, »Dual-SNOM investigations of multimode interference in plasmonic strip waveguides«,
Nanoscale **9**, 6695, (2017).

Peer-reviewed conference contributions

[TKtalk01] T. Kaiser, B. Lüdge, S. Schröter, D. Kauffmann, and M. Duparré, »Detection of mode conversion effects in passive LMA fibres by means of optical correlation analysis«, in: *Solid State Lasers and Amplifiers III*, ed. by J. A. Terry, T. Graf, and H. Jelinkova, vol. 6998, 1, Strasbourg, France: SPIE, 2008, 69980J.

[TKtalk02] O. A. Schmidt, T. Kaiser, B. Lüdge, S. Schröter, and M. Duparré, »Laser-beam characterization by means of modal decomposition versus M^2 method«, in: *Laser Resonators and Beam Control XI*, ed. by A. V. Kudryashov, A. H. Paxton, V. S. Ilchenko, and L. Aschke, vol. 7194, 1, San Jose, CA, USA: SPIE, 2009, 71940C.

[TKtalk03] T. Kaiser, S. Schröter, and M. Duparré, »Modal decomposition in step-index fibers by optical correlation analysis«,
in: *Laser Resonators and Beam Control XI*,
ed. by A. V. Kudryashov, A. H. Paxton, V. S. Ilchenko, and L. Aschke, vol. 7194, 1, San Jose, CA, USA: SPIE, 2009, 719407.

[TKtalk04] T. Kaiser, C. Helgert, T. Paul, S. B. Hasan, F. Lederer, C. Rockstuhl, and T. Pertsch, »Resonant coupling of dielectric waveguides with plasmonic metaatoms«, in: *Proc. SPIE 8093*, 2011, 809322.

[TKtalk05] T. Kaiser, S. B. Hasan, T. Paul, and T. Pertsch, »The relative impedance of waveguiding structures«, in: *Meta: 2012*, 2012.

[TKtalk06] T. Kaiser, S. Diziain, C. Helgert, C. Rockstuhl, and T. Pertsch, »Plasmonic nanoparticle interaction in hybrid plasmonic-dielectric waveguides«, in: *CLEO: 2013*, Washington, D.C.: OSA, 2013, QW3N.3.

[TKtalk07] F. Eilenberger, A. Brown, S. Minardi, T. Kaiser, and T. Pertsch, »Imaging cross-correlation FROG: retrieval of ultrashort, complex, spatiotemporal fields«, in: *CLEO: 2013*, Washington, D.C.: OSA, 2013, QM4E.6.

[TKtalk08] T. Kaiser, M. Falkner, J. Qi, M. Steinert, C. Menzel, C. Rockstuhl, and T. Pertsch, »Advanced Disc-Ring Optical Nanoantennas Investigated by Photoelectron Emission Microscopy (PEEM)«, in: *CLEO: 2015*, Optical Society of America, 2015, FTh1E.2.

[TKposter01] O. A. Schmidt, T. Kaiser, M. Duparré, and R. Kowarschik, »Laser beam characterization by means of modal decomposition versus M^2 method«, in: *Proc. DGaO*, 2009, P30.

[TKposter02] D. Flamm, T. Kaiser, M. Duparré, and R. Kowarschik, »Field reconstruction by modal decomposition in passive optical fibers used for brilliant laser beam transmission«, in: *Proc. DGaO*, 2009, P79.

[TKposter03] T. Kaiser, C. Helgert, C. Rockstuhl, F. Lederer, M. Arens, T. Pertsch, T. Paul, R. Wolf, C. Rockstuhl, F. Lederer, and T. Pertsch, »Metamaterials in Waveguide Geometries«, in: *CLEO/Europe and EQEC: 2011*, Optical Society of America, 2011, EJ_P3.

Acknowledgements

Many people helped making this thesis possible. I am thankful to Prof. PERTSCH for giving me the possibility to explore the world of nanooptics in his work group and providing funding for my work. Prof. ROCKSTUHL, now with the Karlsruhe Institute of Technology, contributed a number of scientific ideas that found their way into this thesis.

Prof. LALANNE, now with the University Bordeaux, helped me understand many of the conceptual and numerical concepts considering BLOCH modes. The scientific discussions with a number of collaborators opened my view on many aspects of the field. I would like to particularly mention Prof. TRETYAKOV, Prof. MORTENSEN, Prof. NESHEV and PD Dr. VOGELGESANG.

From my colleagues, I owe special thanks to Dr. CHRISTIAN HELGERT and Dr. THOMAS PAUL for their guidance and explanations when I started my work. Many other people also provided help with experiments and numerical calculations, in particular Dr. SÉVERINE DIZIAN, Dr. ANGELA KLEIN, MATTHIAS FALKNER, JING QI, and Dr. SHAKEEB BIN HASAN. CHRISTIANE OTTO invested substantial effort into the sample preparation of nanostructured waveguides.

I am indebted to Dr. REINHARD GEISS for this valuable comments after proof-reading the manuscript. I would also like to thank the reviewers of the thesis for their efforts.

A very special thanks goes to Dr. MICHAEL DUPARRÉ who is now retired and has been a scientific mentor since my first year in university and later became a personal mentor and friend. I still remember our early days when we wondered how modal decomposition could work for the full vectorial field in the presence of loss. It is done, MICHAEL! Not at last, this thesis is for you.

Without the help and encouragement of my friends and family, I would not have finished this work. From my very heart I am thankful for their patience and sacrifice, especially to my wife KATHARINA and my kids JOHANNA and JAKOB.

Ehrenwörtliche Erklärung

Ich erkläre hiermit ehrenwörtlich, dass ich die vorliegende Arbeit selbständig, ohne unzulässige Hilfe Dritter und ohne Benutzung anderer als der angegebenen Hilfsmittel und Literatur angefertigt habe. Die aus anderen Quellen direkt oder indirekt übernommenen Daten und Konzepte sind unter Angabe der Quelle gekennzeichnet. Bei der Auswahl und Auswertung folgenden Materials haben mir die nachstehend aufgeführten Personen in der jeweils beschriebenen Weise unentgeltlich geholfen:

1. THOMAS PAUL, vorher Inst. für Festkörpertheorie und Optik (FSU Jena), jetzt Fraunhofer Institut für Angewandte Optik und Feinmechanik, stellte seine Implementation einer FMM zur Verfügung auf deren Basis ich die Erweiterung zur a-FMM implementierte.

2. Die FDTD Simulation in Kapitel IV wurde durchgeführt von JING QI, Inst. für Festkörpertheorie und Optik (FSU Jena).

3. Die Herstellung der Proben in den Kapiteln IV und V wurden durchgeführt von MICHAEL STEINERT und CHRISTIAN HELGERT, beide Inst. für Angewandte Physik (FSU Jena).

4. Die SNOM Experimente in den Kapiteln IV und V wurden zusammen mit SÉVERINE DIZIAIN und ANGELA KLEIN, beide zu dieser Zeit am Inst. für Angewandte Physik (FSU Jena), an deren Setups durchgeführt.

5. Das n-PEEM Experiment in Kapitel IV wurde durchgeführt von MATTHIAS FALKNER, Inst. für Angewandte Physik (FSU Jena).

Weitere Personen waren an der inhaltlich-materiellen Erstellung der vorliegenden Arbeit nicht beteiligt. Insbesondere habe ich hierfür nicht die entgeltliche Hilfe von Vermittlungs- bzw. Beratungsdiensten (Promotionsberater oder andere Personen) in Anspruch genommen. Niemand hat von mir unmittelbar oder mittelbar geldwerte Leistungen für Arbeiten erhalten, die im Zusammenhang mit dem Inhalt der vorgelegten Dissertation stehen.
Die Arbeit wurde bisher weder im In- noch im Ausland in gleicher oder ähnlicher Form einer anderen Prüfungsbehörde vorgelegt.
Die geltende Promotionsordnung der Physikalisch-Astronomischen Fakultät ist mir bekannt.
Ich versichere ehrenwörtlich, dass ich nach bestem Wissen die reine Wahrheit gesagt und nichts verschwiegen habe.

Ort, Datum Unterschrift